Phase Transition of Quantum Light-Matter Systems

Tesis
entregada a la
Universidad de Chile
en cumplimiento parcial de los requisitos
para optar al grado de
Magíster en Ciencias Físicas
Facultad de Ciencias

por

Joaquín Rubén Jesús Figueroa Álvarez

Octubre, 2018

Director de Tesis : **Dr. Felipe Torres**
Co-Director de Tesis : **Dr. Juan Alejandro Valdivia**

FACULTAD DE CIENCIAS

UNIVERSIDAD DE CHILE

INFORME DE APROBACIÓN

TESIS DE MAGÍSTER

Se informa a la Escuela de Postgrado de la Facultad de Ciencias que la Tesis de Magíster presentada por el candidato

Joaquín Rubén Jesús Figueroa Álvarez

ha sido aprobada por la Comisión de Evaluación de la Tesis como requisito para optar al grado de Magíster en Ciencias Físicas, en el examen de Defensa de Tesis rendido el día 04 de Octubre de 2018.

Director de Tesis

Dr. Felipe Torres _____

Co-Director de Tesis

Dr. Juan Alejandro Valdivia _____

Comisión de Evaluación de la Tesis

Dr. Guillermo Romero _____

Dr. Felipe Barra _____

Dr. Alvaro Nuñez _____

A mi Familia

BIOGRAFÍA

Nacido 20 de septiembre 1986, Licenciado en ciencias mención Física 2010 de la Universidad de Chile y titulado como Ingeniero Civil Electricista en 2012. Trabajo en Synopsys Chile LTDa desde el 2012 al 2016 cuando ingresa al Magíster en Ciencias Mención Física de la Universidad de Chile.

AGRADECIMIENTOS

Primero quiero agradecer a mi Familia, por su apoyo en este proceso.

También quiero agradecer a mis tutores, Felipe Torres y Alejandro Valdivia, por su guía y disposición.

Agradezco también a la Universidad y a la facultad por el apoyo financiero.

Finalmente agradezco a CEDENNA por el apoyo brindado el financiamiento a congresos y otras actividades.

ABSTRACT

Strong correlation effects emerge from light-matter interactions in coupled resonator arrays, such as the Mott-Insulator to superfluid phase transition of atom-photon excitations are among the most interesting phenomena in the field of quantum optics and quantum simulations. This Thesis focuses on the study of the transition from Mott-Insulator to Superfluid phase of weakly coupled resonator arrays each one doped with a two-level system. We discover that quenched dynamics of a finite-sized complex array of coupled resonators induces a first-order like phase transition. We demonstrate that the latter is accompanied by nucleation of superfluid-light domains that can be used to manipulate the photonic transport properties of the simulated superfluid phase; this in turn leads to an empirical scaling law. On the other hand, adiabatic dynamics resembles a second order phase transition inducing a continous change of the state of the system. First, we study the formation of dressed quantum polariton states and the effective photon-photon interaction between them. This system is described by the Jaynes-Cummings-Hubbard model. If the frequency of the resonator mode and the two-level system are close to resonance the effective photonic repulsion prevents the presence of more than one polaritonic excitations in the resonator, due to the photon-blockade effect. Detuning the atomic and photonic frequencies reduces this effect and leads the system to a photonic superfluid phase. We find that a nucleated superfluid photon state emerges in a localized way, which depends on the topology of the array. This avalanche-like behavior leads to a universal scaling law between the critical parameters of the superfluid state and the average connectivity.

The second problem refers to the effect of the anisotropic distribution of light-matter coupling across different sites of the array and the two level system frequency anistropy on the dynamics of the phase transition. We obtain the modulation and

resonance of superfluid states. This highlights the topological properties of the array, and how they can be used to manipulate the photonic transport.

The validity of our results encompasses a wide range of complex architectures that might lead to a promising device for use in scaled quantum simulations.

Keywords: Quantum Phase Transition, Jaynes-Cummings-Hubbard model, Topological Properties.

Contents

List of Figures

Chapter 1

Introduction

Within the next 10 years traditional computational systems, built on semiconductor transistors and based on the *Von-Neuman* architecture, will inexorably reach a limit in their continued technological development due to fundamental physical constraints[1]. In the *Von-Neuman* architecture the processor is physically separated in functional blocks, thus the information must be transferred between the different blocks for each operation. This is the origin of the *Von-Neuman Bottleneck*, which limits information transfer rates[2]. Quantum systems represent one of the most promising fields to surpass current computation technologies, where quantum entanglement and interference provide the system with great computational and storage capabilities due to the large number of degrees of freedom involved[3].

Although the current computational paradigm leverages parallelism to increase the computational performance, the processing power still uses traditional arquitectures bound by the *Von-Neuman Bottleneck*. Quantum computing aims to solve these issues through its intrinsic quantum parallelism[4] and carefully designed algorithms leveraging the quantum properties of the computer.

1.1 Quantum Computing

Richard Feynamm[3] was the first to introduce the idea of a quantum computer as new mechanism to study the phenomena of physical systems in situations where traditional computers (classical computers in this context) are not adequate, due to the difficulty to keep track of the large number of variables involved in the study of quantum systems, and the memory requirements which increase exponentially with the system size[5]. In quantum computing, the basic premise is that everything is governed by quantum mechanics, even classical computers, which are used for calculations and modeling of nature. However, no classical computation takes advantage of quantum mechanics, therefore, the idea is to use quantum phenomena for general computations, where the main goal is the development of a universal quantum computer capable of executing any instruction or tasks taking advantage of quantum physics to perform them at a much higher speed by levaring quantum parallelism[6]. Typical examples of universal quantum computing are the quantum cryptography algorithms[7], which would break current cryptography jeopardizing financial transactions [8], and could also promise secure communication between two parties without the possibility of eavesdropping, far beyond anything available through the use of current computers[7]. Since its inception, Quantum Computing has gathered a great interest from the community; however, the complexity of isolating and controlling the quantum states have hindered the development of quantum computers[6].

Even if a universal quantum computer is not yet attainable, it is still possible to use quantum mechanics to "simulate nature, with nature", which is known as quantum simulation. In quantum simulation one can study a controllable laboratory system that exhibits the same or similar properties as another system of interest,

that would not be tractable using conventional computers. Manipulating states of the laboratory system is possible to discover new phenomena for the systems in study[9]. In recent years there has been an increasing focus on quantum simulations, as the techniques for controlling the small scale systems have experienced continuous improvement[10, 11, 12, 13, 14, 15, 16, 17, 18, 19, 20, 5, 21, 22].

1.2 Quantum Simulators

In Quantum Computing, the field of quantum simulations have showed success as multiple quantum systems can be used for computation and analysis, each quantum system is known as a platform[5]. Some of them are mentioned here with their corresponding applications as introduction. Therefore, one can mention the ultra-cold gasses platform[18], which operates in the Bose-Einstein condensate state, and used to simulate superconductivity phenomena based on the BCS theory, Mott insulator states and similar phenomena. Another interesting system is the trapped ions architecture in radio-frequency traps, used in the study of magnetism phenomena produced by spin interaction[12]. Quantum Chemistry phenomena can also be studied through the use of the quantum photonic platform, which has the advantage of being usable at room temperature[9]. Finally the superconducting circuits is one of the most interesting platforms due to the wide range of the parameters and the possibility of building the system with great precision as they can be built using techniques that are similar to the ones used in semiconductor industry[13, 23, 11, 24].

Finally, and most important platform for this study, Cavity quantum electrodynamics (CQED) describes light-matter interactions. The physics in this architecture can be described through multiple models, such as the Jaynes-Cummings model, Dicke model, Bose-Hubbard model. Multiple coupled cavities can be used to study additional phenomena including many-body physics [21, 25, 26]. These characterist-

ics make the study CQED systems important and the object of this work for both, the additional insights revealed for multiple physics fields and the potential technological applications which can be developed with these systems. In the framework of CQED systems and many-body physics phenomena, we focus our analysis on the simulation of phase transitions.

1.3 Simulated phase transition

Phase transitions are phenomena observed in a range of physical systems and characterized by a drastic change in an extensive wide range variable of the system. For instance, solid-liquid-gas phase transition observed in materials like water, superconductivity in metals, the magnetic phase transition at curie temperature or the liquid Helium superfluid phase transition, etc[27, 28, 29, 30, 31].

In this thesis, we explore, the Mott-Insulator/Superfluid phase transition in the Jaynes-Cummings-Hubbard (JCH) model through the analysis of emergent phenomena in the polaritonic states. Here the JCH model is analyzed in three different conditions. First, we use quench dynamics and topology to show a first-order like phase transition with accompanied nucleation. Second, we also consider Hall-like states through anisotropy on the light-matter coupling. Finally, we study the resonance in a Meta-stable phase produced by the anisotropy of between the doping two-level system frequency.

To understand the properties of the phase transition in the JCH model, it is required to understand the Jaynes-Cummings (JC) model. The JC model [32, 33] is one of the most studied CQED models, because of its successful experimental realizations, particularly in superconducting circuits. The JC model is one of the most simple models describing light-matter interaction where the excitations for the system form hybrid light-matter dressed known as polaritons. This system has been

comprehensively studied and will be used as building block in this work[34, 35, 36].

The Jaynes-Cummings-Hubbard(JCH) model[37], is an extension to the JC model by coupling multiple JC cavities through a hopping constant so that excitations can move between cavities. The JCH model extension exhibits multiple interesting phenomena such as the Mott-Insulator/Superfluid phase transition, which appears due to the interaction of the hybrid light-matter states (polaritons) and the photon blockade effect[38, 39, 40, 41, 42].

The main objective of this thesis is to explore the Mott-Insulator/Superfluid phase transition in the Jaynes-Cummings-Hubbard (JCH) model through the analysis of emergent phenomena in the polaritonic states. Here the JCH model will be analyzed in three different situations. First, through use quench dynamics and topology. Second through anisotropy on the light-matter coupling and finally through the anisotropy of between the doping two-level system frequency.

1.4 Methodology

This work explores the JCH model through analytical and numerical analysis performed using computer simulation. For numerical simulations the quantum toolkit QuTip [34, 35] is used, as it allows the analysis of the temporal evolution of the system observable quantities through a variety of numerical methods, which include the Lindblad Master equation Solver, and Mote-Carlo wavefunction approach.

1.5 Outline of this Thesis

This thesis is divided in chapters describing the theoretical background, and the results of obtained through the development of this work, thus this first chapter provides a brief introduction.

The Second chapter provides an introduction to different models including the

Jaynes-Cummings model, describing its origin, properties, spectrum and some physical phenomena including the photon blockade effect. Then, we move to the Bose-Hubbard model as an approach to many-body physics; the Bose-Hubbard model is also used to shown that the properties of the system can be described using different order parameters. Finally this, we focus on the Jaynes-Cummings-Hubbard model and how physical phenomena such as Mott-Insulator/Superfluid phase transitions arise on it by the manipulation of the different variables of the model.

The Third chapter provides a theoretical description of phase transitions, and how they relate to the Quantum phase transition observed in many-body physics, as well as the CQED models discussed in this work. This chapter shows how a first-order-like quantum phase transition arises in the JCH model using quench dynamics. This behavior is accompanied by nucleation of the superfluid light domains which may be manipulated via the topology of the array. The latter may also allow for the indirect manipulation of the photonic superfluid state. All results are verified through numerical simulations and a mean field theory.

The Fourth chapter includes a theoretical analysis of the JCH model from an energy perspective using quantum perturbation theory as an analysis tool. Then this chapter discusses the effects of the detuning induced anisotropy in the JCH model, which originates a new resonant phase on the model different to both the Mott-Insulator phase and the superfluid phase with its own set of properties. Finally we show that anisotropy on the light-matter coupling produces a modulated integer-filling phase transition in the JCH model, which resembles Quantum-Hall effects.

The final chapter provides the conclusions of this Thesis and possible developments originating from the results here presented.

Chapter 2

Phase transition in Light-Matter Quantum Systems

2.1 Introduction

Coupled resonator arrays allow us to study several physical phenomena in a wide array of different platform, ranging from superconducting circuits to doped optical crystals. Furthermore, CQED models are capable of simulating many-body physics phenomena including phase transitions. In this thesis we focus on the Mott-Insulator/Superfluid phase transitions, specifically in the Jaynes-Cummings-Hubbard and Bose-Hubbard model.

2.2 The Jaynes-Cummings Model

The JC model describes a two level system (TLS), such as a trapped ion inside an optical cavity, interacting with photons as shown in figure 2.1.

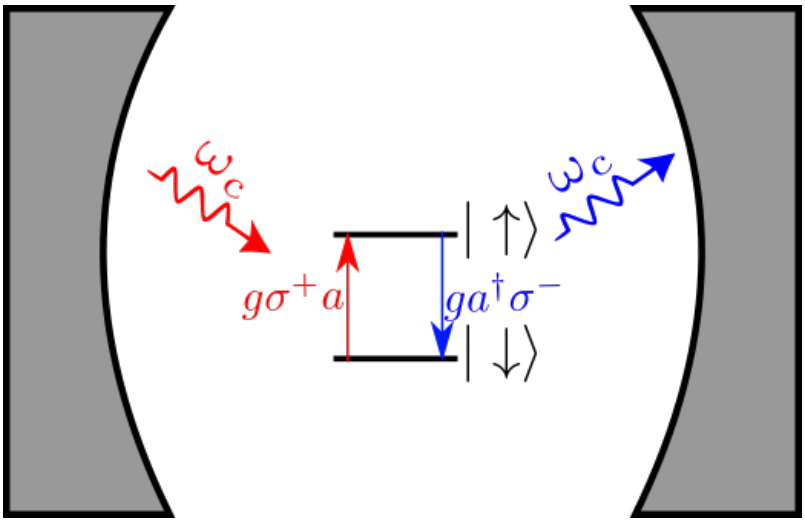

Figure 2.1: Schematic representation of the Jaynes-Cummings model. The JC model describes the absorption(Red) and emission(Blue) of a photon by a TLS inside a cavity. In this figure $a(a^\dagger)$ is the photonic lowering(rising) operator, while $\sigma^+(\sigma^-)$ is the TLS rising(lowering) operator

The JC model is described by the Hamiltonian

$$H_{JC} = \omega_c a^\dagger a + \omega_a \sigma^+\sigma^- + g(a^\dagger\sigma^- + a\sigma^+), \tag{2.1}$$

where ω_a is the TLS frequency, ω_c is the photonic frequency, and g the light-matter coupling strength. The first term of equation (2.1) correspond to a single mode electromagnetic field of the cavity, the second term is a free TLS system and the last term describes the light-matter coupling between the photons and the TLS, see figure 2.1.

Equation (2.1) shows the Jaynes-Cummings Hamiltonian, which is an approximation of the Rabi Hamiltonian obtained through the rotating wave approximation (RWA), considering $\omega_c - \omega_a \ll \omega_c + \omega_a$. For the JC model, the total number of exitations $N = a^\dagger a + \sigma^+\sigma^-$ is a conserved quantity, hence $[H_{JC}, N] = 0$. The conserved total excitations allows for the diagonalization of the JC model, which is not possible for the Rabi model[47].

2.2.1 Properties of the Jaynes-Cummings model

The JC model has interesting properties, the first one comes from the usage of the (RWA), since the interaction terms describe the process in which the TLS and the cavities exchange energy or excitations, thus the term $a\sigma^+$ represents the absorption of a photon in the cavity by the TLS going from the ground state to the excited state, while $a^\dagger\sigma^-$ corresponds to the release of a photon from the TLS going from the exited state to the ground state (Figure 2.1). $a^\dagger\sigma^+$ shows a spontaneous creation of a photon in the cavity with an spontaneous transition in the TLS from the ground state to the exited state, similarly $a\sigma^-$ is the spontaneous destruction of a photon and the transition of the TLS from the exited state to the ground state, while these process are possible, they are less intuitive than the other terms, and represent process that are much more energetic or faster, thus are discarded in the study of the system(See A for a more detailed discussion).

The constant number of excitations in the JC model, allows for convenient writing of the Hamiltonian in matrix form, using the basis $\{|n,\downarrow\rangle, |n,\uparrow\rangle\}$, built from the tensor product of the photon basis $|n\rangle$ for n photons in the cavity and the two-level system basis $\{|\downarrow\rangle, |\uparrow\rangle\}$ which represent states with the system in the ground state and the exited state respectively. Furthermore, for a total number of excitations(n) the matrix form of the JC Hamiltonian is shown in equation (2.2).

$$H^n_{JC} = \begin{array}{c} \begin{matrix} \langle n,\downarrow| & \langle (n-1),\uparrow| \end{matrix} \\ \begin{bmatrix} n\omega_c & g\sqrt{n} \\ g\sqrt{n} & (n-1)\omega_c + \omega_a \end{bmatrix} \end{array} \begin{array}{l} |n,\downarrow\rangle \\ |(n-1),\uparrow\rangle \end{array} . \tag{2.2}$$

From the matrix form the standard procedure is to compute the eigenvalues and eigenvectors of the Hamiltonian, from which the physical properties of the system can be computed, including but not limited to the energies, the states and the time evolution of the system[48]. At this point the diagonalization procedure will be

detailed, however before performing the procedure, it is convenient to perform the following identifications. The detuning $\Delta = \omega_a - \omega_c$ is defined as an auxiliary variable, representing the difference between the energies of the photonic cavity and the TLS transition energy. The cavity resonant frequency is re-labeled as $\omega_c \to \omega$, so it can be identified as system's Hamiltonian frequency, hence the modified Hamiltonian is shown in equation (2.3), which will have a more convenient representation.

$$H_{JC}^{n} = \begin{bmatrix} n\omega & g\sqrt{n} \\ g\sqrt{n} & n\omega - \Delta \end{bmatrix}. \tag{2.3}$$

The eigenvalues of the Hamiltonian above are $E_n^{\pm} = n\omega + \frac{\Delta}{2} \pm \chi_n$ with $\chi_n = \sqrt{\left(\frac{\Delta}{2}\right)^2 + g^2 n}$, then the eigenvectors are $|n-\rangle = \sqrt{n}\,|n,\downarrow\rangle - (\chi_n - \frac{\Delta}{2})\,|n,\uparrow\rangle$ and $|n+\rangle = g\sqrt{n}\,|n,\downarrow\rangle + (\chi_n + \frac{\Delta}{2})\,|n,\uparrow\rangle$, where $|n-\rangle$ corresponds to the lowest energy eigenvalue for n total excitations($E_n^{-} = n\omega + \frac{\Delta}{2} - \chi_n$), and $|n+\rangle$ corresponds to the highest energy eigenvalue.

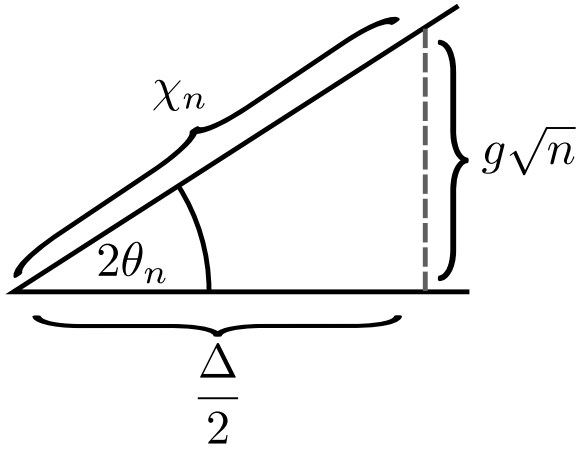

Figure 2.2: Graphical representation of the Jaynes-Cummings model energy constants which

From the definition of χ_n is observed that the quantities in the eigenvectors satisfy a trigonometrical relationship, as shown in figure 2.2, from which the mixing angle θ_n is defined as $tan(2\theta_n) = \frac{g\sqrt{n}}{\Delta/2}$ to simplify the expressions for the eigenvectors shown

in equation (2.4). This method to represent the JC Hamiltonian is known as the Polariton mapping [49]

$$\begin{pmatrix} |n-\rangle \\ |n+\rangle \end{pmatrix} = \begin{bmatrix} \cos(\theta_n) & -\sin(\theta_n) \\ \sin(\theta_n) & \cos(\theta_n) \end{bmatrix} \cdot \begin{pmatrix} |n,\downarrow\rangle \\ |n-1,\uparrow\rangle \end{pmatrix}. \tag{2.4}$$

Equation (2.4) shows the polariton mapping on the left side, where the states $|n\pm\rangle$ are labeled according to their corresponding eigen-energies $E_n^{\pm}$, hence these are associated with different energy branches. The equation (2.4) also shows how to perform the linear transformation between the cavity-TLS system to the polariton mapping where the states of the form $|n,\downarrow\rangle = |n\rangle\otimes|\downarrow\rangle$ are the tensor product between the cavity system basis and the TLS system basis.

2.2.2 The Energy spectrum of the Jaynes-Cummings model

Consider the energies of the system given by $E_n^{\pm} = n\omega + \frac{\Delta}{2} \pm \chi_n(\Delta)$, then is clear that is possible to study the system and its properties based on the detuning parameter Δ, while keeping in consideration that represents the mismatch between the cavity and TLS resonant frequencies. Figure 2.3 shows the energy spectrum of an empty cavity and compares them with the energies of the JC model in the resonant case ($\Delta = 0$). For the empty cavity in figure 2.3 (Left) is possible to observe the harmonic energy spectrum, so that the spectrum is coherent. For the JC system at the right side of figure 2.3, the energy of the system is not uniquely determined by the number of polaritons (n), in fact for a given number of polaritons there are two distinct energy levels, which allow for the identification of different branches, the lower branch characterized by E_n^- and $|n-\rangle$ and the upper branch characterized by E_n^+ and $|n+\rangle$, which has a higher energy than the lower branch. In comparison with the empty cavity spectrum, the light matter interaction in the JC model produces a dopant splitting of the spectrum, and the spectrum becomes anharmonic as there is a non

uniform energy gap between the different branches and a non uniform energy gap between different number of excitations in the same branch.

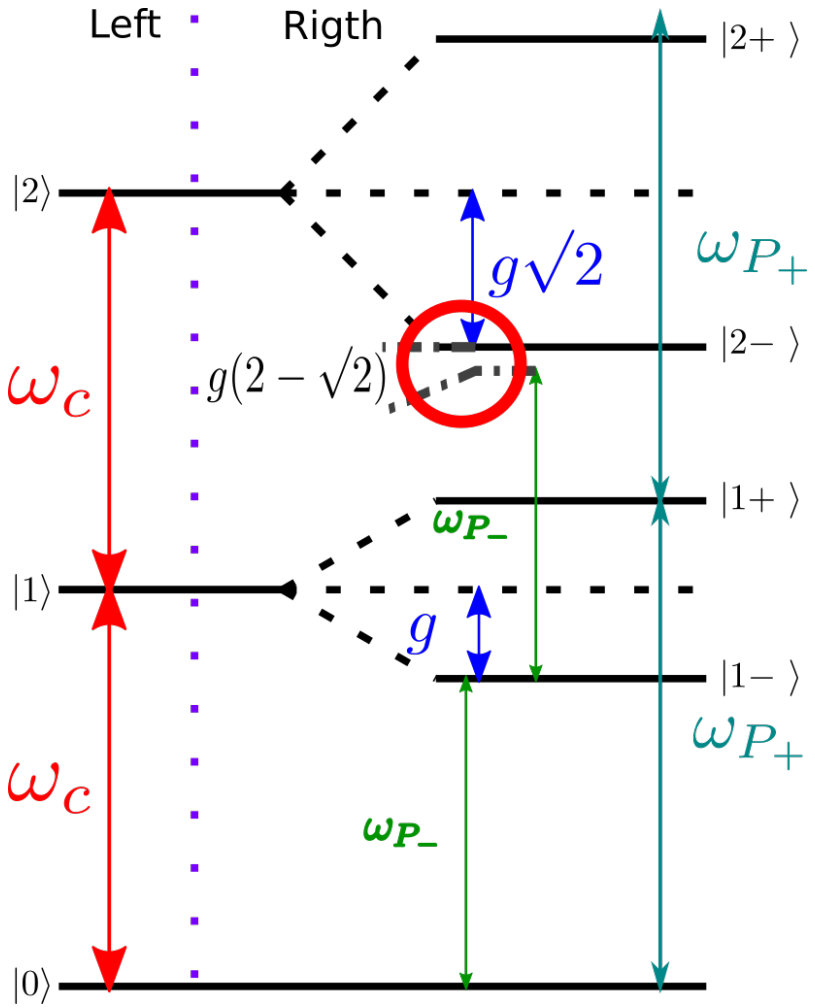

Figure 2.3: The energy spectrum of the Jaynes-Cummings model in the resonant case. Left shows the spectrum of an empty cavity of frequency ω_c. Right the modified spectrum through the interaction between the cavity and the two level system, where for each total number of excitations (polaritons) the lower and upper branch can be observed, associated to the frequencies $\omega_{P_-} = \frac{1}{\hbar}E_{|1-\rangle}$ and $\omega_{P_+} = E_{|1+\rangle}$ respectively.

There is another case of interest in the JC model, which is given by the off-resonance case $\Delta \gg g$ in such scenario shown in figure 2.4, the light-matter interaction losses its influence over the dynamics of the system so that the cavity behaves almost as if it was empty, as there is a lifting of the lower branch which matches

with the empty cavity spectrum. Although the JC model has a similar spectrum to an empty cavity, there are still two distinct branches, the lower branch for which the TLS remains empty, and the upper branch where the TLS remains occupied for any number of photons in the cavity. The lack of resonance between the TLS and the cavity mode, means that a photon in the cavity can not effectively interact with the TLS, which means that the TLS and the cavity are not coupled anymore.

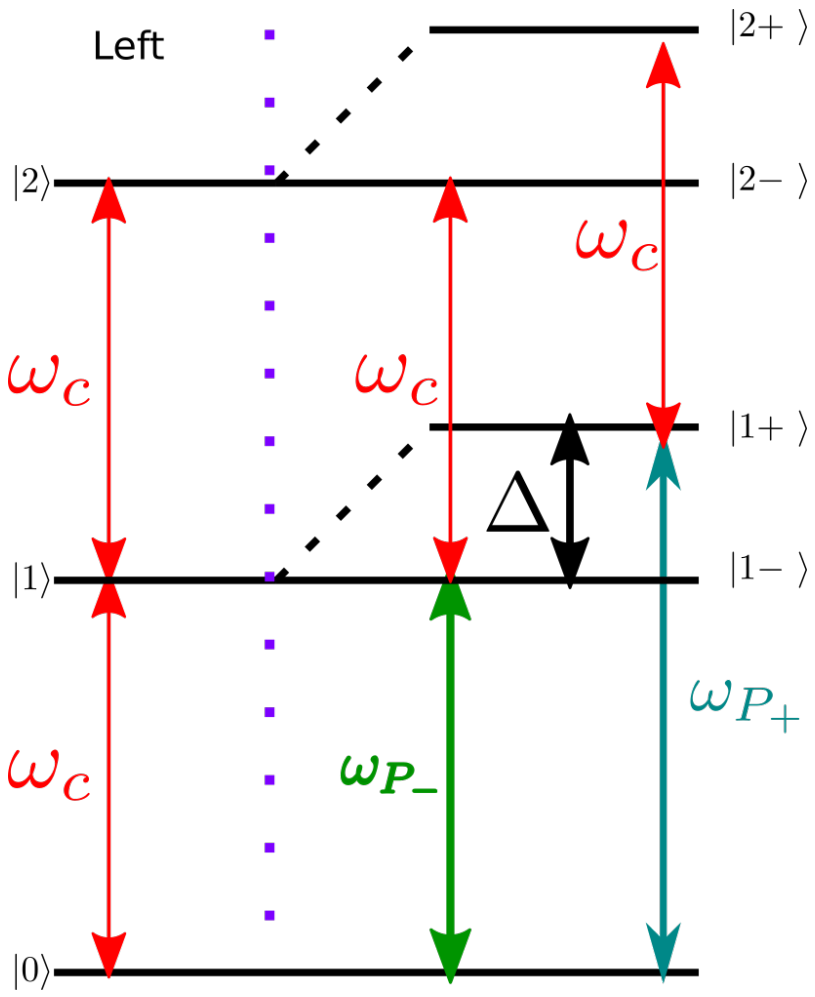

Figure 2.4: The energy spectrum of the Jaynes-Cummings model in the off-resonant case ($\Delta \gg g$). Left shows the spectrum of an empty cavity. Right the modified spectrum through the interaction between the cavity and the two level system, where the lifting of the lower branch to match the empty cavity spectrum can be observed

A more detailed analysis of figure 2.4 shows that the spectrum of both branches

becomes harmonic. This can be understood through the analysis of the energies $E_n^{\pm} = n\omega - \frac{\Delta}{2} \pm \frac{\Delta}{2}\sqrt{1 + \frac{n}{\left(\frac{\Delta}{2g}\right)^2}}$ which in the limit $\Delta \gg g$ becomes $E_n^- = n\omega$ and $E_n^+ = n\omega + \Delta$. The spectrum of the polariton branches in the JC model as function of the detuning is shown in figure 2.5

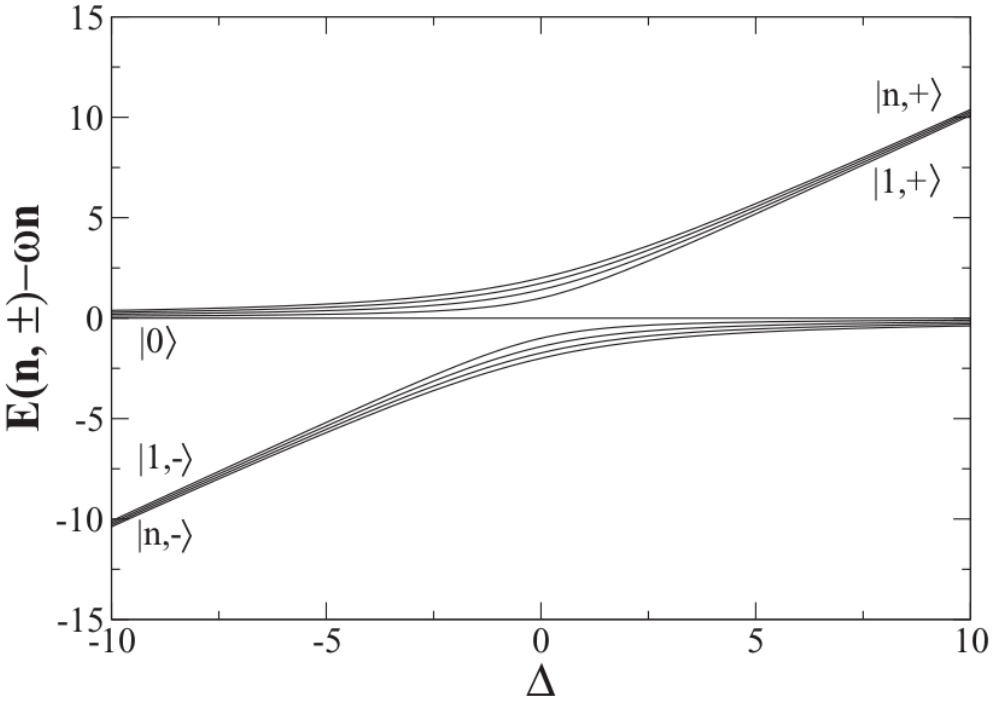

Figure 2.5: The energy spectrum of the Jaynes-Cummings model for multiple number of polaritons as function of Δ. This figure shows how the energy of the lower polariton branch is always smaller than for the upper polariton, and that these do not cross at any point. [50]

2.2.3 Photon Blockade

One of the most interesting phenomena which can be observed in a non linear optical cavity is the appearance of the photon blockade[36]. If the frequency of the resonator mode and the two-level system are close to resonance the effective photonic repulsion prevents the presence of more than one excitations in the resonator.Experimentally this can be demonstrated using the setup shown in figure 2.6, in which a coherent

photon source is used to drive a JC cavity, but it can only populate the $|1-\rangle$ state, never higher energy levels[36].

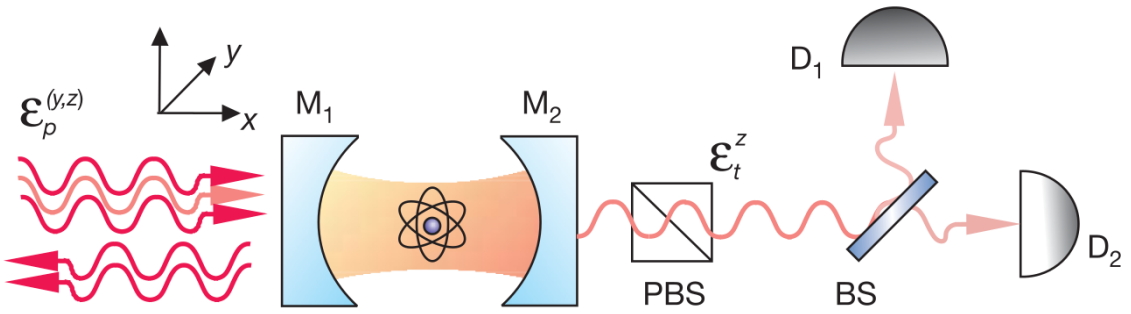

Figure 2.6: Schematic representation of the experimental setup used to study the photon blockade. A JC cavity is pumped with a coherent beam of photons, however due to the photon blockade, they can only pass through the cavity at a reduced rate, which is measured with the detectors [36]

2.3 The Bose-Hubbard Model

With the development of the quantum theory, also came the development of statistical theory for the different types of particles: Fermi statistics for fermions and Bose statistics for bosons[31]. From the statistics of a gas of particles arise the properties of the system such as the Fermi pressure and the Bose-Einstein condensate (BEC); however, is the interplay of particles with different statistics that give rise to more interesting phenomena such as superconductivity, superfluidity, and the fractional quantum hall effect[52, 53].

Is in this context that the Bose-Hubbard model[54] is used, as it has the optical non-linearities that give rise to interesting phenomena, and being a multiple cavity model, has the potential to simulate phenomena present in Many-Body systems

2.3.1 Photon Blockade in the Bose-Hubbard model

The Bose-Hubbard model describes a system of coupled non-linear optical cavities[54], in a similar manner as the Hubbard model[55] describes spin-chains.

$$H_{BH} = \mu \sum_{i}^{N} n_i - J \sum_{\langle i,i' \rangle}^{N} (a_i^\dagger a_{i'} + h.c.) + U \sum_{i}^{N} n_i(n_i - 1) \tag{2.5}$$

The Bose-Hubbard model Hamiltonian, shown in equation (2.5), describes a system on non-linear optical cavities in the grand-canonical ensemble where μ represents the chemical potential for the photon occupation for each cavity, U represents the on-site photon-photon repulsion originated by the non-linearities of the cavity, J represents the nearest-neighbors hopping strength, or the strength of the coupling between the cavities, $a_i^\dagger(a_i)$ is the creation(destruction) operators for the photons inside the cavity and n_i represents the total number of photons inside the cavity.

The Bose-Hubbard model exhibits a photon blockade effect produced by the on-site repulsion of the cavities. In this model, the competition between the on-site repulsion and the hopping produces a Mott-Insulator/Superfluid phase transition as shown in figure 2.7, where the Mott-Insulator phase is the result of a strong on-site repulsion ($\frac{J}{U} \ll 1$), resulting in localized photons. On the other hand the Superfluid phase is the result of a weak on-site repulsion ($\frac{J}{U} \gg 1$) where the photons are delocalized.

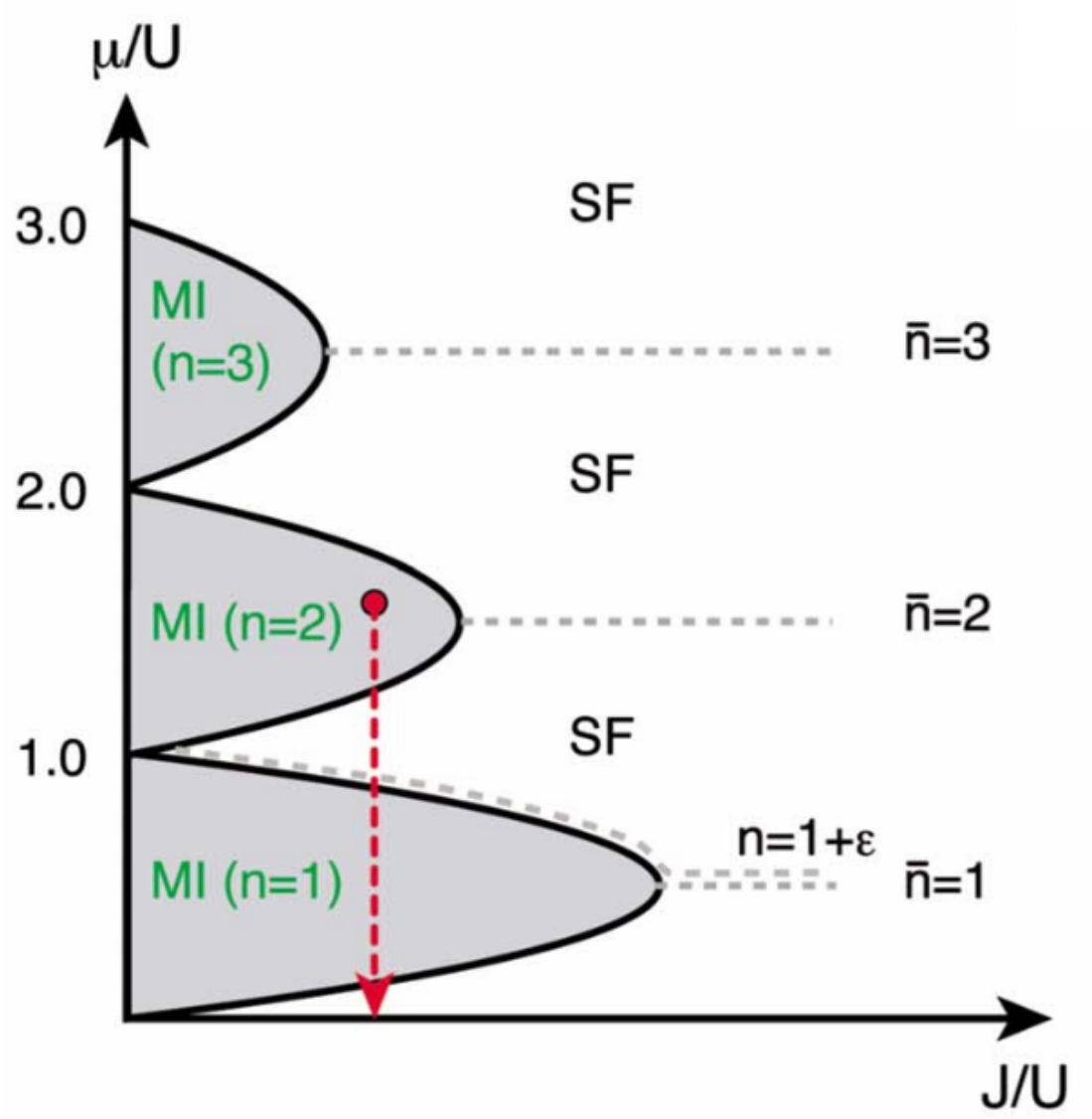

Figure 2.7: Phase diagram of the Bose-Hubbard model, which shows multiple Mott-Insulator lobes and the superfluid phase, which depend on the competition between the chemical potential (μ) and the hopping (J)[56].

Figure 2.7, also shows the effect of the chemical potential on the phase diagram in the form of multiple Mott-Insulator lobes. Each lobe represent a different integer-filling factor, meaning that the ration between the total number of photons of the system and the number of cavities is an integer number, so the first lobe ($n = 1$),

means that there is a single photon in each cavity.

2.3.2 Variance in the BH model

In the Mott-Insulator phase the excitations are localized. In contrast, the Superfluid phase is characterized by the delocalization of the excitations. The order parameter describing this phase transition, is the total variance.

$$\Delta N = \sum_{i}^{N} \Delta N_i = \sum_{i}^{M} \frac{1}{T} \int_0^T dt \left(\langle n_i^2 \rangle - \langle n_i \rangle^2 \right), \tag{2.6}$$

with ΔN_i is the time averaged variance for the site i. When the total variance is close to zero the excitations are localized at the different sites of the system. In this case, the number of photons in each site does not fluctuate. On the other hand, when the system is in the superfluid phase, the excitations are delocalized and can move freely through the different sites of the arrangement. Thus the number of photons in each site has larger quantum fluctuations[26].

2.3.3 Bipartite Fluctuation

A generalization of the previous order parameter are bipartite fluctuations, defined as

$$\mathscr{F}_A = \sum_{i,j \in A} C_{i,j} = \sum_{i \in A} \frac{1}{T} \int_0^T dt \left(\langle n_i n_j \rangle - \langle n_i \rangle \langle n_j \rangle \right) \tag{2.7}$$

where A is a partition of the system, and $C_{i,j}$ are the time averaged correlation coefficients between cavities i and j, notice that for $C_{i,i} = \Delta N_i$. The bipartite fluctuations was introduced as a different order parameter to characterize the Bose-Hubbard's model Mott-Insulator/Superfluid transition. The fluctuations of a system provide a description of the of the exchange of excitations of the system with the environment. For a closed system the fluctuations are zero. For a closed system divided in two partitions, then the fluctuations of both are equal in magnitude.

The use of bipartite fluctuations, require the analysis of multiple partitions schemes of the system, so it allows for the study of long range correlations. Therefore are better suited to quantify a system going from an ordered state to a disordered state, in which the long range correlations are increased[59]. Bipartite fluctuations exhibit scaling behavior between the gapless and gapfull phases according to the dimension of the system, which allows for the detection of quantum critical points[60, 61]

2.4 The Jaynes-Cummings Hubbard model

The JCH model an extension of the traditional JC model [37, 39] using the Hubbard model [62] as inspiration for multiple coupled cavities. The first characteristic of the JCH model is that being a multiple cavity system, in a similar fashion as other Hubbard based models, is that it can exhibit behaviors that mimics the phenomenology studied in many body physics. The JCH model is built from multiple JC cavities coupled through photon hopping.

$$H_{JCH} = \omega_c \sum_{i}^{N} H_{JC} - J \sum_{\langle i,j \rangle}^{N} \left(a_i^\dagger a_j \right) \tag{2.8}$$

The JCH model shown in equation (2.8) as a collection of JC cavities, coupled through the hopping term $a_i^\dagger a_j$, where H_{JCH} is the JCH Hamiltonian. This model has been used in the study of multiple many-body physics phenomena [39, 49, 63, 64, 65, 66, 67]

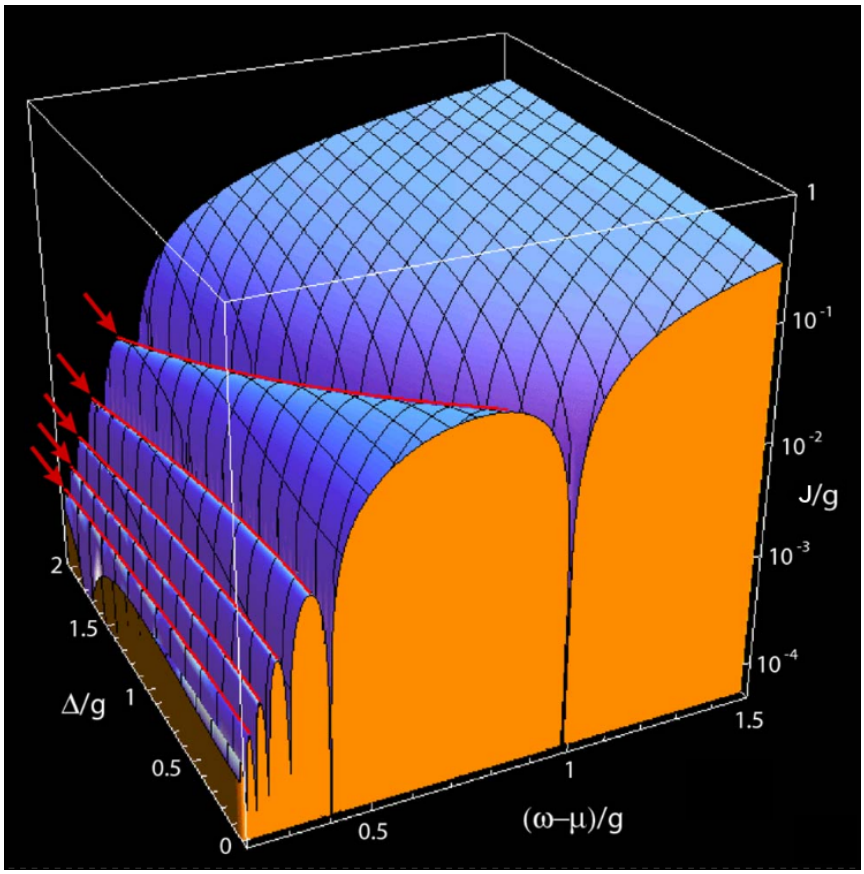

Figure 2.8: Phase diagram of the JCH model as described in the literature[49]. This figure, shows the phase boundary between the Mott-Insulator phase and the superfluid phase in the grand-canonical ensemble. The competition between the chemical potential (μ) and the cavity frequency determines the Mott-Insulator phase lobes for different occupation number. The lobes limit depend on the competition between the hopping (J) and the light-matter coupling (g), and the shape is affected by the detuning Δ compared with the light-matter coupling

Figure 2.8 shows the Mott-Insulator phase boundary of the JCH [49]. Notice that at large hoppings or large detunings, the photon blockade is no longer dominant, so the system becomes superfluid.

In a similar way as the JC model, the JCH model has conserved quantities the total number of excitations in the array of cavities $N = \sum_k^M N_i$ as a conserved quantity of the Hamiltonian, however an analytical treatment of the system is not practical anymore, as number of elements in the matrix representation of the Hamiltonian

grows exponentially with the number of sites, and even if diagonalized there is no clear interpretation for the states, in contrast to the single cavity Hamiltonian.

2.4.1 Polariton Mapping in the JCH model

It was previously established that is not practical or possible to diagonalize the JCH model from the analytical perspective, as the difficulties involved in tracking the number of states for any given configuration prevent the development of the physical intuition of the behavior of the model, therefore it can be convenient to consider the polariton mapping for the JC model from equation (2.4).

From the polariton mapping, is possible to define the creation and annihilation polariton operators[49] $P^{\dagger}_{n\pm} = |n\pm\rangle\langle 0|$ so that the JC Hamiltonian is written as $H_{JC} = \sum_{n,\alpha\in\{\pm\}} E_{n\alpha} P^{\dagger}_{n\alpha} P^{\dagger}_{n\alpha}$, and the photon creation operators for a single cavity are written as $a^{\dagger} = \sum_{n,\alpha,\beta} t_{n\alpha\beta} P^{\dagger}_{n\alpha} P_{(n-1)\beta}$, where the coefficients $t_{n\alpha\beta} = \langle n\alpha| a^{\dagger} |(n-1)\beta\rangle$ represent the probability amplitude of interchange in polariton number in the cavity and the mixing of polariton branches.

$$\begin{aligned} t_{n--} &= \sqrt{n}\cos(\theta_n)\cos(\theta_{n-1}) + \sqrt{n-1}\sin(\theta_n)\sin(\theta_{n-1}), \\ t_{n-+} &= \sqrt{n}\cos(\theta_n)\sin(\theta_{n-1}) - \sqrt{n-1}\sin(\theta_n)\cos(\theta_{n-1}), \\ t_{n+-} &= \sqrt{n}\sin(\theta_n)\cos(\theta_{n-1}) - \sqrt{n-1}\cos(\theta_n)\sin(\theta_{n-1}), \\ t_{n++} &= \sqrt{n}\sin(\theta_n)\sin(\theta_{n-1}) + \sqrt{n-1}\cos(\theta_n)\cos(\theta_{n-1}). \end{aligned} \tag{2.9}$$

Equation (2.9) shows the values for all the coefficients $t_{n\alpha\beta}$[63]. Finally the polariton mapping for the full JCH model[63] is

$$\begin{aligned} H_{JCH} &= \sum_{i}\sum_{n,\alpha} E_{n\alpha} P^{\dagger}_{n\alpha i} P_{n\alpha i} \\ &\quad -J\sum_{i,j} A_{ij} \sum_{n,n'} \sum_{\alpha,\alpha',\beta,\beta'} t_{n\alpha\beta} t_{n'\alpha'\beta'} P^{\dagger}_{n\alpha i} P_{(n-1)\beta i} P^{\dagger}_{(n'-1)\beta' j} P_{n'\alpha' j}, \end{aligned} \tag{2.10}$$

where $A_{i,j}$ is the connectivity matrix given by $A_{ij} = 1$ if the cavities i and j are connected, and $A_{ij} = 0$ otherwise.

2.4.2 Phase transition in the JCH model

One of the most interesting phenomenon observable in the JCH model is the availability to study quantum phase-transitions due to the Mott-Insulator/Superfluid phase transitions. For the analysis of the phase transitions, is convenient to consider that there are two basic limits for the JCH model: the atomic limit $J \ll g$ and the hopping dominated limit $J \gg g$[49].

Atomic limit $J \ll g$

In the atomic limit of the JCH model, the hopping term of the Hamiltonian is considered as a perturbation of the system, so the analysis of the phase transition can be developed through the formalism developed for a single cavity JC model.

In a single cavity JC model, it was established that for the resonant case, the mismatch between the energy levels with different number of excitations prevents the change in the polariton number for the cavity using a specific photonic source, hence a JC cavity driven by an optical source with the cavity frequency can only hold a single excitation with that energy, and the same source cannot force the system to a double exited state. This phenomenon is known as photon blockade[36]

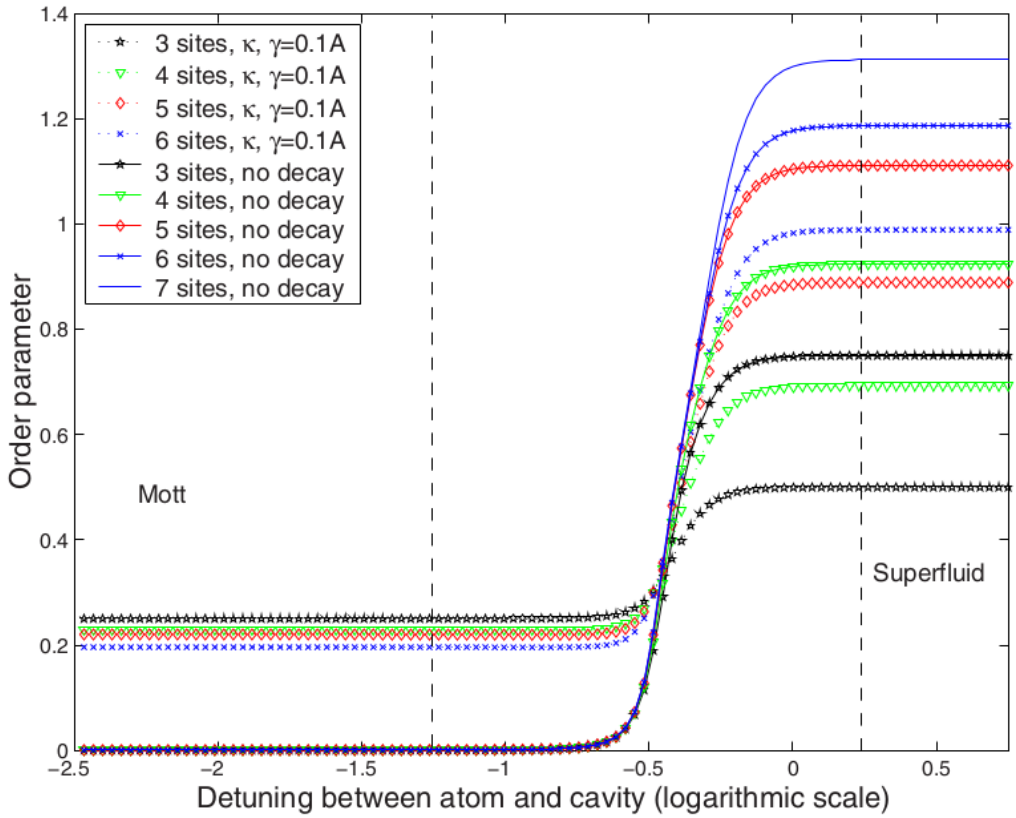

Figure 2.9: Phase transition in the JCH model defined by a change in the order parameter $\langle \Delta N \rangle_T$ as a function of the detuning $\frac{\Delta}{g}$ This figure shows the robustness of the phase transition to the coupling with the environment modeled through the parameters κ and γ which represent the cavity and TLS decay rates. In this figure the hopping strength is A [39].

Now for a multiple cavity system, the photon blockade phenomenon is observed in absence of an energy driver. In a JCH system prepared with a single polariton for each cavity, the evolution of the photonic dynamics exhibit the photon blockade as the lack of occupancy of higher energy states and the low variance of the polariton number for each site[39].The phase transition is observed by changing the detuning between the cavity and the TLS, the higher energy states for any given cavity can be occupied with probability greater than zero. similarly the variance of the polariton number for each site is also increased and can be used as order parameter in order

to characterize the phase transition, as shown in figure 2.9

Hopping domiated limit $J \gg g$

For the Hopping dominated limit in the JCH model, the TLS light-matter interaction can be treated perturbatively, regardless of the detuning, so at this limit the system is considered to be mainly an array of coupled cavities where the photons can move mostly free, so the increase of the hopping constant (J) drives the phase transition from the Mott-Insulator to the Superfluid phase.

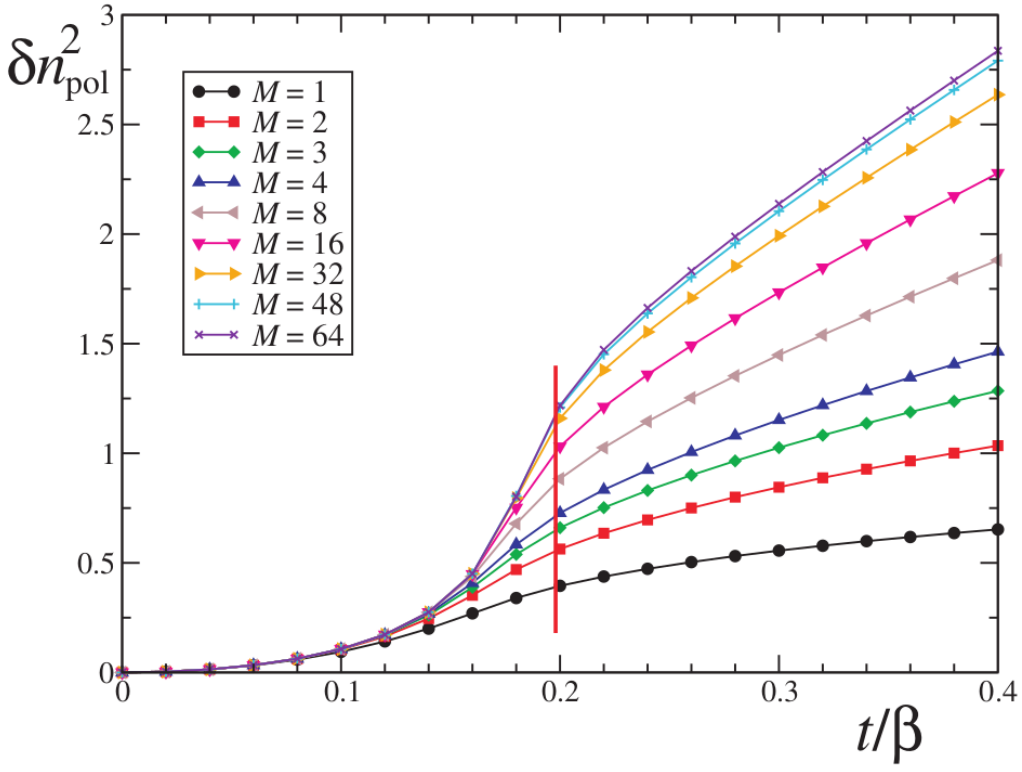

Figure 2.10: Phase transition in the JCH model defined by bipartite fluctuation as the order parameter δn^2 as a function of the hopping parameter[61]. In this figure the hopping parameter is t and the light matter interaction is β

Figure 2.10 characterizes the quantum phase transitions using bipartite fluctuations of the polariton number for the different partitions of the system[61, 60]. Bipartite fluctuations show that the phase transition is an universal phenomena which

does not depend on the order parameter used for describing the system.

$$\delta n^2(M) = \left\langle \left(\sum_{i \in M} n_i \right)^2 \right\rangle - \left\langle \sum_{i \in M} n_i \right\rangle^2 \tag{2.11}$$

Equation (2.11) shows the method to compute the bipartite fluctuations of a given size M. Another mechanism to compute the bipartite fluctuations is to use the two-point correlation functions $C_{ij} = \langle n_i n_j \rangle - \langle n_i \rangle \langle n_j \rangle$ so that $\delta n(M) = \sum_{\{i,j\} \in M} C_{ij}$.

2.5 Conclusions

Coupled Cavity QED systems, provide a mechanism to bridge the different scales of the physical phenomena involved, on one side the individual interactions between atoms, and the macroscopic phenomena in condensed matter systems, as they provide with a platform to perform controllable and precisely measurable experiments[25] involving only a few cavities, only each one encompasses a wealth of phenomena, such as the photon blockade, as was already discussed 2.2.3, in order to study and broaden the understanding of Many-Body physics. In this context, the Jaynes-Cummings-Hubbard (JCH) model is used as a Many-Body quantum simulation tool for the research of new physical phenomena.

This section has provided an introduction to the CQED models, starting with the jaynes-Cummings model, its theoretical description and properties analysis. Following the JC model, we discussed how a Coupled resonating array is capable of simulating many body physics and in particular the Mott-Insulator/Superfluid phase transition.

We also discussed how this Mott-Insulator/Superfluid phase transition can be analyzed in the BH model and JCH model through different order parameters that

are in agreement, and in particular that for the JCH model there are multiple mechanisms to trigger the phase transition through the competence between the hopping and light-matter interaction, or through the detuning of the cavity.

Chapter 3

Quantum Phase Transitions: Topology and Nucleation

3.1 Introduction

In the previous chapter, we discussed different CQED model, and their properties, as well as the Mott-Insulator/Superfluid phase transition in the Bose-Hubbard and Jaynes-Cummings Hubbard models. This chapter provides a small introduction to phase transitions and quantum phase transition from a theoretical perspective including the classification of phase transitions and the use of order parameters to describe them.

This chapter, also provides an introduction to the numerical analysis tools used through this work, to validate the procedure and ensure the correctness of the results, before describing the effect of topology on the phase transition in Coupled resonating arrays (CRAs).

3.2 Phase Transitions

Phase transitions are examples of collective phenomena, because phase transition arise through the mutual interaction of large groups of atoms, molecules, spins, etc, rather than the single behavior [28]

Statistical mechanics provides a mechanism to describe an extensive physical system, and also provides a theoretical framework for thermodynamics, when the system is in the thermodynamic limit. A system is considered to be in the thermodynamic limit where the number of particles is large enough to be considered infinite ($N \to \infty$), and the volume of the same system is also considered infinite($V \to \infty$), however the particle density is still finite($\frac{N}{V} \to \nu$). [68]

The thermodynamic limit is important, not only because it provides a link between statistical mechanics and thermodynamics, but also, because is in this limit, where the different statistical ensembles can be considered equivalent, therefore allowing for the rigorous mathematical study of physical phenomena.

The order parameter concept arise in the landau theory of phase transitions providing a description of the local macroscopic state of the system. Within this context, the order parameter is conveniently chosen for the phase transition to be described, thus in ferromagnetism the local magnetization is the order parameter, while in the superconductivity theory, the order parameter is the macroscopic wavefunction[30].

3.2.1 Phase transition classification

As there are multiple systems undergoing phase transitions, these transitions have different characteristics, therefore there is the need to classify the phase transitions in categories which share common properties. Ehrenfest devised the most influential classification mechanism of phase transitions[69], where he differentiated between first and second order phase transitions, based on the Gibbs free-energy description.

Consider a system on the neighborhood of a phase transition, with Gibbs free energies g_1 and g_2 for the respective phases, so that at the transition point $g_1 = g_2$. The system undergoes a first order phase transition if the first derivative of the Gibbs

energy over thermodynamic variables has a discontinuity across the phases

$$\left(\frac{\partial g_1}{\partial T}\right)_P - \left(\frac{\partial g_2}{\partial T}\right)_P \neq 0 \tag{3.1}$$

$$\left(\frac{\partial g_1}{\partial P}\right)_T - \left(\frac{\partial g_2}{\partial P}\right)_T \neq 0, \tag{3.2}$$

where T and P are the temperature and the pressure respectively[68]. Second order phase transitions, exhibit a discontinuity on the second derivative of the Gibbs free energy. Higher order phase transitions could be defined, however no additional information can be obtained through a finer grained representation, so the custom is to label all higher order phase transitions a second order[68].

$$\left(\frac{\partial^n g_1}{\partial T^n}\right)_P - \left(\frac{\partial^n g_2}{\partial T^n}\right)_P \neq 0 \tag{3.3}$$

$$\left(\frac{\partial^n g_1}{\partial^n P}\right)_T - \left(\frac{\partial^n g_2}{\partial P^n}\right)_T \neq 0. \tag{3.4}$$

3.2.2 Quantum Phase Transitions

Most phase transitions have a thermodynamical origin, where the ordering of the system is destroyed by thermal fluctuations, as in the solid-liquid transition where the lattice order is destroyed, or the ferromagnetic transition at Curie point, where the thermal fluctuations destroy the magnetic order. Quantum phase transitions, are a phenomenon occurring at low temperatures, where the system order is destroyed by quantum fluctuations derived from Heisenberg uncertainty principle, and become the example of a wide array of interesting phenomena such as the rare-earth magnetic insulators, and the already mentioned superconductivity and the liquid helium phase transition[70].

Just as in the separation between classical mechanics and quantum mechanics, quantum phase transitions can only occur in systems where quantum mechanics is dominant, which means that quantum fluctuations dominate over thermal fluctu-

ations ($\hbar\omega \ll k_B T$); this is possible only at low temperatures and smaller scale systems.

Classical phase transition theory provides insights for quantum phase transitions[70], such as the description of the phase transition through order parameters and the analysis of the classical and quantum crossover. However classical theories cannot provide a complete description of quantum phase transitions due to the prevalence of quantum phenomena. Which prevents an adequate mapping between classical and quantum descriptions, due to phenomena such as the berry phase which does not have a classical counterpart. Similarly the decoherence time rules over the dynamics of quantum systems, which does not have an analogue in classical phase transitions

Considering that quantum phase transitions occur close to absolute zero temperatures, it becomes useful to analyze the phase transitions through the perspective the singularities in the ground energy eigenstates. Therefore a first order quantum phase transition is produced by single (a small number) crossings of the ground states, and second order phase transitions are characterized by multiple ground states.

3.2.3 Nucleation and Domains formation

First-order transitions are characterized by the phase coexistence due to local domains nucleation. In a nonequilibrium metastable state, thermal (or quantum) fluctuations drive small fractions of the system to be locally stable forming a "nucleus" [31]. For instance, the vapor-liquid phase transition, where a supercooled vapor is a meta-stable phase, so is expected to transition into the liquid phase. This process is mediated by fluctuations in which water droplets are continuously formed and destroyed. Nonetheless statistically some droplets will be large enough to be stable, forming a condensation nucleus around which the rest of the vapor will become liquid until reaching equilibrium. In a similar fashion, magnetic materials subject

to a strong enough magnetic field will change their magnetization surrounding the different magnetization nucleus[71].

3.3 Phase transition in JCH and BH models

In this section we show that the phase transition described in terms of the order parameter is a universal characteristic and can be observed in both the Jaynes-Cummings-Hubbard and the BH models

3.3.1 Phase Transition in the JCH model

Let us consider a 2-sites (Dimer) JCH array as shown in figure 3.1, described by the JCH hamiltonian from equation (2.8), which for a Dimer configuration becomes $H^{JCH} = H_1^{JC} + H_2^{JC} - J(a_1^\dagger a_2 + a_2^\dagger a_1)$, now considering the atomic limit for the JCH model ($J \ll g$), and having the system set up in a particular detuning $\Delta = \tau$, define the intial state $|\Psi_0\rangle_\Delta = |1-\rangle_1 \otimes |1-\rangle_2$, and let the system evolve in time for a time $T > J^{-1}$, which is the natural timescale for the JCH model as it represents the minimum time the system needs to evolve so that the effect of the hopping is significant.

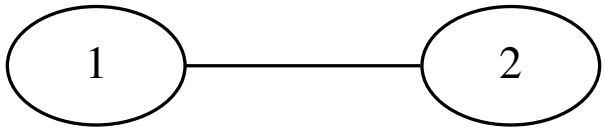

Figure 3.1: A graph representation of a 2-sites (Dimer) Coupled resonating arrays (CRA), each node of the graph represents a cavity, and each line represents a coupling between nodes

Now for the simulations, the following constants values were used for the parameters of the system considering the cavity frequency ω as the unity, the light-matter coupling was defined as $g = 10^{-2}\omega$ and the hopping as $J = 10^{-4}\omega$, then from the simulations take the data for the expectation values for the operators $\langle N_1\rangle$,$\langle N_2\rangle$,$\langle N_1^2\rangle$,$\langle N_2^2\rangle$ and $\langle N_1 N_2\rangle$ as function of time, which means $\langle N_1\rangle = \langle\Psi(t)|\, N_i\, |\Psi(t)\rangle$. Then we take their respective time average up to $T = J^{-1}$, therefore $\langle N_1\rangle_T = \frac{1}{T}\int_0^T \langle N_1\rangle$, in order to build the order parameter $\Delta N = \sum_{i=\{1,2\}}(\langle N_i^2\rangle_T - \langle N_i\rangle^2)$. Repeating this process for different values of the detuning allows to build the phase transition diagram for a Dimer JCH network shown in figure 3.2, where is possible to observe that the sharp rise of the order parameter when the for higher values of the detuning and that the order parameter of both sites is equal, which is consistent with the symmetry of the network.

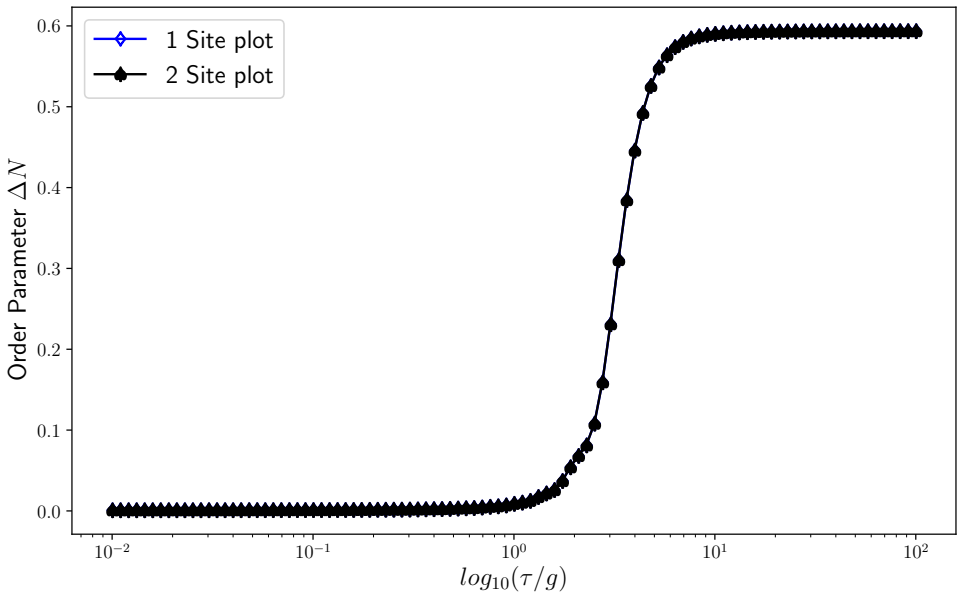

Figure 3.2: Phase transition Diagram for a Dimer JCH network, using as order parameter the variance for site

3.3.2 Phase Transition in the BH model

To verify the procedure for the BH model, a similar mechanism was used, considering again a Dimer CRA as shown in figure 3.1, but in this case the system Hamiltonian becomes $H^{BH} = \omega(N_1 + N_2) - U\left(N_1(N_1 - 1) + N_2(N_2 - 1)\right) - J(a_1^\dagger a_2 + a_2^\dagger a_1)$. For numerical simulations, the initial state of the system is prepared with a single photon in each cavity ($|\Psi_0\rangle = |1\rangle_1 \otimes |1\rangle_2$) with the hopping strength of the system was set to $J = 10^{-4}\omega$. Now for a given on-site repulsion ($U \in [10^{-2}J, 10^2 J]$) let the system evolve for a time $T > J^{-1}$ and in the same manner as proceeded for the JCH model, build the order parameter as the time averaged variance for site at every on-site repulsion simulated in order to get the phase diagram shown in figure 3.3. Notice again that due to the symmetry of the network, both sites have the same order parameter through the phase transition, which has the same overall second order nature as the one shown in the JCH model

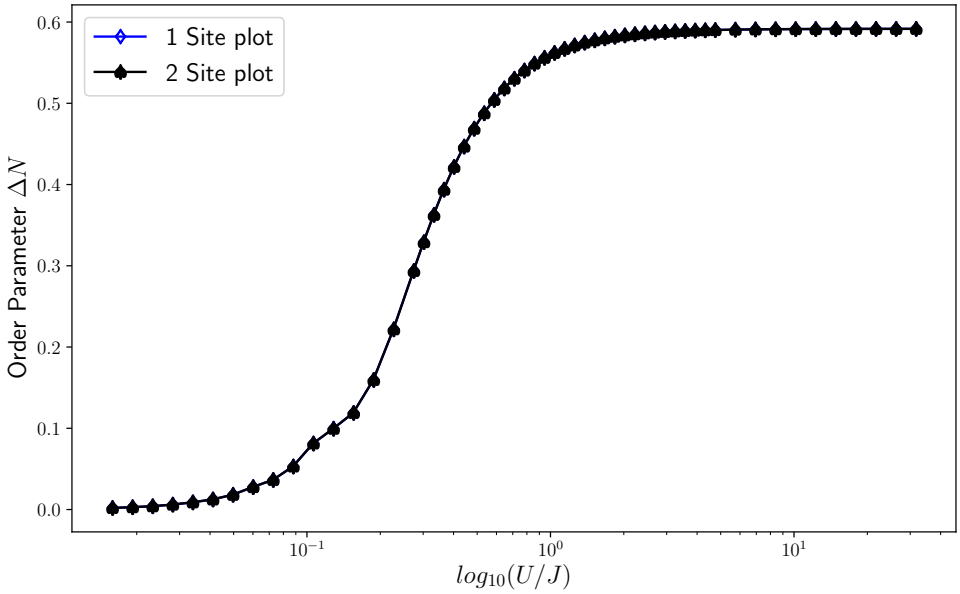

Figure 3.3: Phase transition Diagram for a Dimer BH network, using as order parameter the variance for site

Now that the method for obtaining the phase transition for both models has been shown to be successful, it can be used with confidence moving forward.

3.4 Topology and Nucleation in the JCH model

This section discusses the effect that the topology has on the dynamics and the phase transition of CRA, leading to the previously unknown discovery of first order like phase transition for the JCH model and accompanying nucleation.

Before discussing the topology effects in a JCH CRA network, is convenient to discuss the effect of using the quench dynamics in the system. A quantum system subject to an abrupt change, reflected in the Hamiltonian, evolves through quench dynamics. For the JCH model, an abrupt change in the detuning parameter Δ triggers the quench dynamics

$$\begin{pmatrix} |n-\rangle \\ |n+\rangle \end{pmatrix} = \begin{bmatrix} \cos(\theta_n) & -\sin(\theta_n) \\ \sin(\theta_n) & \cos(\theta_n) \end{bmatrix} \cdot \begin{pmatrix} |n,\downarrow\rangle \\ |n-1,\uparrow\rangle \end{pmatrix}. \tag{3.5}$$

The sudden change in the detuning Δ, produces a change in the basis of the system, so in the new basis, the initial state is a superposition of the upper and lower polariton states. For clarity consider a single cavity, where the relation between the polariton mapping and the photon-TLS exitation is given by equation (3.5) as discussed in 2.2.1. notice that $\theta_n = \tan^{-1}(\frac{2g\sqrt{n}}{\Delta})$ is a function of the detuning Δ, so for an initial state $|\Psi_0\rangle = |n-\rangle_{\Delta_0}$ subject to an abrupt quench $\Delta_0 \to \Delta_1$, can be written in the new basis as $|\Psi_0\rangle = \cos(\theta_{\Delta_1} - \theta_{\Delta_0})\,|n-\rangle_{\Delta_1} + \sin(\theta_{\Delta_1} - \theta_{\Delta_0})\,|n+\rangle_{\Delta_1}$, therefore as consequence from quench dynamics the initial state is a linear superposition of the upper and lower polariton states ($\Delta \neq 0$).

The experimental realization of the JCH model can be achieved through circuit QED [72, 73] where one might cool down the whole system reaching temperatures around $T_0 \sim 15$[mK]. In this case, the system will be prepared in its global ground state $|G\rangle = \bigotimes_{i=1}^{L} |0,-\rangle_i$, with L the total number of sites. Then, one can apply individual magnetic fields on the TLSs, each implemented via a transmon qubit [74], such that the resonance condition $\Delta = 0$ is achieved. This way one can address individually each cavity with an external AC microwave current or voltage tuned to the transition $|0,-\rangle_i \to |1,-\rangle_i$, with a driving frequency $\omega_D = \omega - g$, such that the system will be prepared in the desired initial state $|\psi_0\rangle$. The sudden quench of the detuning can be achieved by applying magnetic fields to the transmon qubits in order to reach the desired superfluid phase.

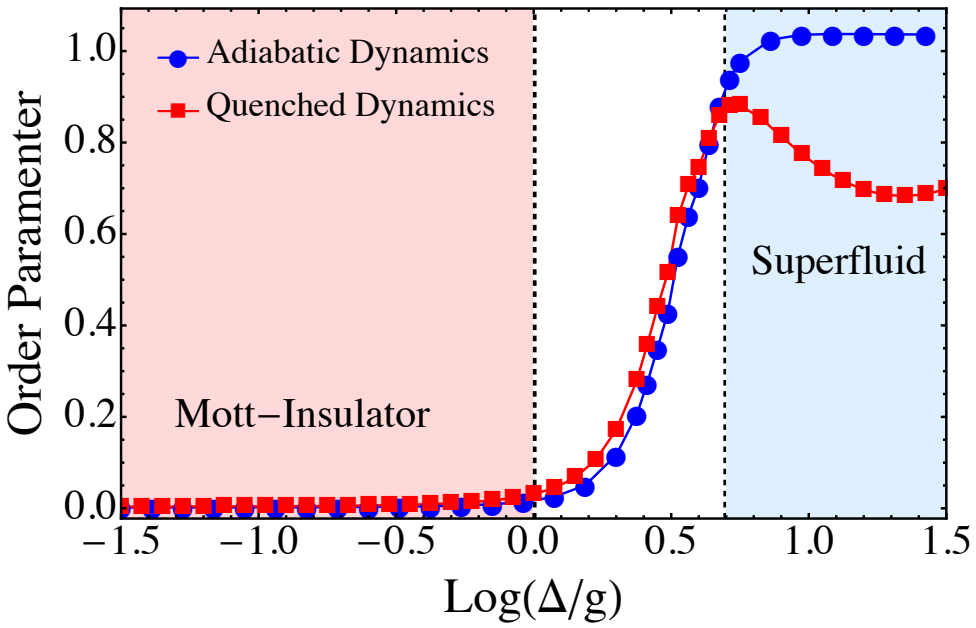

Figure 3.4: First and Second order phase transition diagram simulated in a dimer array. Quench are shown in Red, and adiabatic dynamics is shown in blue for comparison

Figure 3.4 shows the phase transition for a JCH model dimer array subject to adiabatic dynamics (blue) and quench dynamics (red). This figure shows that for low detunings the system remains in the Mott-Insulator phase, while for large detunings the system goes to a superfluid phase, regardless of the involved dynamics. For adiabatic dynamics notice the sharp increase in the order parameter during the transition, and its stabilization after reaching the superfluid state, which is a defining characteristic of a second-order type phase transition. In contrast, the quenched dynamics exhibits a peak in the phase transition diagram before settling to its superfluid value, this behavior is consistent with a first-order like phase transition, analogous to the Metal-Insulator transition of oxides [75].

3.4.1 Domain Nucleation in the JCH model

Now we see that the topology of the array dominates the phase transition in this system. Indeed, let us consider four CRA, which can be arranged in six different topologies as shown in figure 3.5. Studying a reduced number of cavities is different from the usual approach of using large number of cavities for simulating many-body phenomena, as with few cavities is already possible to simulate many-body phenomena, but we focus on the topology of the cavity array to find the key factors which dominate the phenomena. Thus we chose only 4 cavities arrays as a good compromise between the variety of arrays and the number of possibilities allowing for a systematic analysis of the properties of the arrays.

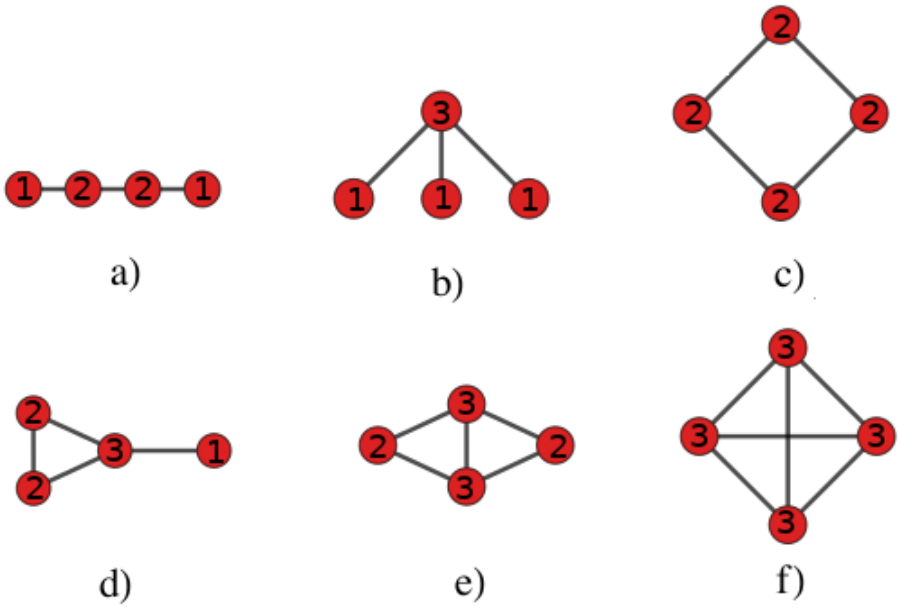

Figure 3.5: Schematic representation of all the possible topologies that can be arranged for four-sites JC nodes. Notice that each site has a number which represent the total number of sites to which it is connected

Figure 3.6 compares the results obtained through the analysis of the variance for site, and the order parameter obtained through bipartite fluctuations for a 4-sites

array connected in a cyclic fashion.

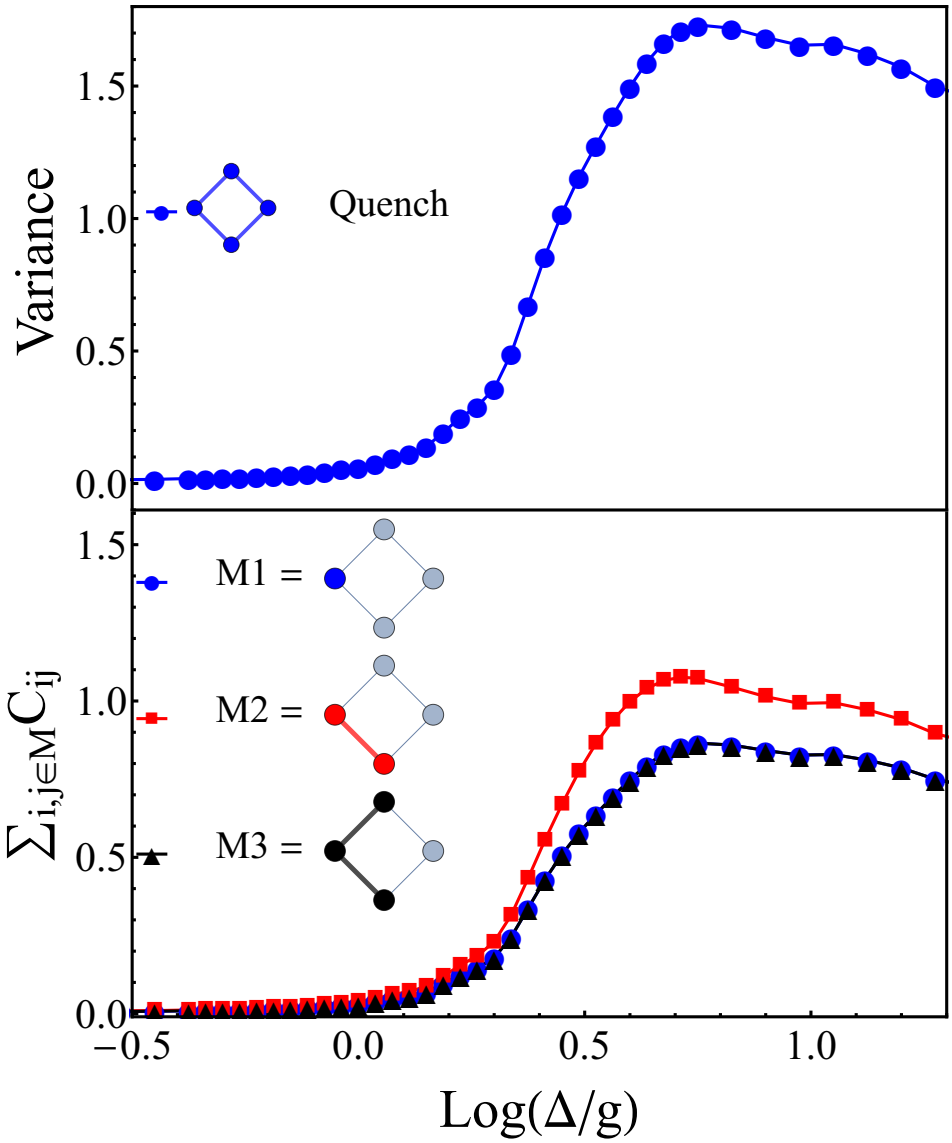

Figure 3.6: Comparison between the different order parameters to describe the phase transition for quench dynamics. (Top) Phase transition described using the variance for site. (Bottom) Phase transition described using bipartite fluctuations. Notice that regardless of the order parameter used, the nature of the phase transition remains the same

Considering that the nature of the phase transition remains the same regardless of the order parameter chosen, is possible to analyze the phase transition for each array

as shown in figure 3.7, which shows the order parameter as function of the detuning, which reinforces the idea of using these topologies to determine the influence over the phase transition.

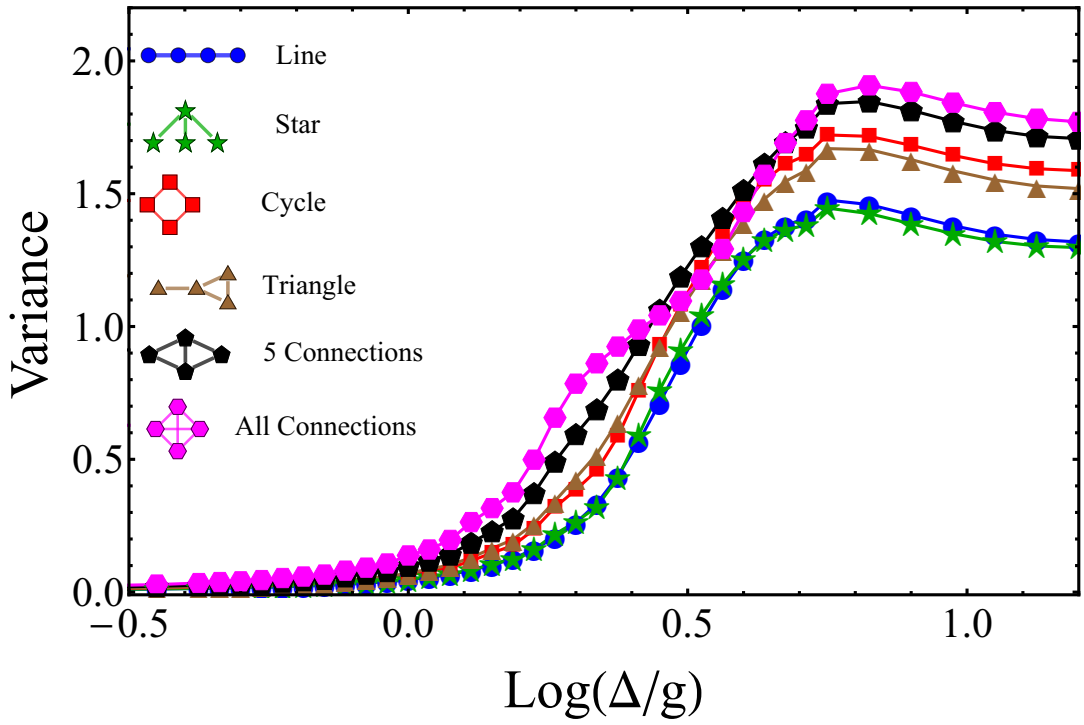

Figure 3.7: This figure shows the Mott-Insulator to superfluid phase transition for the different 4-sites arrays, where is possible to observe that each different topology has a different transition.

Now that there are clear difference between the each array, the following will show that the key factor driving the difference between the multiple topologies is the local connectivity of each site, which is shown in figure 3.8.

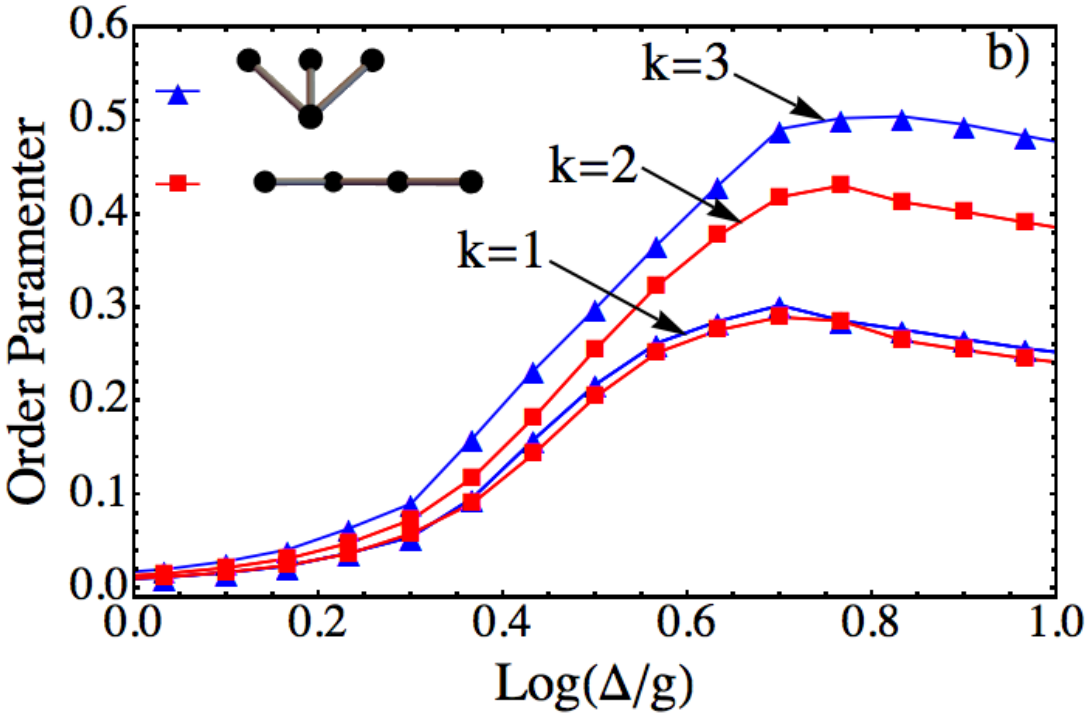

Figure 3.8: This figure shows the phase transition for 2 different arrays, analyzing the order parameter for each connectivity. Notice that all the sites that have the same connectivity, here noted by k, have the same behavior

Careful analysis of figure 3.8, shows that the number of local connections, or connectivity, of each site dominates the phase transition, determines the detuning at which the phase transition starts, which is different for each site, and also determines the superfluid phase order parameter, which confirms that the local connectivity is the key factor in the phase transition of quench dynamics JCH model.

Now that is clear that the connectivity dominates the quenched dynamics phase transition, and in particular the limit value of the superfluid phase order parameter, is possible to extend the analysis beyond 4 sites, up to 5 sites with carefully selected arrays to show that the averaged standard deviation depends linearly on the connectivity of the CRAs As shown in Fig. 3.9(a). Consider a set of CRAs with four and five interconnecting resonators as shown in Fig. 3.9(b). In contrast to these results,

the adiabatic dynamics does not exhibit a monotone or linearly growing behavior as function of the connectivity.

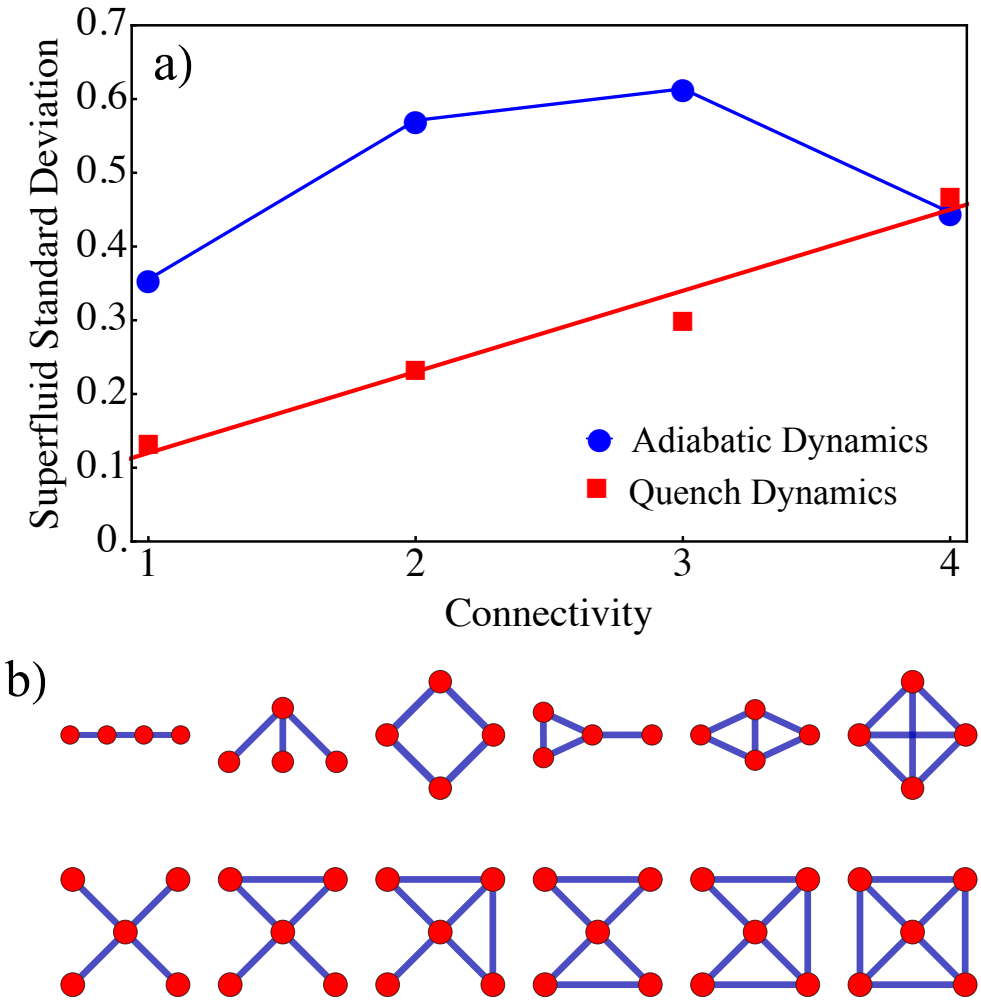

Figure 3.9: a) Standard deviation of the superfluid phase as a function of the connectivity. Adiabatic dynamics (blue circles) and quench dynamics (red squares). A set of CRAs with four and five interconnecting resonators, as shown in b) are considered. Continuous lines have been added as a guide to the eye.

3.4.2 Mean field theory and Nucleation

In the thermodynamics limit, the emergent superfluid phase behaves as a quantum liquid [37]. Superfluidity is achieved by means of a transition of the excitations from polaritonic to photonic. In order to describe the simulated superfluid phase in our

system, we introduce the mean-field photonic order parameter [37] ψ in which we use the ansantz $\psi = \langle a_i \rangle$. Using the decoupling approximation $a_i^\dagger a_j \approx \langle a_i^\dagger \rangle a_j + a_i^\dagger \langle a_j \rangle - \langle a_i^\dagger \rangle \langle a_j \rangle$, the resulting mean-field JCH Hamiltonian can be written as

$$H_{JCH} = \sum_i H_i^{JC} - J \sum_i k_i (\psi a_i^\dagger + \psi^* a_i). \tag{3.6}$$

Therefore, the simulated Mott-Insulator phase is described by the on site repulsion, which suppresses the fluctuations of the number of per site excitations $|\psi| = 0$. On the contrary, the superfluid phase is dominated by the hopping and the quantum fluctuations $|\psi| \neq 0$. Introducing the identity $\sigma^+\sigma^- + \sigma^-\sigma^+ = \mathbb{1}$, we obtain an effective light-matter coupling, since it retains the mixed products of photonic and two level operators,

$$h_i^{LM} = \tilde{g}_i a_i^\dagger \sigma_i^- + \tilde{g}_i^\dagger a_i \sigma_i^+ + \text{h.c.} \tag{3.7}$$

Here $\tilde{g}_i = \mathbb{1} g - J k_i \psi^* \sigma_i^-$ is the effective light-matter coupling per site, which therefore turns out to be an operator. In the simulated superfluid phase the atomic transitions are expected to be suppressed against the photonic dressed states. Moreover, the total excitation number does not change, hence when the photonic excitations increase the atomic excitations decrease. Note that when $\tilde{g}_i = 0$, i.e. when there are no hopping or topological effects,

$$\langle \sigma_i^+ \rangle = \frac{g}{J k_i} \frac{1}{\psi}, \tag{3.8}$$

which indicates that the increase of the photonic states leads to a reduction of the atomic excitations, due to the conservation of the number excitations. Figure 3.10 shows the effect of the quench dynamics on the simulated phase transition of the JCH model for different arrays. In this case the nucleation of superfluid states emerges due to the variation of the order parameter, according to Eq. (3.8). In the Mott-Insulator state $\langle \sigma_i^+ \rangle > 0 \, \forall i$, when the detuning is increased $\langle \sigma_i^+ \rangle$ decreases

by a factor $1/(k_i\psi)$, until the superfluid phase is reached. Therefore the mean field theory strongly supports the scaling law of the order parameter shown in figure 3.9(a) ; namely, as the connectivity of CRAs is increased locally, the light superfluid phase is achieved for a smaller detuning strength, which is evindence for nucleation.

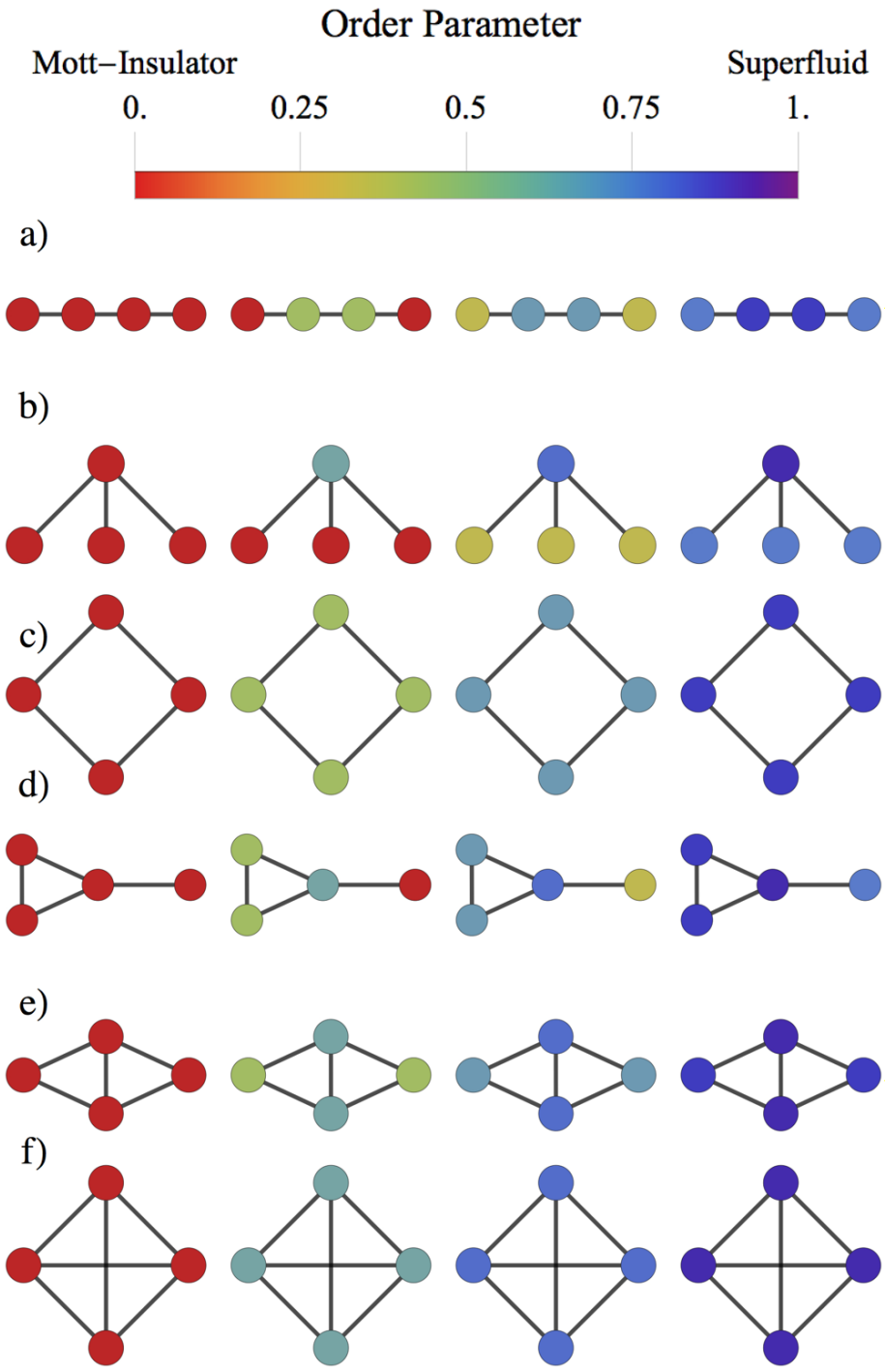

Figure 3.10: Numerical simulation of the quench dynamics using the variance per site as order parameter. The full set of four node arrays, with (a-b) three; (c-d) four; (e) five; and (f) six connections. Connectivity per site a) (1,2,2,1), b) (3,1,1,1), c) (2,2,2,2), d) (3,2,2,1), e) (3,2,3,2), and f) (3,3,3,3). Notice that as the local connectivity increases, the system reaches the superfluid phase with a lower detuning strength. For each array and from left to right we have considered parameters $\log(\Delta/g) = (0.5, 0.7, 0.75, 0.8)$, and $g = 10^{-2}\omega$, $J = 10^{-4}\omega$, where ω is the resonator frequency.

3.4.3 Topology effect on Adiabatic dynamics and BH model

In the previous section, the topology effect on the quench dynamics for the JCH model was demonstrated, while the superfluid phase of adiabatic dynamics showed no obvious dependence of the topology. Figure 3.11 shows the little dependence of the order parameter in the superfluid phase of the BH model as function of the local connectivity. This reinforces that the quench dynamics is required for the appearance of nucleation and ties the topology to the superfluid phase.

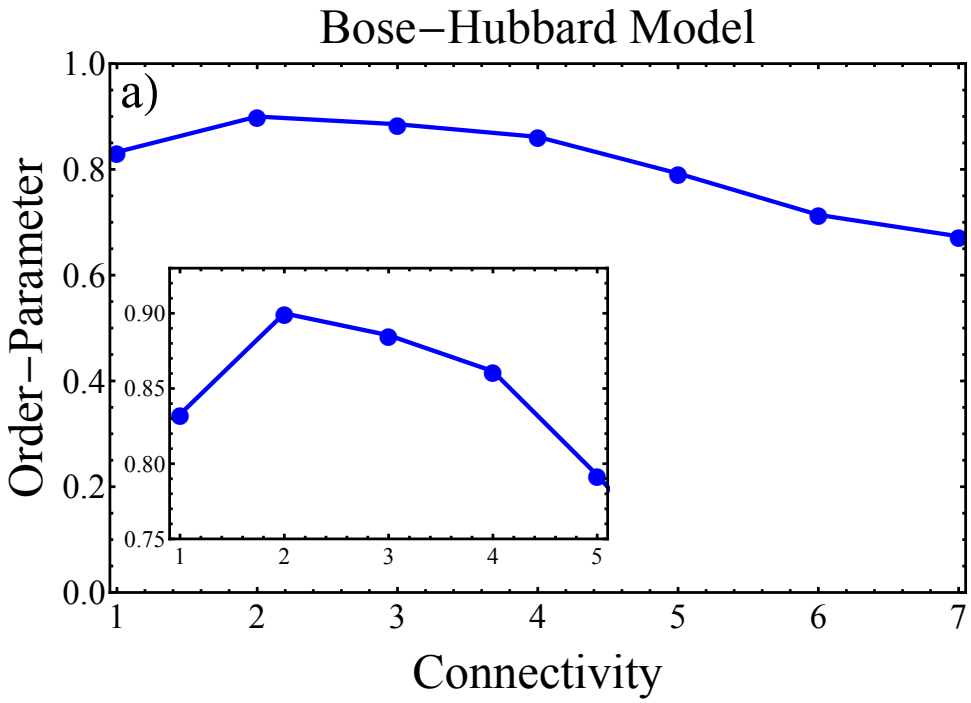

Figure 3.11: Standard deviation of the variance of the polariton occupation number as a function of connectivity in the Bose-Hubbard model. (Inset)Standard deviation of the variance of the polariton occupation number as a function of connectivity in the JCH model.

3.5 Conclusions

This chapter demonstrated that quench dynamics induce a first-order like phase transition in coupled resonator arrays doped with a two-level system governed by

the JCH model, where nucleation of simulated superfluid states has been validated through numerical simulation and by a mean field theoretical approach. In the quench dynamics the change of the order parameter, is explained by the non uniform transition from Mott-Insulator to superfluid, which depends on the local connectivity. Since the quench dynamics exhibits the same behavior independent of the choice of the order parameter, the standard deviation of the polariton number or the bipartite fluctuation, the results reveal the universality of the simulated first order phase transition. In particular, as far as we understand, there is no known microscopic mechanism for predicting nucleation in first-order phase transitions. In this context, our results provide an exact geometrical description for the appearance of domain nucleation due to the number of connections.

Chapter 4

Light-Matter Anisotropy and Dimerization

4.1 Introduction

The previous Chapter, showed the effects topology has in Coupled resonator arrays, and in particular in the Mott-Insulator/Superfluid phase transition of the JCH model. This chapter focused on the effect that other sources of anisotropy have on the dynamics of the same model, and how they modify the phase transition, but first is required to describe the JCH model from the energy perspective for additional insights of the model.

4.2 Phase Transition from the Energy perspective

Up to this point the JCH model phase transition has been discussed only through the order parameters that describe the system, however this chapter shows that additional insight can be obtained through the analysis of the energy of the system

Now to have a better understanding of the related phenomenon, we rely on an energy level description of the system, nevertheless as the Hamiltonian cannot be diagonalized, we proceed to describe the energy levels through perturbation theory for the uniform case using that $J \ll g$, therefore we can treat the hopping part

of the Hamiltonian as a perturbation over the on-site JC Hamiltonian. The JCH Hamiltonian can be written in the polariton basis [39, 49] as

$$\begin{aligned} H_{JCH} = &\sum_{i}^{M}\sum_{n,\alpha} E_{n\alpha} P_{in}^{\dagger\alpha} P_{in}^{\alpha} \\ &+ J\sum_{i,j} A_{ij} \sum_{n,n'} \sum_{\alpha,\alpha',\beta,\beta'} t_{n\alpha\beta} t_{n'\alpha'\beta'} P_{in}^{\dagger\alpha} P_{i(n-1)}^{\beta} P_{j(n'-1)}^{\dagger\beta'} P_{jn'}^{\alpha'}, \end{aligned} \tag{4.1}$$

where we recognize the JC Hamiltonian as $\sum_{n,\alpha} E_{n\alpha} P_{in}^{\dagger\alpha} P_{in}^{\alpha} = H^{JC}$ with $E_{n\alpha}$ the energy levels of the cavity for polariton number (n) and polariton branch $(\alpha \to \pm)$. $P_{in}^{\dagger\alpha} P_{im}^{\beta} = |n\alpha\rangle_i \langle m\beta|_i$ are the polariton creation destruction operators for site.

We identify the terms in the Hamiltonian for perturbation theory as $H_{JCH} = H_0 + JH^{hop}$, where $H_0 = \sum_i H_i^{JC}$ is the unperturbed Hamiltonian, and H^{hop} as the perturbation. Choosing the basis for the unperturbed state as

$$\left|\psi^0\right\rangle = \bigotimes_{k}^{M} |n_k\alpha_k\rangle_k \tag{4.2}$$

so that each state has a unique defined number of polaritons per site and belongs to a specific polariton branch, the first correction to the energy is

$$\begin{aligned} E_{\psi}^{1} &= \langle\psi^0| H^{hop} |\psi^0\rangle \\ &= \langle\psi^0| P_{im}^{\dagger\alpha} P_{i(m-1)}^{\beta} P_{j(m'-1)}^{\dagger\beta'} P_{jm'}^{\alpha'} |\psi'^0\rangle \\ &= \bigotimes_{k}^{M} \langle n_k\gamma_k| \left(|m_i\alpha_i\rangle \langle m_i - 1\beta_i| |m_j - 1\beta_j\rangle \langle m_j\alpha_j|\right) \bigotimes_{k}^{M} |n'_k\gamma'_k\rangle \\ &= \langle n_i\gamma_i| \langle n_j\gamma_j| |m_i\alpha_i\rangle \langle m_i - 1\beta_i| \langle m_j - 1\beta_j| |m_j\alpha_j\rangle |n'_i\gamma'_i\rangle |n'_j\gamma'_j\rangle \\ &= \delta_{m_i}^{n_i} \delta_{m_i-1}^{n'_i} \delta_{\alpha_i}^{\gamma_i} \delta_{\gamma'_i}^{\beta_i} \delta_{m_j-1}^{n_j} \delta_{m_j}^{n'_j} \delta_{\beta_j}^{\gamma_j} \delta_{\gamma'_j}^{\alpha_j} \\ &= 0 \qquad\qquad \text{if } |\psi'^0\rangle = |\psi^0\rangle \end{aligned} \tag{4.3}$$

For equation 4.3, different basis states were used for the algebra ($|\psi'^0\rangle$,$|\psi^0\rangle$) for simplicity, and later were made the same state as required for perturbation theory. Also the ortogonality of the polariton basis was used allowing to determine that $E_{\psi}^{1} \equiv 0$, meaning that there is no first order energy correction. Following a similar procedure, we find that

$$E_\psi = E_\psi^0 + J^2 \sum_k \frac{\left|\langle\psi_k^0| H^{hop} |\psi^0\rangle\right|}{E_\psi^0 - E_{\psi_k}^0}, \tag{4.4}$$

where $|\psi_k^0\rangle$ are the unperturbed basis states with different energy than the analyzed state. At this point we see that unless the energy levels for different states are near-degenerate, perturbation theory shows that we can properly describe the states of the system through the unperturbed energy states only. Notice that for precise analysis in near degenerate state, one would need to identify the relevant degenerate states and perform the corresponding analysis, however, as we will show next, this is not necessary for a qualitative picture.

Now that we have a good theory for the energy levels through the perturbation theory, we proceed to show that the energy levels can also be correlated to the states of the phase transition in the JCH model, to do so consider the lower branch unperturbed states for the JCH model with two total exitations $|\psi_{1,1}\rangle = |1-\rangle_1 \otimes |1-\rangle_2$, $|\psi_{2,0}\rangle$ and $|\psi_{0,2}\rangle$. Now for an initial state with a single polariton per site in the resonant case, the system remain in the $|\psi_{1,1}\rangle$, consistently with the Mott-insulating phase. In the superfluid phase the polaritons flow freely through the cavities. For instance considering an initial state $|\psi_{1,1}\rangle$, in the superfluid phase, the states $|\psi_{2,0}\rangle$ and $|\psi_{2,0}\rangle$ are also allowed.

Now the energies of the described states, are $E_{1,1} = 2\omega + \Delta - 2\sqrt{\frac{\Delta^2}{4} + g^2}$ for $|\psi_{1,1}\rangle$ and $E_{2,0} = 2\omega + \frac{\Delta}{2} - \sqrt{\frac{\Delta^2}{4} + 2g^2}$ for $|\psi_{2,0}\rangle$, notice that symmetry dictates that $E_{0,2} = E_{2,0}$. For convenience we define the effective energy levels $\tilde{E}_{1,1} = \frac{E_{1,1} - 2\omega}{g} = 2\delta - 2\sqrt{\delta^2 + 1}$ and $\tilde{E}_{2,0} = \delta - \sqrt{\delta^2 + 2}$, where $\Delta = 2g\delta$, to give a measure of the energy difference between states with the same number of polaritons.

Figure 4.1 shows that the energies of the JCH Hamiltonian corrected up to first order quantum perturbation theory describe the phase transition as degeneracy of the different energy levels so that for states which have different energy levels in the

dimer ($E_{1,1} \neq E_{2,0}$) at the Mott-insulating phase ($\Delta \approx 0$) become degenerate as the system transitions to the superfluid phase ($E_{1,1} \simeq E_{2,0}$ if $\Delta \gtrapprox g$). From this point it becomes possible to describe and engineer CRA systems to exhibit a wide array of physical phenomena.

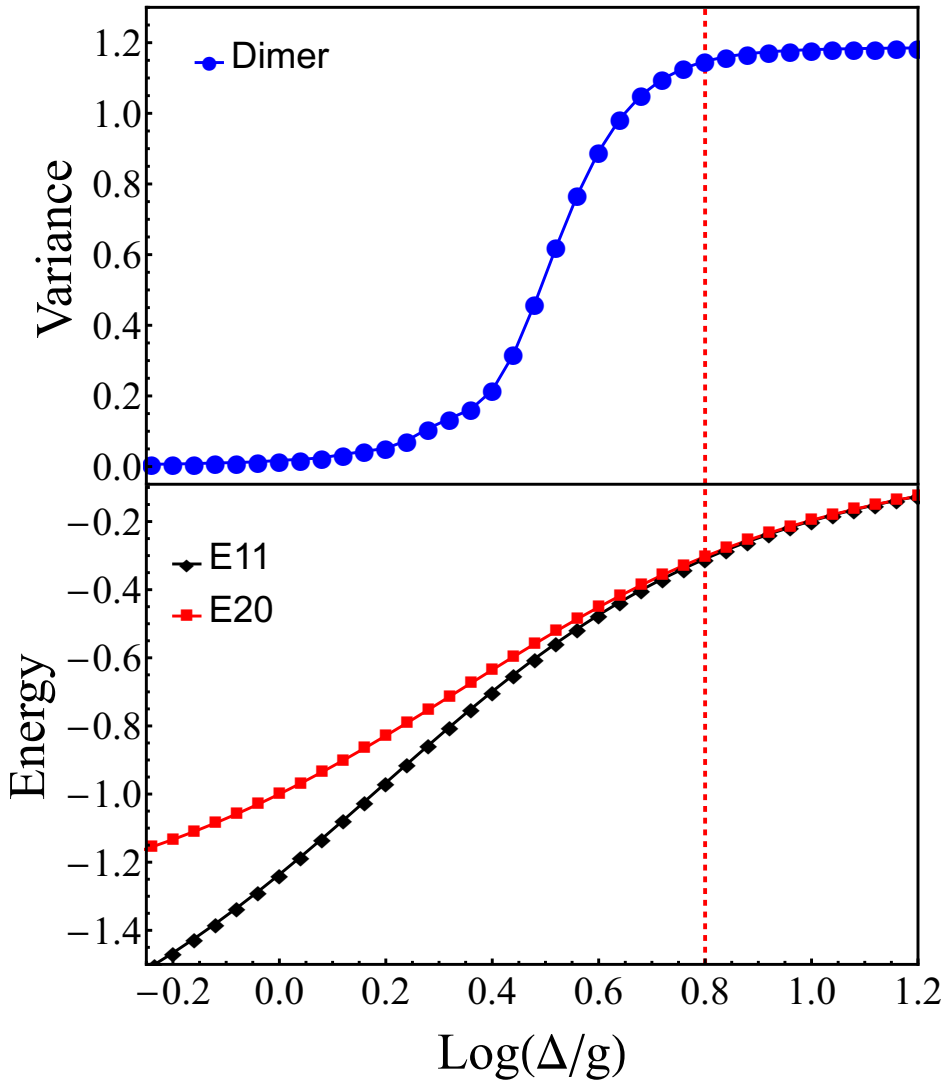

Figure 4.1: (Top) JCH Mott-Insulator/Superfluid phase transition for a dimer CRA, as function of the detuning parameter Δ and described using the total variance of the polariton number. (Bottom) Effective energy levels as function of the detuning. The vertical red dashed line shows the point in which both analysis describe a superfluid phase

This section has shown that the phase Mott-Insulator to Superfluid phase transition can be understood from the energy perspective using quantum perturbation theory as the transition from a gaped energy system considering the spectrum across the different states of the system in the Mott-Insulator phase to the Superfluid phase in which the energy spectrum of the system is highly degenerate

4.3 JCH Model detuning anisotropy and resonance.

This Chapter shows that detuning anisotropy exhibits new phenomena for the adiabatic dynamics of the JCH model, through the interplay between the different accessible quantum states. For reference consider Figure 4.2, which shows the archetypal behavior of the order parameter as a function of the detuning Δ in the adiabatic dynamics regime, and for an integer filling factor of one net excitation per site [39]. Here we also show the expectation value for the polariton number for each site. Notice that although the system is in the superfluid phase, the polariton number remains constant, this is because in the superfluid phase all states are considered to be equally probable, therefore a state with two poalritons in one site 1, and 0 polaritons in site 2, has the same possibility than the state with two polaritons in site 2 and 0 polaritons in site 1 so in average is the same as having a single polariton in each cavity.

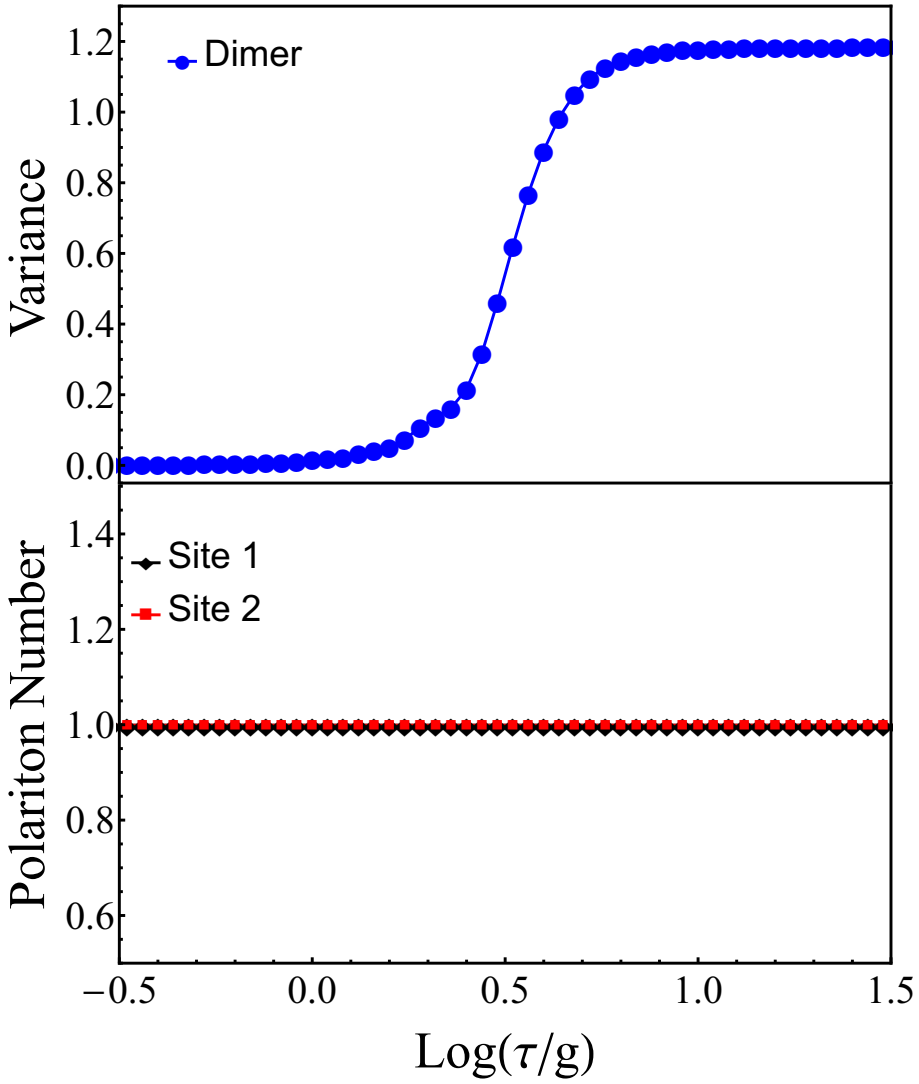

Figure 4.2: (Top) JCH Mott-Insulator/Superfluid phase transition for a dimer CRA, as function of the detuning τ and using the total variance of the polariton number as order parameter with $g = 10^2\omega$, $J = 10^{-2}g$ and 3 fock states per site. (Bottom) Expectation value for the polariton number per site, notice that the polariton number per cavity remains constant through the experiment

We show that the introduction of detuning anisotropy in CRA described by the JCH model, produces a resonant phenomenon which gives rise to the appearance of directional dynamics through the cavities in contrast to the usual superfluid dynamics in the model.

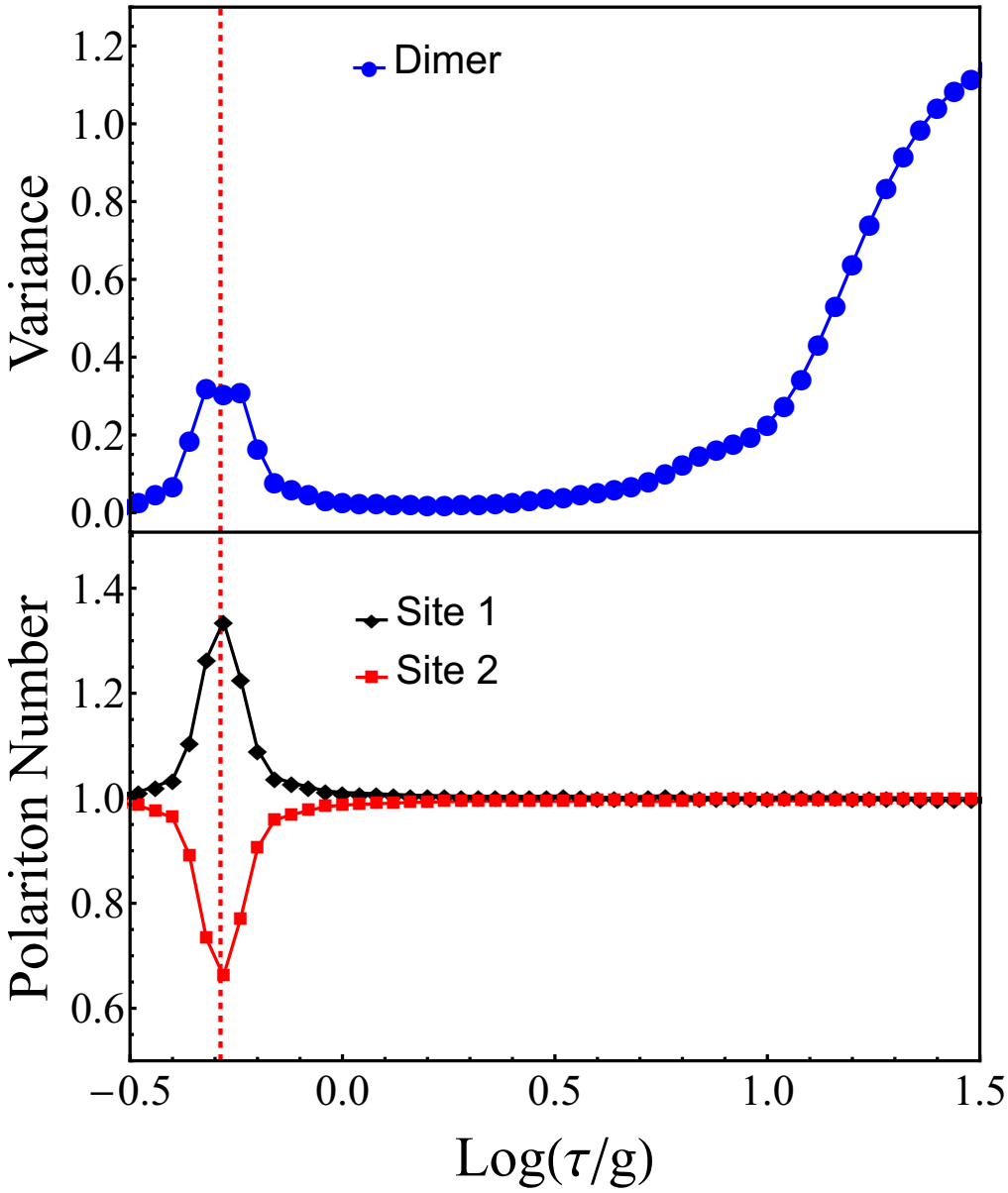

Figure 4.3: (Top) JCH Mott-Insulator/Superfluid phase transition for a dimer with detuning anisotropy ($\Delta_1 \neq \Delta_2$) CRA as function of the detuning parameter and described using the total variance of the polariton number as order parameter using $g = 10^2\omega$ and $J = 10^{-2}g$ considering up to 3 fock states per polaritonic mode, Notice the spike in the order parameter on the Mott-insulating phase. (Bottom) Expectation value for the polariton number per site during the same phase transition, notice that the polariton number per cavity shows a distinctive occupation difference at the point in which the order parameter exhibits a spike

Figure 4.3 shows the phase transition of a dimer with a detuning anisotropy ($\Delta_2 \neq \Delta_1$) in which the index represents the cavities. For analysis purposes, consider a global detuning parameter (τ), and for each simulation point set the detuning of the respective cavities as $\Delta_1 = \tau$ and $\Delta_2 = 2\tau$. The total variance per site in the top panel of figure 4.3 exhibits a peak on the order parameter in for a global detuning , in the Mott-insulating phase zone, this peak has a parallel in for the polariton number for site, which shows a departure from the initial state of one polariton in each site to different occupation numbers for sites depending on the frequencies of the cavities.

Figure 4.4 shows the simulation of the time evolution up to $T = 6J^{-1}$ of the polariton number for site at $\log \frac{\Delta}{g} = -0.28$, which shows the peak in the order parameter of figure 4.3. Figure 4.4 shows how the system oscillates periodically between the states $|1-\rangle \otimes |1-\rangle$ and $|2-\rangle \otimes |0\rangle$, with no large deviations, which in turn demonstrate its robust behavior.

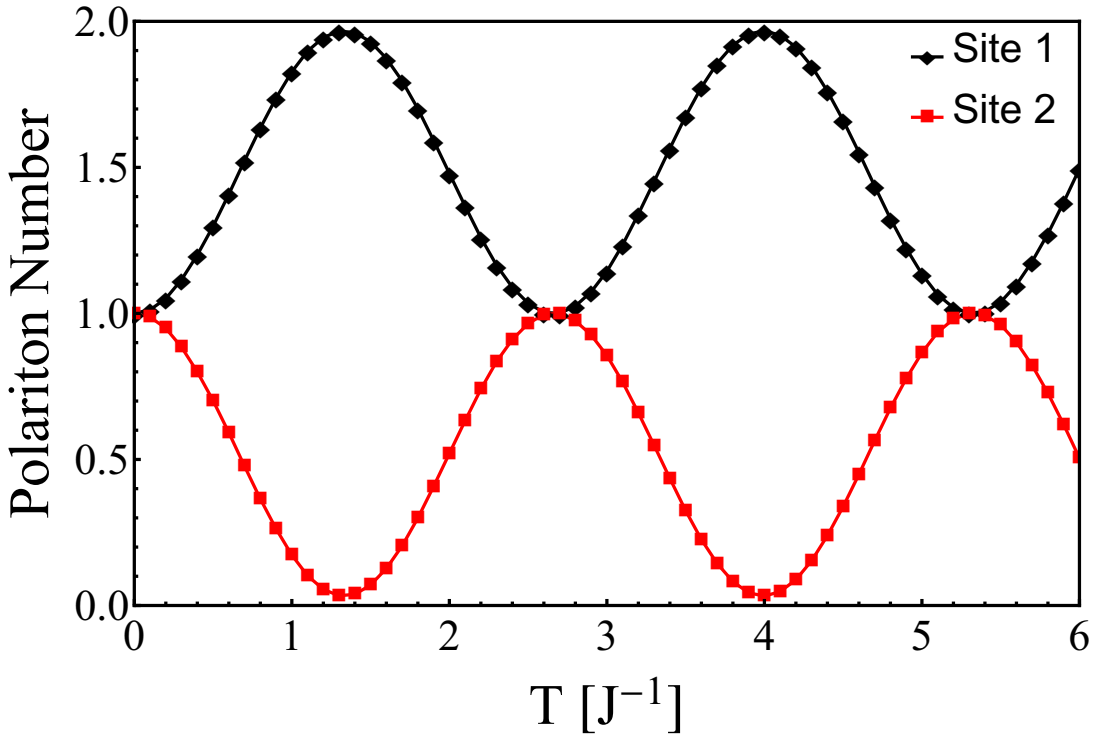

Figure 4.4: Time data for the polariton number for site at the resonant detuning ($\log \frac{\Delta}{g} = -0.28$). Notice simulations times going over $T = 6^{-1}J$. At resonant frequency we observe that the system goes periodically from state $|1,1\rangle$ to $|2,0\rangle$.

Now we show that the energy perspective provides a good theoretical framework for modeling and predicting resonance, considering the states and respective energies of uncoupled JC cavities as the initial point of analysis and using that figure 4.4 suggest that the relevant states are $|1,1\rangle$ and $|2,0\rangle$ with their corresponding energies $E_{1,1} = 2\omega + \frac{\Delta_1}{2} + \frac{\Delta_2}{2} - \frac{1}{2}\sqrt{\Delta_1^2 + 4g^2} - \frac{1}{2}\sqrt{\Delta_2^2 + 4g^2}$ and $E_{2,0} = 2\omega + \frac{\Delta_1}{2} - \frac{1}{2}\sqrt{\Delta_1^2 + 8g^2}$ to determine at which point these energies are equal ($E_{11,} = E_{2,0}$). Using the definitions $\Delta_1 = 2g\delta$, $\Delta_2 = 2g\alpha\delta$, we get that $\delta_c = \frac{1}{\sqrt{\alpha^2-1}}$, from which $\tau_c = \frac{2g}{\sqrt{\alpha^2-1}}$. Our numerical simulation gave the closest value for τ_c from $\log \frac{\tau_c}{g} = -0.28$ which is in close accordance to the theoretical value $\log \frac{\tau_c}{g} \approx -0.287$ considering our simulation did not cover all the spectrum of possible values for τ.

Now we proceed to show how our theory can predict the resonance in the phase transition diagram for a dimer with $\Delta_1 = \tau$ and $\Delta_2 = \alpha\tau$, from which we get that $\omega_2 = \omega + \alpha(\omega_1 - \omega)$ so by using the relationship $\delta_c = \frac{1}{\sqrt{\alpha^2-1}}$ we get the critical frequency

$$\omega_2^c = \omega + \sqrt{(\omega_1 - \omega_2)^2 + 4g^2} \tag{4.5}$$

as function of ω_1, thus for any detuning factor α used to study the phase transition, the point in which the second cavity frequency intersects the theoretical resonant frequency will mark the resonant point as shown in figure 4.3.

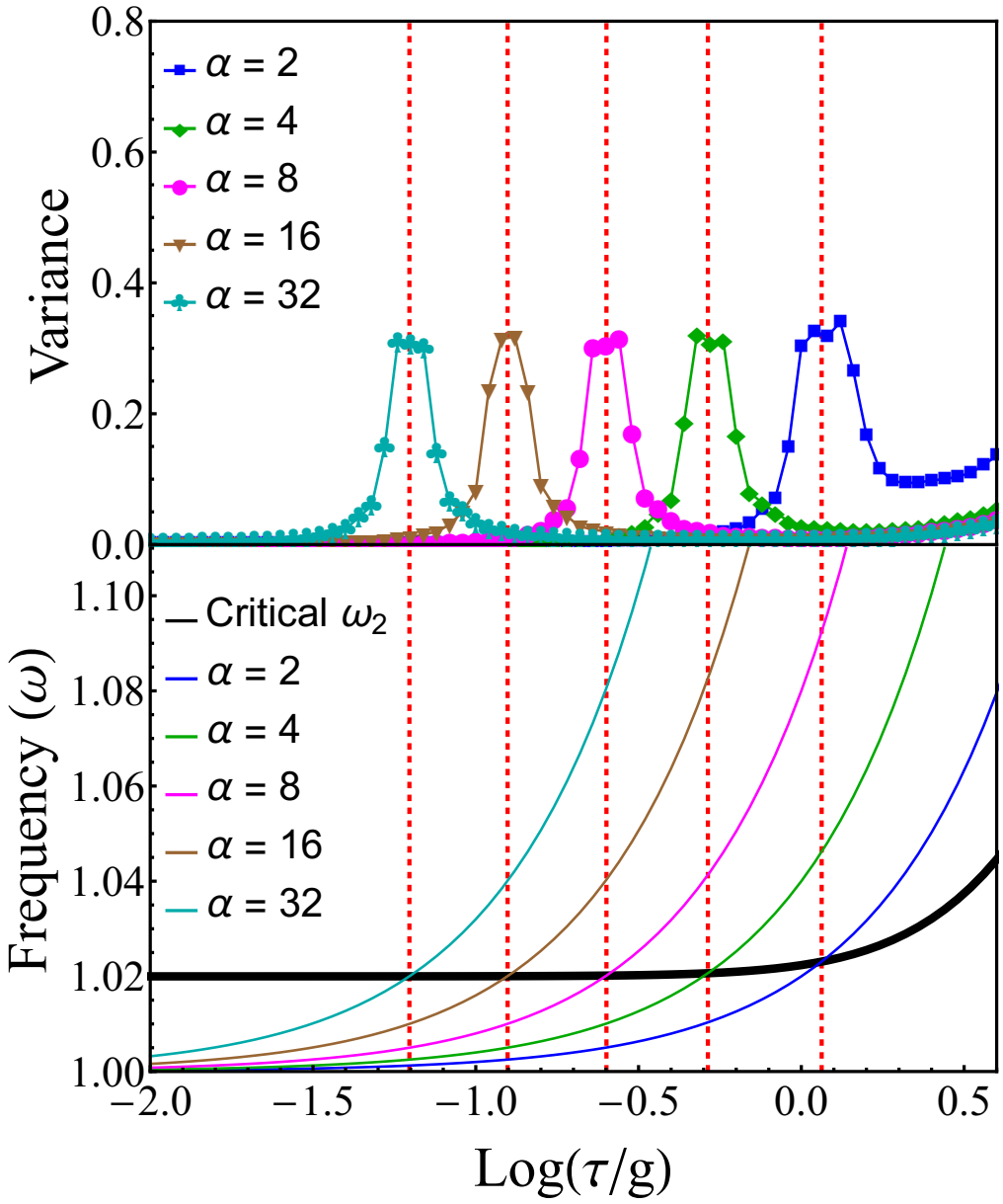

Figure 4.5: (Color online) (Top) Order parameter as function of the global detuning (τ) for a dimer network with different anisotropy factors between Δ_1 and Δ_2 exhibiting a peak at different detunings. (Bottom) Critical frequency ω_2 at which the cavities enter in resonance as a function of the detuning, and compared with the frequencies for the cavities according to a detuning factor α; the crossing points between the cavity frequency according to the detuning factor and the theoretical resonant frequency predicts the point the phase transition diagram where the resonance is observed

Now that the theory has proven itself as predictive, is possible to use it for designing CRA with specific resonance for a subset of states, as shown in figure 4.3, where a CRA of three cavities connected in line was designed specifically to exhibit resonance between the states $|1,1,1\rangle$ and $|0,3,0\rangle$, so at no point a single cavity actually have 2 polaritons, but goes straight to three, which shows the predictive power of our analysis and provides a designing mechanism for JCH CRA which exhibit new phenomena

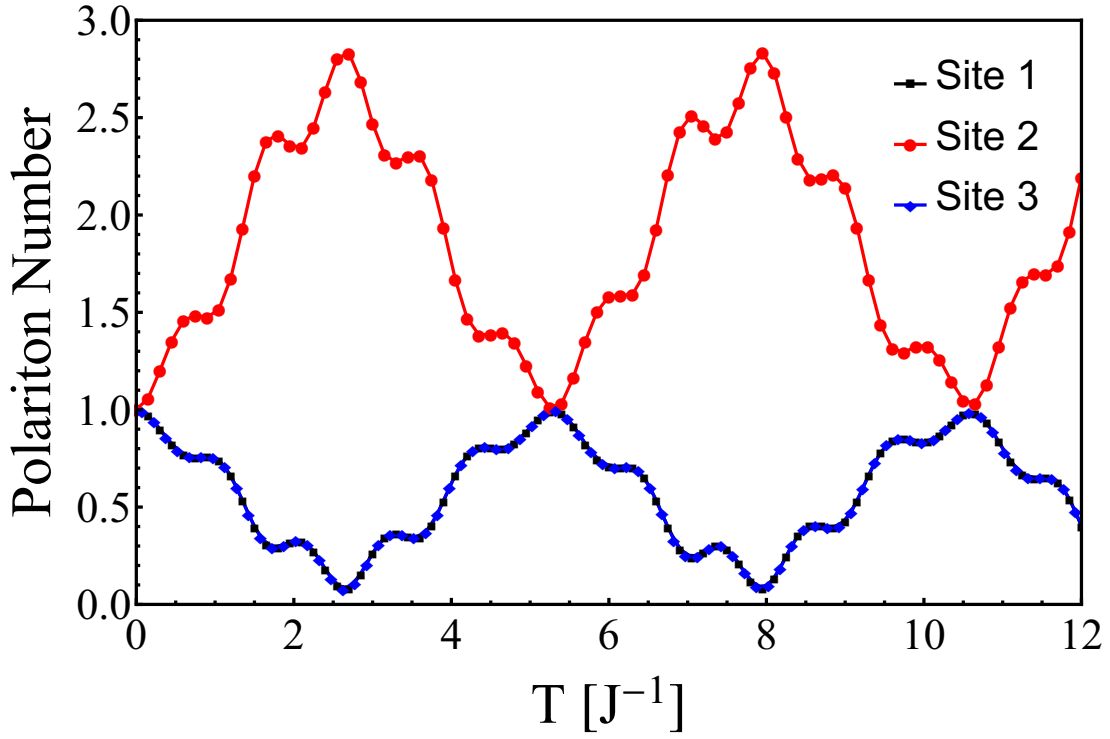

Figure 4.6: Time data for the polariton number for site at the resonant detuning ($\log \frac{\Delta}{g} = -0.2132$). Notice simulations times going over $T = 12^{-1}J$. At resonant frequency we observe that the system goes periodically from state $|1,1,1\rangle$ to $|0,3,0\rangle$.

We have proven that through the individual manipulation of the TLS in a JCH model, is possible to induce a resonant phenomenon which is both highly configurable and robust. Furthermore, although is possible to tailor the anisotropy and structure

of the array, the exact dynamics is still to be completely determined, therefore the resonance could provide additional understanding of the JCH model.

4.4 Hall effect in JCH model

This section shows that through the analysis of the JCH model phase transition from the energy perspective and building a system with light-matter coupling anisotropy, is possible to engineer a stepped phase transition with a similar profile to the quantum hall-effect conductivity behaves under magnetic influence.

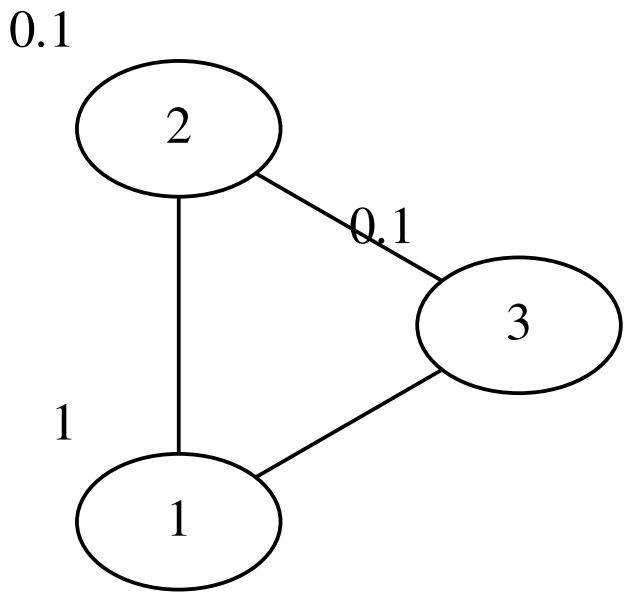

Figure 4.7: Tree sites CRA connected in a cyclic fashion, with anisotropy in the light-matter couplings between the TLS and the cavity frequency

Consider a 3-cavity CRA system connected in a cyclic formation as shown in

figure 4.4, with light-matter coupling anisotropy engineered so that for one cavity is $g_1 = 10^{-2}\omega = g$ and for the other two cavities $g_2 = g_3 = 10^{-1}g$, while the hopping strength remains constant for all connections at $J = 10^{-2}g$.

We show that consistently with the theory described in 4.2, this system exhibits a 2-step superfluid phase transition as the different energy levels become degenerate to the initial state $|\psi_0\rangle = |1,1,1\rangle$ for adiabatic dynamics over the lower polariton branch. Considering the effective energies for the meaningful states $|\psi_0\rangle = |1,1,1\rangle$, $|\psi_1\rangle = |1,2,0\rangle$ and $|\psi_2\rangle = |2,0,1\rangle$ in which $|\psi_1\rangle$ represent the process in which the sites labeled as 2 and 3 transition to a partial superfluid and $|\psi_2\rangle$ represents the process in which the sites labeled as 1 and 2 transition to a partial superfluid, we have that their corresponding effective energies are

$$\tilde{E}_{1,1,1} = 3\delta - \sqrt{\delta^2+1} - 2\sqrt{\delta^2+0.1} \tag{4.6}$$

$$\tilde{E}_{1,0,2} = 2\delta - \sqrt{\delta^2+1} - \sqrt{\delta^2+0.2} \tag{4.7}$$

$$\tilde{E}_{2,0,1} = 2\delta - \sqrt{\delta^2+2} - \sqrt{\delta^2+0.1} \tag{4.8}$$

where we notice that we can define δ_{c_1} and δ_{c_2}, as points in which we can perform a first-order taylor approximation over $\sqrt{\delta^2+0.1}$ and $\sqrt{\delta^2+1}$ respectively so that

$$\tilde{E}_{1,1,1} \xrightarrow[\delta>\delta_{c_1}]{} \delta - \sqrt{\delta^2+1} - \frac{0.1}{\delta^2} \tag{4.9}$$

$$\tilde{E}_{1,1,1} \xrightarrow[\delta>\delta_{c_2}]{} -\frac{0.5}{\delta^2} - \frac{0.1}{\delta^2} \tag{4.10}$$

$$\tilde{E}_{1,0,2} \xrightarrow[\delta>\delta_{c_1}]{} \delta - \sqrt{\delta^2+1} - \frac{0.1}{\delta^2} \tag{4.11}$$

$$\tilde{E}_{2,0,1} \xrightarrow[\delta>\delta_{c_2}]{} -\frac{1}{\delta^2} - \frac{0.05}{\delta^2} \tag{4.12}$$

where it becomes clear that for $\delta > \delta_{c_1}$ $\tilde{E}_{1,1,1} = \tilde{E}_{1,0,2}$, thus we have the first partial superfluid phase transition. Similarly for $\delta > \delta_{c_2}$ $\tilde{E}_{1,1,1} \approx \tilde{E}_{2,0,1}$ and if δ is large enough the difference becomes negligible, therefore the states are considered to have

the same energy and the nodes become superfluid. This process is shown in figure 4.8

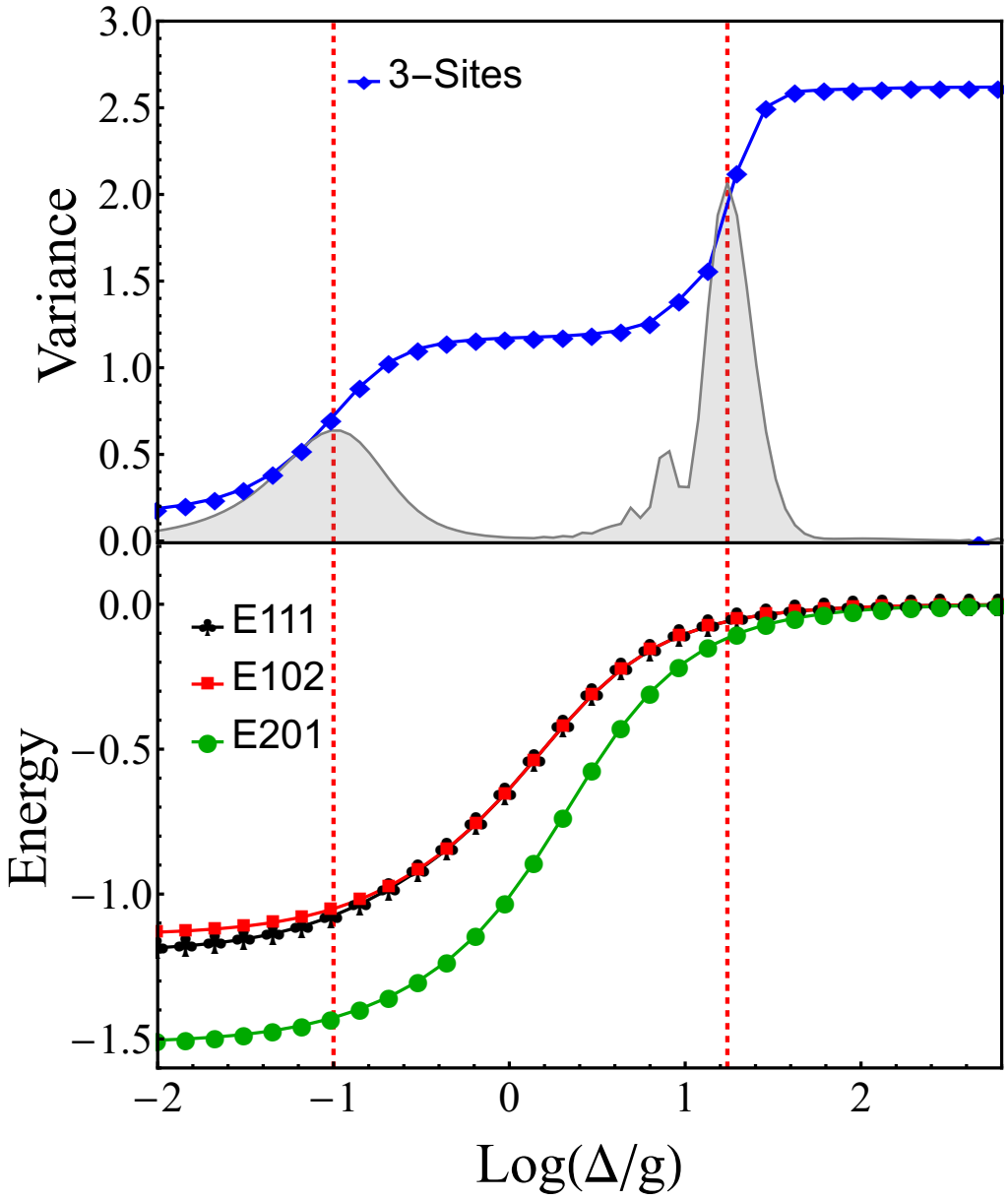

Figure 4.8: (Top) JCH Mott-Insulator/Superfluid phase transition for 3-sites cycle CRA with anisotropy on the light-matter coupling, as function of the detuning parameter Δ and described using the total variance of the polariton number, where 2 plateaus are observed. The shaded area shows the first derivative of the order parameter and the highlighted peaks exhibit the point in which a transition is observed. (Bottom) Effective energy levels as function of the detuning, where the different levels become degenerate as the detuning is increased. The vertical red dashed line shows the point in which both analysis describe a superfluid phase

We have shown how the CRA array with anisotropy on the light-matter coupling exhibits multiple plateaus through the Mott-Insulator/Superfluid phase transition. Now is possible to have Hall behavior present in CRA beyond 3-cavities with a corresponding theory within the same energy analysis previously discussed. Figure 4.9 shows the Mott-Insulator to superfluid phase transition for a 4-sites CRA in line configuration where three plateaus are possible through the transition as the different sites start to interact with each other.

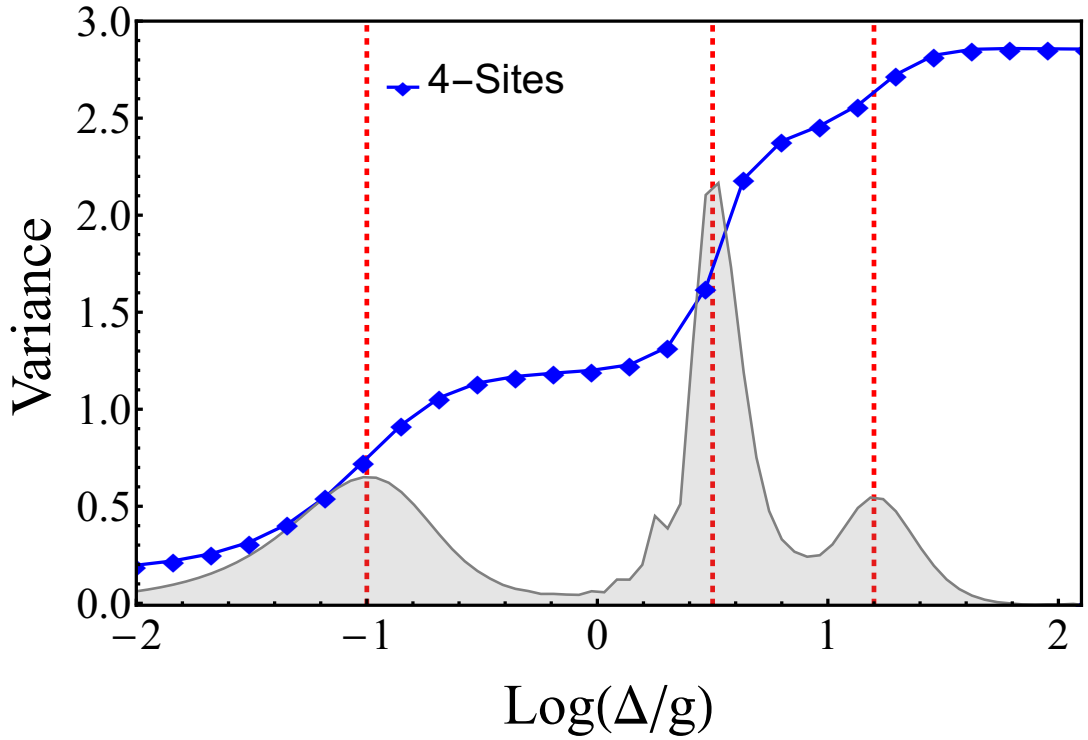

Figure 4.9: 4-sites line network with light-matter couplings $g_1 = g_2 = 10^{-2}\omega = g$ and $g_3 = g_4 = 10^{-1}g$. In this configuration there are plateaus for each pair with the same light-matter coupling superfluid dimerization and an additional plateau for larger detunings (Δ) as the sites with different light-matter couplings start interacting with each-other

Now that 4-sites networks are considered, it becomes interesting to check if topology has an impact through the phase transition under light-matter coupling an-

isotropy. Figure 4.10 shows that there is small impact on the phase transition when considering the topology effects, as there is a minor overshot beyond the superfluid phase value for a cycle topology accompanied by an additional peak in the first derivative of the order parameter, which means that the topology has an impact which requires further investigation.

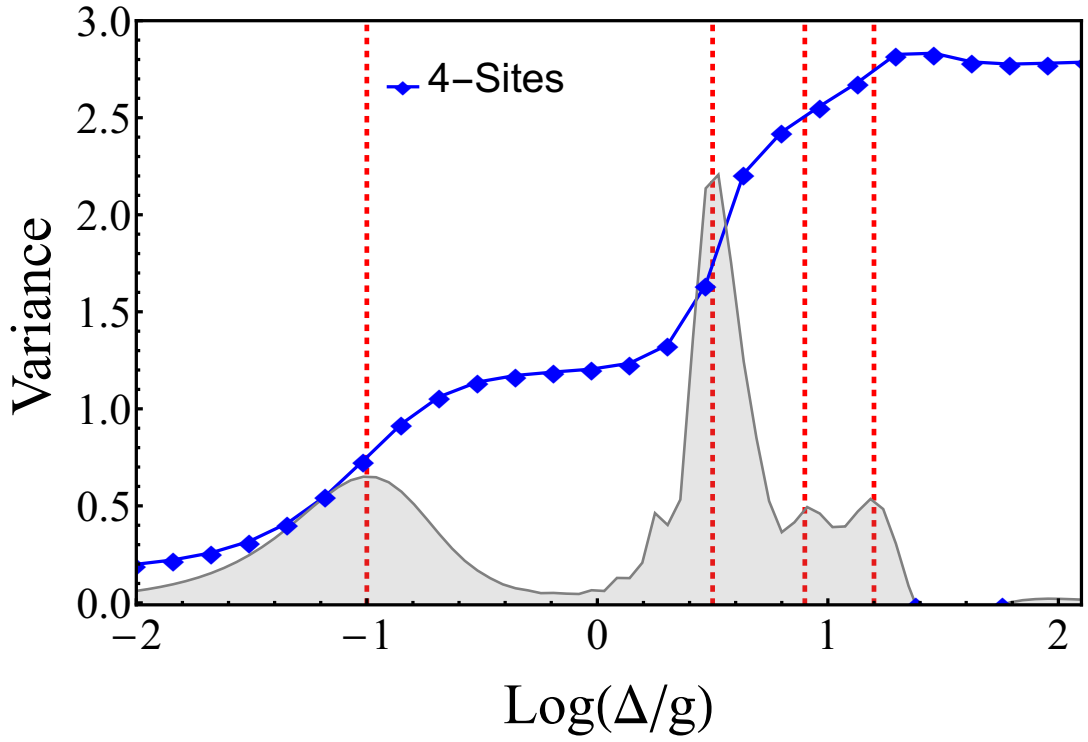

Figure 4.10: 4-sites cycle network with light-matter couplings $g_1 = g_2 = 10^{-2}\omega = g$ and $g_3 = g_4 = 10^{-1}g$. In this configuration there are plateaus for each pair with the same light-matter coupling superfluid dimerization and an additional plateau for larger detunings (Δ) as the sites with different light-matter couplings start interacting with each-other

As we have seen in this section, the use of the light-matter coupling anisotropy allows for fine grained control over the Mott-Insulator to superfluid phase transition of a JCH system, so while there are some cavities in the superfluid phase, some other cavities remain in a Mott-insulating phase, thus it could be used for technological

applications where selective transport is needed.

4.5 Conclusions

This chapter has shown that the energy perspective for the JCH model provides additional insight for the model, including the phase transition and becomes the most useful tool in the analysis of the anisotropy based phenomena.

This chapter also showed that the different sources of anisotropy, produce different changes in the dynamics of the system, so that the individual manipulation of the TLS induces a new phase on the model, here named as resonant dynamics which are easily configurable and robust. On a similar fashion, the light-matter coupling anisotropy modifies the phase transition in multiple steps according to the dimerization induced by the competence between the light-matter coupling anisotropy and the detuning of the cavities.

Chapter 5

Summary and Outlook

Through this work anisotropy has shown new and interesting phenomena in coupled resonating arrays described by the JCH Model, which open additional research oportunities for quantum simulations and potential technological applications taking advantage of the new phenomena.

We have shown that quench dynamics induce a first-order like phase transition in coupled resonator arrays doped with a two-level system, this behavior is independent of the choice of the order parameter, the standard deviation of the polariton number or the bipartite fluctutation, our results reveal the universality of the simulated first order phase transition. Thus quench dynamics provides a new mechanism to study many-body systems using CRAs as quantum simulation platorm.

A topologycal anisotropy of the network in presence of quench dynamics so that the nucleation of simulated superfluid states, demonstrated by numerical simulation, is a function of the local connectivity as demonstrated by the mean field theory. This dependence of the superfluid phase with the local connectivity explains the nucleation in CRAs where as far as we understand, there is no known microscopic mechanism for predicting nucleation in first-order phase transitions. In this context, our results

provide an exact geometrical description for the appearance of domain nucleation due to the number of connections. Thus, our results may be used to predict, and manipulate, the nucleation of a superfluid phase of light in complex-random networks

A CRA system described by the JCH model subject to a detuning anisotropy has exhibited a resonance phenomenon, which can be understood a new phase different from either the Mott-Insulating phase and the Superfluid phase. In contrast to the usual Superfluid phase, not all possible quantum states are available, which gives rise to a different dynamics in which the system oscillates. These oscillations show evidence of complex directional dynamics which in larger arrays could exhibit new phenomena not previously observed in other quantum systems. Similarly careful design of such cavities could have additional technological applications in quantum computing circuits.

The rise of the quantum Hall-like phase transition on Coupled JCH cavities under light-matter anisotropy, broadens the scope in which the JCH model can be used for quantum simulations as, to our best knowledge, this is the first evince of quantum Hall-like curves in these systems, which allow for the study of many-Body phenomena not previously accessible through smaller systems, which can provide additional insights for materials research and development.

The energy perspective of the JCH model demonstrated through perturbation theory has exhibited good predictive capabilities, which can be used to determine if a CRA is in the Mott-Insulator or superfluid phase, and can be further utilized in the design of complex systems for research and technological applications, taking advantage of the different discussed in this work and elsewhere.

As discussed, the different types of anisotropy discussed through this work, each exhibit new and interesting phenomena, which have yet to yield all the results they could individually provide. Furthermore, additional research is possible through

combinations of the previously mentioned anisotropies in the system in search for new phenomena and applications.

Bibliography

[1] Ivan K. Schuller and Rick Stevens, "Neuromorphic Computing: From Materials to Systems Architecture - NCFMtSA_rpt.pdf," https://science.energy.gov/~/media/bes/pdf/reports/2016/NCFMtSA_rpt.pdf, Oct. 2015.

[2] Thomas Potok, Catherine Schuman, Robert Patton, Todd Hylton, Hai Li, and Robinson Pino, "Neuromorphic Computing Workshop," http://ornlcda.github.io/neuromorphic2016/, Jul. 2016.

[3] R. P. Feynman, "Simulating physics with computers," *Int J Theor Phys*, vol. 21, no. 6-7, pp. 467–488, Jun. 1982.

[4] K. L. Pudenz and D. A. Lidar, "Quantum adiabatic machine learning," *Quantum Inf Process*, vol. 12, no. 5, pp. 2027–2070, May 2013.

[5] I. M. Georgescu, S. Ashhab, and F. Nori, "Quantum simulation," *Rev. Mod. Phys.*, vol. 86, no. 1, pp. 153–185, Mar. 2014.

[6] R. Di Candia, "Embedding quantum simulators," Ph.D. dissertation, Jun. 2015.

[7] M. Nakahara and T. Ohmi, *Quantum Computing: From Linear Algebra to Physical Realizations*. CRC Press, Mar. 2008.

[8] D. Aggarwal, G. K. Brennen, T. Lee, M. Santha, and M. Tomamichel, "Quantum attacks on Bitcoin, and how to protect against them," Oct. 2017.

[9] A. Aspuru-Guzik and P. Walther, "Photonic quantum simulators," *Nature Physics*, vol. 8, no. 4, pp. 285–291, Apr. 2012.

[10] D. Willsch, M. Nocon, F. Jin, H. De Raedt, and K. Michielsen, "Gate-error analysis in simulations of quantum computers with transmon qubits," *Phys. Rev. A*, vol. 96, no. 6, p. 062302, Dec. 2017.

[11] L. Lamata, "Digital-analog quantum simulation of generalized Dicke models with superconducting circuits," *Scientific Reports*, vol. 7, p. 43768, Mar. 2017.

[12] R. Blatt and C. F. Roos, "Quantum simulations with trapped ions," *Nat Phys*, vol. 8, no. 4, pp. 277–284, Apr. 2012.

[13] A. A. Houck, H. E. Türeci, and J. Koch, "On-chip quantum simulation with superconducting circuits," *Nat Phys*, vol. 8, no. 4, pp. 292–299, Apr. 2012.

[14] D. S. Abrams and S. Lloyd, "Simulation of Many-Body Fermi Systems on a Universal Quantum Computer," *Phys. Rev. Lett.*, vol. 79, no. 13, pp. 2586–2589, Sep. 1997.

[15] S. Schmidt and J. Koch, "Circuit QED lattices: Towards quantum simulation with superconducting circuits," *Annalen der Physik*, vol. 525, no. 6, pp. 395–412, Jun. 2013.

[16] J. I. Cirac and P. Zoller, "Goals and opportunities in quantum simulation," *Nat Phys*, vol. 8, no. 4, pp. 264–266, Apr. 2012.

[17] D. L. Underwood, W. E. Shanks, J. Koch, and A. A. Houck, "Low-disorder microwave cavity lattices for quantum simulation with photons," *Phys. Rev. A*, vol. 86, no. 2, p. 023837, Aug. 2012.

[18] I. Bloch, J. Dalibard, and S. Nascimbène, "Quantum simulations with ultracold quantum gases," *Nat Phys*, vol. 8, no. 4, pp. 267–276, Apr. 2012.

[19] A. Trabesinger, "Quantum simulation," *Nat Phys*, vol. 8, no. 4, pp. 263–263, Apr. 2012.

[20] M. J. Hartmann, "Quantum simulation with interacting photons," *J. Opt.*, vol. 18, no. 10, p. 104005, 2016.

[21] E. Jané, G. Vidal, W. Dür, P. Zoller, and J. I. Cirac, "Simulation of quantum dynamics with quantum optical systems," *Quantum Information & Computation*, vol. 3, no. 1, Jul. 2002.

[22] R. Gerritsma, G. Kirchmair, F. Zähringer, E. Solano, R. Blatt, and C. F. Roos, "Quantum simulation of the Dirac equation," *Nature*, vol. 463, no. 7277, pp. 68–71, Jan. 2010.

[23] M. Mariantoni, H. Wang, R. C. Bialczak, M. Lenander, E. Lucero, M. Neeley, A. D. O'Connell, D. Sank, M. Weides, J. Wenner, T. Yamamoto, Y. Yin, J. Zhao, J. M. Martinis, and A. N. Cleland, "Photon shell game in three-resonator circuit quantum electrodynamics," *Nature Physics*, vol. 7, no. 4, pp. 287–293, Apr. 2011.

[24] A. Mezzacapo, U. L. Heras, J. S. Pedernales, L. DiCarlo, E. Solano, and L. Lamata, "Digital Quantum Rabi and Dicke Models in Superconducting Circuits," *Scientific Reports*, vol. 4, p. 7482, Dec. 2014.

[25] A. Tomadin and R. Fazio, "Many-body phenomena in QED-cavity arrays [Invited]," *J. Opt. Soc. Am. B, JOSAB*, vol. 27, no. 6, pp. A130–A136, Jun. 2010.

[26] M. Hartmann, F. Brandão, and M. Plenio, "Quantum many-body phenomena in coupled cavity arrays," *Laser & Photon. Rev.*, vol. 2, no. 6, pp. 527–556, Dec. 2008.

[27] C. Domb, M. S. Green, and J. L. Lebowitz, Eds., *Phase Transitions and Critical Phenomena. Vol. 1: Exact Results*, 2nd ed. London: Acad. Press, 1976, oCLC: 256425090.

[28] ——, *Phase Transitions and Critical Phenomena. Vol. 2: ...* London: Acad. Press, 1972, oCLC: 830722336.

[29] ——, *Phase Transitions and Critical Phenomena. Vol. 5B: ...* London: Acad. Press, 1976, oCLC: 830722363.

[30] C. Domb and M. S. Green, *Phase Transitions and Critical Phenomena Vol5A*. Academic Press, 1976.

[31] L. D. Landau and E. M. Lifshitz, *Statistical Physics*. Elsevier, Oct. 2013.

[32] E. T. Jaynes and F. W. Cummings, "Comparison of quantum and semiclassical radiation theories with application to the beam maser," *Proceedings of the IEEE*, vol. 51, no. 1, pp. 89–109, Jan. 1963.

[33] F. Deppe, M. Mariantoni, E. P. Menzel, A. Marx, S. Saito, K. Kakuyanagi, H. Tanaka, T. Meno, K. Semba, H. Takayanagi, E. Solano, and R. Gross, "Two-photon probe of the Jaynes–Cummings model and controlled symmetry breaking in circuit QED," *Nature Physics*, vol. 4, no. 9, pp. 686–691, Sep. 2008.

[34] J. R. Johansson, P. D. Nation, and F. Nori, "QuTiP: An open-source Python framework for the dynamics of open quantum systems," *Computer Physics Communications*, vol. 183, no. 8, pp. 1760–1772, Aug. 2012.

[35] ——, "QuTiP 2: A Python framework for the dynamics of open quantum systems," *Computer Physics Communications*, vol. 184, no. 4, pp. 1234–1240, Apr. 2013.

[36] K. M. Birnbaum, A. Boca, R. Miller, A. D. Boozer, T. E. Northup, and H. J. Kimble, "Photon blockade in an optical cavity with one trapped atom," *Nature*, vol. 436, no. 7047, pp. 87–90, Jul. 2005.

[37] A. D. Greentree, C. Tahan, J. H. Cole, and L. C. L. Hollenberg, "Quantum phase transitions of light," *Nature Physics*, vol. 2, no. 12, pp. 856–861, Dec. 2006.

[38] M. T. C. Wong and C. K. Law, "Two-polariton bound states in the Jaynes-Cummings-Hubbard model," *Phys. Rev. A*, vol. 83, no. 5, p. 055802, May 2011.

[39] D. G. Angelakis, M. F. Santos, and S. Bose, "Photon-blockade-induced Mott transitions and XY spin models in coupled cavity arrays," *Phys. Rev. A*, vol. 76, no. 3, p. 031805, Sep. 2007.

[40] C. Y. Hu, "Photonic transistor and router using a single quantum-dot-confined spin in a single-sided optical microcavity," *Scientific Reports*, vol. 7, p. 45582, Mar. 2017.

[41] Y.-P. Wang, W.-L. Yang, Y. Hu, Z.-Y. Xue, and Y. Wu, "Detecting topological phases of microwave photons in a circuit quantum electrodynamics lattice," *npj Quantum Information*, vol. 2, p. 16015, Jun. 2016.

[42] S. Schmidt and G. Blatter, "Strong Coupling Theory for the Jaynes-Cummings-Hubbard Model," *Phys. Rev. Lett.*, vol. 103, no. 8, p. 086403, Aug. 2009.

[43] J. W. Negele and H. Orland, *Quantum Many-Particle Systems*. Westview Press, Dec. 2008.

[44] S. Haroche and J.-M. Raimond, *Exploring the Quantum: Atoms, Cavities, and Photons*. OUP Oxford, Aug. 2006.

[45] Christian Nietner, "Quantum Phase Transition of Light in the Jaynes-Cummings Lattice," Ph.D. dissertation, University of Kaiserslautern, Sep. 2010.

[46] I. I. Rabi, "On the Process of Space Quantization," *Phys. Rev.*, vol. 49, no. 4, pp. 324–328, Feb. 1936.

[47] D. Braak, "Integrability of the Rabi Model," *Phys. Rev. Lett.*, vol. 107, no. 10, p. 100401, Aug. 2011.

[48] J. J. Sakurai and J. Napolitano, *Modern Quantum Mechanics*. Addison-Wesley, 2011.

[49] J. Koch and K. Le Hur, "Superfluid–Mott-insulator transition of light in the Jaynes-Cummings lattice," *Phys. Rev. A*, vol. 80, no. 2, p. 023811, Aug. 2009.

[50] A. Halu, S. Garnerone, A. Vezzani, and G. Bianconi, "Phase transition of light on complex quantum networks," *Phys. Rev. E*, vol. 87, no. 2, p. 022104, Feb. 2013.

[51] M. A. Kastner, "The single-electron transistor," *Rev. Mod. Phys.*, vol. 64, no. 3, pp. 849–858, Jul. 1992.

[52] D. R. Tilley and J. Tilley, *Superfluidity and Superconductivity*. CRC Press, Jan. 1990.

[53] X.-G. Wen, *Quantum Field Theory of Many-Body Systems:From the Origin of Sound to an Origin of Light and Electrons: From the Origin of Sound to an Origin of Light and Electrons.* OUP Oxford, Jun. 2004.

[54] M. P. A. Fisher, P. B. Weichman, G. Grinstein, and D. S. Fisher, "Boson localization and the superfluid-insulator transition," *Phys. Rev. B*, vol. 40, no. 1, pp. 546–570, Jul. 1989.

[55] J. Hubbard, "Electron correlations in narrow energy bands," *Proc. R. Soc. Lond. A*, vol. 276, no. 1365, pp. 238–257, Nov. 1963.

[56] I. Bloch, J. Dalibard, and W. Zwerger, "Many-body physics with ultracold gases," *Rev. Mod. Phys.*, vol. 80, no. 3, pp. 885–964, Jul. 2008.

[57] H. F. Song, S. Rachel, and K. Le Hur, "General relation between entanglement and fluctuations in one dimension," *Phys. Rev. B*, vol. 82, no. 1, p. 012405, Jul. 2010.

[58] H. F. Song, S. Rachel, C. Flindt, I. Klich, N. Laflorencie, and K. Le Hur, "Bipartite fluctuations as a probe of many-body entanglement," *Phys. Rev. B*, vol. 85, no. 3, p. 035409, Jan. 2012.

[59] D. Gioev and I. Klich, "Entanglement Entropy of Fermions in Any Dimension and the Widom Conjecture," *Phys. Rev. Lett.*, vol. 96, no. 10, p. 100503, Mar. 2006.

[60] S. Rachel, N. Laflorencie, H. F. Song, and K. Le Hur, "Detecting Quantum Critical Points Using Bipartite Fluctuations," *Phys. Rev. Lett.*, vol. 108, no. 11, p. 116401, Mar. 2012.

[61] D. Rossini, R. Fazio, and G. Santoro, "Photon and polariton fluctuations in arrays of QED-cavities," *EPL*, vol. 83, no. 4, p. 47011, 2008.

[62] A. Altland and B. Simons, *Condensed Matter Field Theory*. Cambridge University Press, Jun. 2006.

[63] D. G. Angelakis, Ed., *Quantum Simulations with Photons and Polaritons: Merging Quantum Optics with Condensed Matter Physics*, ser. Quantum Science and Technology. Springer International Publishing, 2017.

[64] D. Rossini and R. Fazio, "Mott-Insulating and Glassy Phases of Polaritons in 1D Arrays of Coupled Cavities," *Phys. Rev. Lett.*, vol. 99, no. 18, p. 186401, Oct. 2007.

[65] A. C. Y. Li, F. Petruccione, and J. Koch, "Perturbative approach to Markovian open quantum systems," *Scientific Reports*, vol. 4, p. 4887, May 2014.

[66] Muhammed Kutty, "PHASE TRANSITION IN JAYNES- CUMMINGS-HUBBARD MODEL," Ph.D. dissertation, Sep. 2011.

[67] WONG Tsz Ching Max, "Topics in Jaynes-Cummings-Hubbard Model – CUHK Digital Repository," Ph.D. dissertation, Nov. 2012.

[68] K. Huang, *Statistical Mechanics*. Wiley, 1987.

[69] G. Jaeger, "The Ehrenfest Classification of Phase Transitions: Introduction and Evolution," *Arch Hist Exact Sc.*, vol. 53, no. 1, pp. 51–81, May 1998.

[70] M. Vojta, "Quantum phase transitions," *Rep. Prog. Phys.*, vol. 66, no. 12, p. 2069, 2003.

[71] N. Bo, G. P. Zhao, H. W. Zhang, L. Chen, and X. B. Wang, "Nucleation field, hysteresis loop, coercivity mechanism and critical thickness in composite multilayers with perpendicular anisotropy," *Solid State Communications*, vol. 151, no. 5, pp. 346–350, Mar. 2011.

[72] J. Raftery, D. Sadri, S. Schmidt, H. E. Türeci, and A. A. Houck, "Observation of a Dissipation-Induced Classical to Quantum Transition," *Phys. Rev. X*, vol. 4, no. 3, p. 031043, Sep. 2014.

[73] M. Fitzpatrick, N. M. Sundaresan, A. C. Y. Li, J. Koch, and A. A. Houck, "Observation of a Dissipative Phase Transition in a One-Dimensional Circuit QED Lattice," *Phys. Rev. X*, vol. 7, no. 1, p. 011016, Feb. 2017.

[74] J. Koch, T. M. Yu, J. Gambetta, A. A. Houck, D. I. Schuster, J. Majer, A. Blais, M. H. Devoret, S. M. Girvin, and R. J. Schoelkopf, "Charge-insensitive qubit design derived from the Cooper pair box," *Phys. Rev. A*, vol. 76, no. 4, p. 042319, Oct. 2007.

[75] M. J. Rozenberg, "Integer-filling metal-insulator transitions in the degenerate Hubbard model," *Phys. Rev. B*, vol. 55, no. 8, pp. R4855–R4858, Feb. 1997.

[76] A. Das, *Lectures on Quantum Field Theory*. World Scientific, 2008.

Appendix A

Rotating Wave Approximation for the JC model

The Rabi model is a complete description of a two level system inside an optical cavity and interacting with it, however the treatment of the Rabi model is complex, because it does not have conserved quantities which can be used for the diagonalization of the system. Consider the Rabi's model Hamiltonian $H_R = \omega_c a^\dagger a + \omega_a \sigma^+ \sigma^- + g(a^\dagger \sigma^- + a\sigma^+ + a^\dagger \sigma^+ + a\sigma^-)$, with $\hbar = 1$, where ω_c is the cavity frequency, ω_a is the TLS energy gap frequency, and g is the light-matter coupling. Now we see that light-matter coupling term has components that conserve the energy in the cavity, and terms that do not. The energy conserving terms are $a^\dagger \sigma^- + a\sigma^+$, which represent the energy movement from the cavity to the TLS and back, through the absorption of a photon by the TLS to transition to a its exited state, and the reverse process. The non energy conserving terms are $a^\dagger \sigma^+ + a\sigma^-$, which describe the TLS transition from the ground state to a higher energy simultaneous to the creation of a photon in the cavity. Now we analyze the Rabi Hamiltonian using interaction picture[76].

$$H_I = \mathrm{e}^{iH_0 t}\left(H_0 + g(a^\dagger\sigma^- + a\sigma^+ + a^\dagger\sigma^+ + a\sigma^-)\right)\mathrm{e}^{-iH_0 t} \tag{A.1}$$

Equation (A.1), shows the Rabi Hamiltonian in the interaction picture, where $H_0 = \omega_c a^\dagger a + \omega_a \sigma^+\sigma^-$ is the free Hamiltonian. Then we can use the the Baker-Hausdorff lema[48], shown in equation (A.2), over the Rabi hamiltonian

$$\mathrm{e}^{\alpha B} A\,\mathrm{e}^{-\alpha B} = A + \alpha\,[B, A] + \frac{\alpha^2}{2!}\,[B, [B, A]] + \cdots \tag{A.2}$$

Now in order to take advantage of the expansion, the most relevant expressions are shown in equation (A.3).

$$\begin{aligned}
\left[H_0, a^\dagger\sigma^+\right] &= (\omega_c + \omega_a)a^\dagger\sigma^+ \\
[H_0, a\sigma^-] &= -(\omega_c + \omega_a)a\sigma^- \\
\left[H_0, a^\dagger\sigma^-\right] &= (\omega_c - \omega_a)a^\dagger\sigma^- \\
[H_0, a\sigma^+] &= -(\omega_c - \omega_a)a\sigma^-
\end{aligned} \tag{A.3}$$

Finally, the rebuilding the expansion shows the interaction Hamiltonian in equation (A.4)

$$H_I = H_0 + g(\mathrm{e}^{i(\omega_c-\omega_a)t}\,a^\dagger\sigma^- + \mathrm{e}^{-i(\omega_c-\omega_a)t}\,a\sigma^+ + \mathrm{e}^{i(\omega_c+\omega_a)t}\,a^\dagger\sigma^+ + \mathrm{e}^{-i(\omega_c+\omega_a)t}\,a\sigma^-) \tag{A.4}$$

We define two frequencies: $\Delta = \omega_c - \omega_a$ and $\Omega = \omega_c + \omega_a$, then we have that the terms associated to the Δ frequency are slow rotating, and the terms associated to the frequency Ω are fast rotating. In the limit $\Omega \gg \Delta$, we have that the fast rotating terms, in average, do not contribute to the dynamics of the system dominated by the slower rotating terms. Notice that this approximation is possible only if $\frac{g}{\Omega} \ll 1$.

The Rabi Hamiltonian, in the interaction picture, is approximated as

$$H_I \approx H_0 + g(\mathrm{e}^{i(\omega_c-\omega_a)t}\, a^\dagger\sigma^- + \mathrm{e}^{-i(\omega_c-\omega_a)t}\, a\sigma^+), \tag{A.5}$$

from which we can reverse the transformation back to the Heisenberg, in which the approximated Rabi Hamiltonian is

$$H_R \approx \omega_c a^\dagger a + \omega_a \sigma^+\sigma^- + g(a^\dagger\sigma^- + a\sigma^+) = H_{JC}, \tag{A.6}$$

which is known as the Jaynes-Cummings model Hamiltonian.

Appendix B

Detuning sign and the polariton map

The Jaynes-Cummings Hamiltonian can be diagonalized using the polariton map, as discussed in [39, 49], however there are subtle differences in the polariton mapping depending on the sign convention used for the definition of the detuning (Detuning), which can be confusing for someone using a different sign convention, therefore this appendix will discuss the different sign conventions and how these change the polariton mapping allowing for the reader a single handy reference when comparing multiple publications

B.1 The $\Delta = \omega_a - \omega_c$ Convention

Consider the single cavity Jaynes-Cummings Hamiltonian shown in equation (B.1), which has already been discussed, as the starting point for the discussion on the $\Delta = \omega_a - \omega_c$ convention.

$$H_{JC} = \omega_c a^\dagger a + \omega_a \sigma^+ \sigma^- + g\left(a^\dagger \sigma^- + \sigma^+ a\right) \tag{B.1}$$

The Jaynes-Cummings Hamiltonian has the conserved quantity $N = a^\dagger a + \sigma^+\sigma^-$, which corresponds to the polariton number, so we write the Hamiltonian following the $\Delta = \omega_c - \omega_a$ convention, which is traditionally used for analysis in which the resonant photon frequency the cavity will be considered higher than the resonant frequency of the two level system, as shown in equation (B.2)

$$H_{JC} = \omega_c N - (\omega_c - \omega_a)\sigma^+ \sigma^- + g\left(a^\dagger \sigma^- + \sigma^+ a\right) \tag{B.2}$$

Now to study the polariton mapping, the Hamiltonian is written in matrix form, redefining the variables $\omega = \omega_c$ and $\Delta = \omega_c - \omega_a$ for comfort, leaving the Hamiltonian as shown in equation (B.3)

$$H_N = \begin{bmatrix} \omega n & g\sqrt{n} \\ g\sqrt{n} & \omega - \Delta \end{bmatrix} \tag{B.3}$$

At this point, traditional linear algebra techniques are used to compute the eigenvalues of the Hamiltonian in its matrix form, so that the energies of the polariton states are $E_n^{\pm} = \omega n - \frac{\Delta}{2} \pm \chi_n$ where $\chi_n = \sqrt{\left(\frac{\Delta}{2}\right)^2 + g^2 n}$ and the polariton states are described by equations (B.4) and (B.5)

$$|n-\rangle = sen(\theta_n)\,|n, \downarrow\rangle - cos(\theta_n)\,|n-1, \uparrow\rangle \tag{B.4}$$

$$|n+\rangle = cos(\theta_n)\,|n, \downarrow\rangle + sen(\theta_n)\,|n-1, \uparrow\rangle \tag{B.5}$$

Where for the polariton mapping we used the auxiliary variable θ_n defined by the

equation (B.6)

$$Tan(2\theta_n) = \frac{g\sqrt{n}}{\frac{\Delta}{2}} \tag{B.6}$$

B.2 The $\Delta = \omega_c - \omega_a$ Convention

The $\Delta = \omega_c - \omega_a$ can be used in cases where the cavity photon resonant frequency is designed to be lower than the two level system resonant frequency, in such scenarios, the Jaynes-Cummings Hamiltonian shown in equation (B.1) is written as shown by equation (B.7)

$$H_{JC} = \omega_c N + (\omega_a - \omega_c)\sigma^+\sigma^- + g\left(a^\dagger\sigma^- + \sigma^+ a\right) \tag{B.7}$$

Again the Hamiltonian is written in matrix form as shown in B.1, but only now the convention is different so $\omega = \omega_c$ and $\Delta = \omega_a - \omega_c$, leaving the hamiltonian as shown in equation (B.8)

$$H_N = \begin{bmatrix} \omega n & g\sqrt{n} \\ g\sqrt{n} & \omega + \Delta \end{bmatrix} \tag{B.8}$$

Finally by doing the diagonalization procedure on the Jaynes-Cummings Hamiltonian, the polariton map energies are for the $E_n^{\pm} = \omega n + \frac{\Delta}{2} \pm \chi_n$, where $\chi_n = \sqrt{\left(\frac{\Delta}{2}\right)^2 + g^2 n}$, with the polaritons states defined by equations (B.9) y (B.10), with the mixing angle $theta_n$ as shown in equation (B.6):

$$|n-\rangle = cos(\theta_n)\,|n,\downarrow\rangle - sen(\theta_n)\,|n-1,\uparrow\rangle \tag{B.9}$$

$$|n+\rangle = sen(\theta_n)\,|n,\downarrow\rangle + cos(\theta_n)\,|n-1,\uparrow\rangle \tag{B.10}$$

It can be observed that even though the expressions for the different states seems to be different, the energies are the same.

SCIENTIFIC REPORTS

OPEN

Nucleation of superfluid-light domains in a quenched dynamics

Joaquín Figueroa[1,2], José Rogan[1,2], Juan Alejandro Valdivia[1,2], Miguel Kiwi[1,2], Guillermo Romero[3] & Felipe Torres[1,2]

Received: 7 February 2018
Accepted: 24 July 2018
Published online: 24 August 2018

Strong correlation effects emerge from light-matter interactions in coupled resonator arrays, such as the Mott-insulator to superfluid phase transition of atom-photon excitations. We demonstrate that the quenched dynamics of a finite-sized complex array of coupled resonators induces a first-order like phase transition. The latter is accompanied by domain nucleation that can be used to manipulate the photonic transport properties of the simulated superfluid phase; this in turn leads to an empirical scaling law. This universal behavior emerges from the light-matter interaction and the topology of the array. The validity of our results over a wide range of complex architectures might lead to a promising device for use in scaled quantum simulations.

The absence of energy dissipation in the flow dynamics of a quantum fluid is one of the most fascinating effects of strongly correlated condensates[1–6]. Quantum phase transitions, from Mott insulator to superfluid, have been observed in a wide range of physical platforms such as ultracold atoms in optical lattices[7], trapped gases of interacting fermionic atom pairs[8], and exciton-polariton condensates[9–11]. Furthermore, the remarkable progress in controlling light-matter interactions in the microwave regime of circuit quantum electrodynamics (QED) has provided a suitable scenario for studying strongly correlated effects with light[12–14]. In this case, coupled resonator arrays (CRAs) each doped with a two-level system (TLS) allow for the formation of dressed quantum states (polaritonic states) and effective photon-photon interactions. The underlying physics is well described by the Jaynes-Cummings-Hubbard (JCH) model[15–17]. In this case, if the frequencies of the single resonator mode and the TLS are close to resonance, the effective photonic repulsion prevents the presence of more than one polaritonic excitation in the resonator, due to the photon-blockade effect[18–20]. Detuning the atomic and photonic frequencies diminishes this effect and leads the system to a photonic superfluid[16]. Unlike Bose-Einstein condensation in optical lattices, polariton condensation includes two kind of excitations, atomic and photonic, and the transition from Mott-insulator to superfluid is accompanied by a transition of the excitations from polaritonic to photonic[16].

Here we show how a first-order like phase transition of the simulated superfluid phase of polaritons in CRAs can be induced by a quench dynamics as described by the JCH model. We compare full numerical simulations of several arrangements of CRAs with mean-field theory of photonic fluctuations dynamics. In this case, the simulated Mott-superfluid transition relies on the topological properties of the array, since the on-site photon blockade strongly depends on the connectivity of each node, even for small resonator-resonator hopping strength. When the system is prepared in the Mott state with a filling factor of one net excitation per site, and a sudden quench of the detuning between the single resonator mode and the TLS is applied, we find a first-order like phase transition which can be described by two bosonic excitations of the lower and upper polariton band. We find that a nucleated superfluid photon state emerges in a localized way, which depends on the topology of the array. This avalanche-like behavior near the simulated phase transition leads to a universal scaling law between critical parameters of the superfluid phase and the average connectivity of the array.

The Model

The physical scenario that we consider are CRAs in complex arrangements such as the one in Fig. 1(a). Here, each node of the array consists of a QED resonator doped with a TLS to be a real or artificial atom, and the whole system is described by the Jaynes-Cummings-Hubbard model[15–17], whose Hamiltonian reads

[1]Departamento de Física, Facultad de Ciencias, Universidad de Chile, Casilla 653, Santiago, 7800024, Chile. [2]Center for the Development of Nanoscience and Nanotechnology 9170124, Estación Central, Santiago, Chile. [3]Departamento de Física, Universidad de Santiago de Chile (USACH), Avenida Ecuador 3493, 9170124, Santiago, Chile. Correspondence and requests for materials should be addressed to F.T. (email: felestorres@gmail.com)

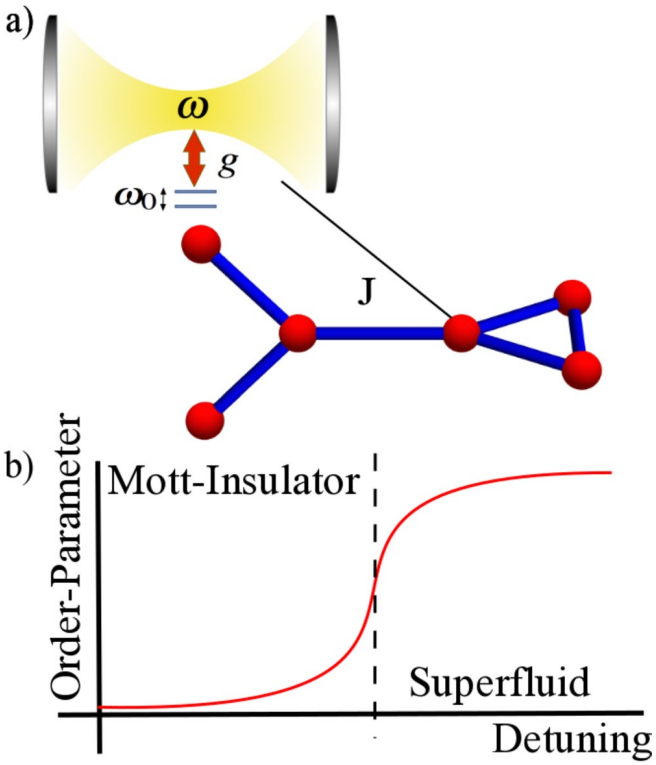

Figure 1. (**a**) Schematic representation of the Jaynes-Cummings-Hubbard lattice in a complex array where each node consists of a single resonator strongly coupled to a two-level system. (**b**) Phase transition from Mott-insulator to superfluid in light-matter CRAs systems as a function of the detuning parameter.

$$H_{\mathrm{JCH}} = \sum_{i=1}^{L} H_i^{\mathrm{JC}} - J\sum_{\langle i,j\rangle} A_{ij} a_i^{\dagger} a_j + \mathrm{h.c.} - \sum_{i=1}^{L} \mu_i n_i, \tag{1}$$

where L is the number of lattice sites, $a_i(a_i^{\dagger})$ is the annihilation (creation) bosonic operator, J is the photon-photon hopping amplitude, A_{ij} is the adjacency matrix which takes values $A_{ij}=1$ if two sites of the lattice are connected and $A_{ij}=0$ otherwise. μ_i stands for the chemical potential at site i and $n_i = a_i^{\dagger}a_i + \sigma_i^{+}\sigma_i^{-}$ represents the number of polaritonic excitations at site i. Also, $H_i^{\mathrm{JC}} = \omega a_i^{\dagger}a_i + \omega_0\sigma_i^{+}\sigma_i^{-} + g(\sigma_i^{+}a_i + \sigma_i^{-}a_i^{\dagger})$ is the Jaynes-Cummings (JC) Hamiltonian describing light-matter interaction[21]. Here, $\sigma_i^{+}(\sigma_i^{-})$ is the raising (lowering) operator acting on the TLS Hilbert space, and ω, ω_0, and g are the resonator frequency, TLS frequency, and light-matter coupling strength, respectively. Notice that the total number of elementary excitations (polaritons) in this system $N = \sum_i^M (a_i^{\dagger}a_i + \sigma_i^{+}\sigma_i^{-})$ is the conserved quantity $[N,H_{JCH}]=0$[22,23].

The quantum dynamics of this model has been studied for linear lattices[15,16], and its equilibrium properties at zero temperature have been studied by means of density matrix renormalization group[24], and by means of mean field (MF) theory, for two-dimensional lattices[17,25,26] and complex networks[27]. The latter studies have provided evidence of a quantum phase transition from Mott-insulating phases to a superfluid polaritonic phase. Beyond the MF approach there have been important contributions from the numerical and analytical viewpoint for extracting the phase boundaries[28–31], the study of critical behavior[30,31], and the excitation spectrum[29–31]. For a general overview on many-body physics with light relevant literature is available[32–34].

Mott-insulator to superfluid phase transition

Here we briefly summarize the Mott-insulator to superfluid phase transition in the JCH model[16]. Our main results are focused on the quantum dynamics of the JCH model (1) in complex networks, where we focus on the canonical ensemble with a fixed total number of polaritons[13,14]. In this case, the JCH Hamiltonian reads

$$H_{\mathrm{JCH}} = \sum_{i=1}^{L} H_i^{\mathrm{JC}} - J\sum_{\langle i,j\rangle} A_{ij} a_i^{\dagger} a_j + \mathrm{h.c.} \tag{2}$$

In the atomic limit, where the photon-hopping can be neglected ($J \ll g$), the JC Hamiltonian at site i (H_i^{JC}) can be diagonalized in the polaritonic basis that mixes atomic and photonic excitations $|n,\pm\rangle_i = \gamma_{n\pm}|\downarrow, n\rangle_i + \rho_{n\pm}|\uparrow, n-1\rangle_i$ with energies $\varepsilon_n^{\pm} = n\omega + \Delta/2 \pm \chi(n)$, where $\chi(n) = \sqrt{\Delta^2/4 + g^2 n}$, $\rho_{n+} = \cos(\theta_n/2)$, $\gamma_{n+} = \sin(\theta_n/2)$, $\rho_{n-} = -\gamma_{n+}$, $\gamma_{n-} = \rho_{n+}$, $\tan\theta_n = 2g\sqrt{n}/\Delta$, and the detuning parameter $\Delta = \omega_0 - \omega$.

Now, one can introduce the polaritonic creation operators at site i defined as $P_i^{\dagger(n,\alpha)} = |n,\ \alpha\rangle_i\langle 0,\ -\ |$, where $\alpha = \pm$ and we identify $|0,-\rangle \equiv |\downarrow, 0\rangle$ and $|0,+\rangle \equiv |\emptyset\rangle$ being a ket with all entries equal to zero, that is, it represents an unphysical state. These identifications imply $\gamma_{0-} = 1$ and $\gamma_{0+} = \rho_{0\pm} = 0$. Using this polaritonic mapping the Hamiltonian (2) can be rewritten as[16,26]

$$H = \sum_{i=1}^{L}\sum_{n=1}^{\infty}\sum_{\alpha=\pm}\varepsilon_n^{\alpha}P_i^{\dagger(n,\alpha)}P_i^{(n,\alpha)} - J\sum_{\langle i,j\rangle}A_{ij}\left[\sum_{n,m=1}^{\infty}\sum_{\alpha,\alpha',\beta,\beta'}t_{\alpha,\alpha'}^{n}t_{\beta,\beta'}^{m}P_i^{\dagger(n-1,\alpha)}P_i^{(n,\alpha')}P_j^{\dagger(m,\beta)}P_j^{(m-1,\beta')} + \text{h.c.}\right], \tag{3}$$

where $t_{++}^{n} = \sqrt{n}\gamma_{n\pm}\gamma_{(n-1)+} + \sqrt{n-1}\,\rho_{n\pm}\gamma_{(n-1)-}$ and $t_{+-}^{n} = \sqrt{n}\gamma_{n\pm}\rho_{(n-1)+} + \sqrt{n-1}\,\rho_{n\pm}\rho_{(n-1)-}$. The first term in Eq. (3) stands for the local polaritonic energy with an anharmonic spectrum and gives rise to an effective on-site polaritonic repulsion. The last term in Eq. (3) represents the polariton hopping between nearest neighbors and long range sites, and it may also allow for the interchange of polaritonic excitations.

If the physical parameters of the Hamiltonian (3) are in the regime $Jn \ll g\sqrt{n} \ll \omega$, and for an integer filling factor, where the total number of excitations N over the lattice is an integer multiple of the number of unit cells L, the lowest energy state is the product $\otimes_{i=1}^{L}|1,\ -\ \rangle_i$ which corresponds to a Mott-insulating phase, and its associated energy is $E = N\varepsilon_1^{-}$. In the thermodynamic limit, the interplay between the on-site polariton repulsion and the polariton hopping leads to a phase transition from a Mott insulator to a superfluid phase. The latter may be reached by diminishing the on-site repulsion by means of detuning the atomic and photonic frequencies. At equilibrium, this phase transition may be quantified by means of bipartite fluctuations[24,35]. In a simulated Mott-insulator transition, where an adiabatic dynamics drives the passage, it has been shown that a suitable order parameter corresponds to the variance of the number of excitations per site. Figure 1(b) shows the archetypal behavior of the order parameter as a function of the detuning Δ in the adiabatic dynamic regime, and for an integer filling factor of one net excitation per site[16].

Quenched dynamics and Topology in finite-size complex lattices

Our aim is to describe how complex arrangements of CRAs, such as the one appearing in Fig. 1(a), affect the simulated phase transition from Mott insulator to superfluid as the detuning parameter Δ is suddenly quenched. In particular, we are interested in how one can manipulate photonic transport properties of the emerging superfluid phase depending on the specific topology of the CRAs. As order parameter we choose the time-averaged standard deviation of the polariton number $\frac{1}{T}\int_0^T dt\sum_i^L(\langle n_i^2\rangle - \langle n_i\rangle^2))$ with $T = J^{-1}$, and we assume the whole system initially prepared in the Mott-insulating state $|\psi_0\rangle = \otimes_{i=1}^{L}|1,\ -\ \rangle_i$, with $\Delta = 0$ at each lattice site. In the Supplementary Material we present another equivalent measure of the order parameter based on the bipartite fluctuation proposed by S. Rachel *et al.*[35], and D. Rossini *et al.*[24]. Of course, due to computational restrictions, we consider relatively small arrangements of CRAs, but with varying degrees of complexity, suggesting that the topology of the network could be used in a nontrivial way to manipulate the emerging of the superfluid phase as these system becomes larger and approach the thermodynamic limit. The initialization process may be achieved by the scheme proposed by Angelakis *et al.*[16]. For instance, in circuit QED[13,14] one might cool down the whole system reaching temperatures around $T_0 \sim 15$ mK. In this case, the system will be prepared in its global ground state $|G\rangle = \otimes_{i=1}^{L}|0,\ -\ \rangle_i$. Then, one can apply individual magnetic fields on the TLSs, each implemented via a transmon qubit[36], such that the resonance condition $\Delta = 0$ is achieved. This way one can address individually each cavity with an external AC microwave current or voltage tuned to the transition $|\downarrow, 0\rangle_i \rightarrow |1, -\rangle_i$, with a driving frequency $\omega_D = \omega - g$, such that the system will be prepared in the desired initial state $|\psi_0\rangle$. The sudden quench of the detuning can be achieved by applying magnetic fields to the transmon qubits in order to reach the desired superfluid phase. It is noteworthy that when the initial state is a linear superposition of upper and lower polariton states ($\Delta \neq 0$) the quantum dynamics will be dominated by these two polaritonic bands. Also, we carry out full numerical calculations for the parameters $g = 10^{-2}\omega$ and $J = 10^{-2}g$, and we consider up to 6 Fock states per bosonic mode. These parameter values allow us to prevent the interchange of polaritonic excitations between different sites.

In order to gain insight into the quench dynamics of the topological CRAs let us consider a dimer array. As shown in Fig. 2, the simulated Mott-insulator to Superfluid phase transition strongly depends on the type of dynamics. Adiabatic dynamics resembles a second order phase transition which leads to a continuous change of the state of the system. On the other hand, the quench dynamics takes place accompanied by a discontinuous change of the state, analogous to the Metal-Insulator transition of oxides[37]. Hence, as we expected, the adiabatic dynamics is not qualitatively affected by the distribution of nearest neighbors. However, the topological properties of the array dominate a first-order like phase transition driving the quench dynamics (see Fig. 2). As the degree of inter-connectivity between the resonators grows the distance between them rapidly diminishes, and thus local correlations become more important due to quantum interference effects. If scaled up to the size of the system, due to the increase in the degrees of freedom, the numerical simulation time grows exponentially. In the next section we obtain an empirical scaling law to address this issue. Indeed, we demonstrate that the photon propagation in the simulated superfluid phase strongly depends of the connectivity per site $k_i = \sum_j A_{ij}$. Let us consider a set of arrays with a fixed number of TLS. As shown in Fig. 3(a) in the quench dynamics case the averaged standard deviation depends linearly on the connectivity, which means that depending on the connectivity the local superfluid states are reached with different detuning scales. We consider a set of CRAs with four and five interconnecting resonators as shown in Fig. 3(b). In contrast to these results, the adiabatic dynamics does not exhibit a monotone or linearly growing behavior, which leads to a sharper phase transition, as illustrated in Fig. 2.

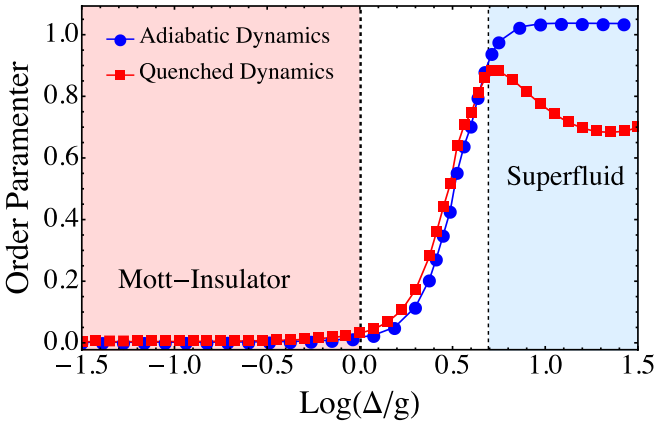

Figure 2. Quantum phase transition of a dimer array. Detuning dependence of the order parameter with two TLS coupled through photon hopping, adiabatic dynamics (blue circles) and quench dynamics (red squares). Continuous lines have been added as guide to the eye.

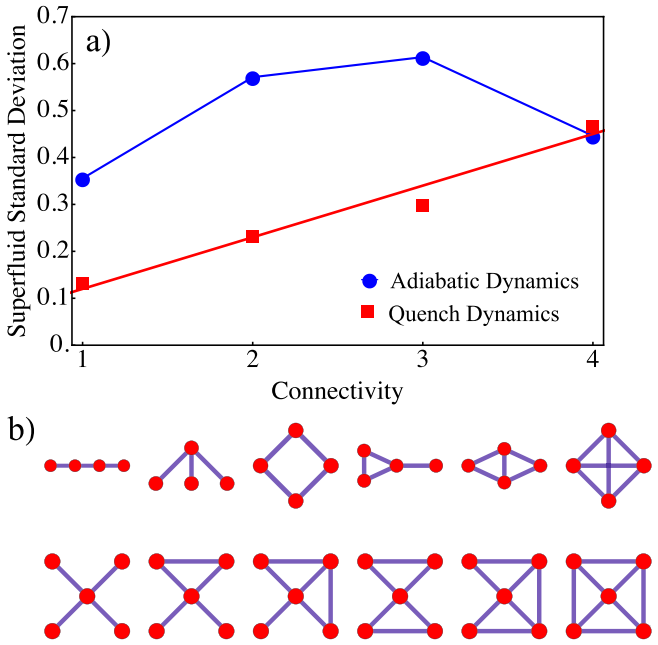

Figure 3. (**a**) Standard deviation of the superfluid phase as a function of the connectivity. Adiabatic dynamics (blue circles) and quench dynamics (red squares). A set of CRAs with four and five interconnecting resonators, as shown in (**b**) are considered. Continuous lines have been added as a guide to the eye.

Mean-field theory of the Superfluid Phase

In the thermodynamic limit, the emergent superfluid phase behaves as a quantum liquid[17]. Superfluidity is achieved by means of a transition of the excitations from polaritonic to photonic. In order to describe the simulated superfluid phase in our system, we introduce the photonic order parameter[17] $\psi = \langle a_i \rangle$. Using the decoupling approximation $a_i^\dagger a_j \approx \langle a_i^\dagger \rangle a_j + a_i^\dagger \langle a_j \rangle - \langle a_i^\dagger \rangle \langle a_j \rangle$, the resulting mean-field JCH Hamiltonian can be written as

$$H_{JCH} = \sum_i H_i^{JC} - J \sum_i k_i (\psi a_i^\dagger + \psi^* a_i). \tag{4}$$

Therefore, the simulated Mott-insulator phase can be characterized by the on site repulsion, which suppresses the fluctuations of the number of per site excitations $|\psi| = 0$. On the contrary, the superfluid phase is dominated by the hopping and the quantum fluctuations $|\psi| \neq 0$. Now we focus on the light-matter coupling induced by the hopping of photons through cavities. Introducing the identity $\sigma^+ \sigma^- + \sigma^- \sigma^+ = I$, we obtain an effective light-matter coupling, since it retains the mixed products of photonic and two level operators,

$$h_i^{LM} = \tilde{g}_i a_i^\dagger \sigma_i^- + \tilde{g}_i^\dagger a_i \sigma_i^+ + \text{h.c.} \tag{5}$$

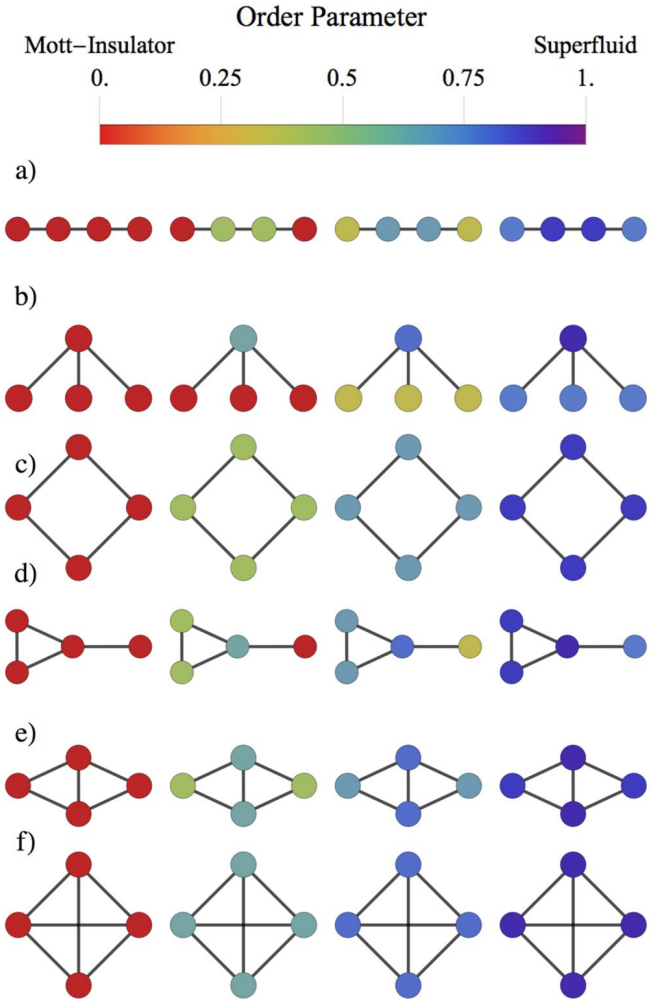

Figure 4. Numerical simulation of the quench dynamics. The full set of four node arrays, with (**a**,**b**) three; (**c**,**d**) four; (**e**) five; and (**f**) six connections. Connectivity per site (**a**) (1, 2, 2, 1), (**b**) (1, 1, 1, 3), (**c**) (2, 2, 2, 2), (**d**) (1, 3, 2, 2), (**e**) (2, 3, 3, 2), and (**f**) (3, 3, 3, 3). As the connectivity is increased locally the superfluid phase is achieved with a lower detuning strength. For each array and from left to right we have considered parameters $log(\Delta/g) = (0.5, 0.7, 0.75, 0.8)$, and $g = 10^{-2}\omega$, $J = 10^{-3}\omega$, where ω is the resonator frequency.

Here $\tilde{g}_i = Ig - Jk_i\psi\sigma_i^+$ is the effective light-matter coupling per site, which therefore turns out to be an operator. In the simulated superfluid phase the atomic transitions are expected to be suppressed against the photonic dressed states. Moreover, the total excitation number does not change, hence when the photonic excitations increase the atomic excitations decrease. Note that when $\tilde{g}_i = Ig$, i.e. when there are no hopping or topological effects,

$$\langle\sigma_i^+\rangle = \frac{g}{Jk_i}\frac{1}{\psi}, \tag{6}$$

which indicates that the total number of excitations is conserved and also demonstrates that the increase of the photonic states leads to a reduction of the atomic excitations, due to the conservation of the number excitations. Figure 4 shows the effect of the quench dynamics on the simulated phase transition of the JCH model for different arrays. In this case the nucleation of superfluid states emerges due to the variation of the order parameter, according to Eq. (6). In the Mott-Insulator state $\langle\sigma_i^+\rangle > 0\,\forall\, i$, when the detuning is increased $\langle\sigma_i^+\rangle$ decreases by a factor $1/(k_i\psi)$, until the superfluid phase is reached.

We have shown that the mean field approach strongly supports the scaling law of the order parameter shown in Fig. 3(a); namely, as the connectivity of CRAs is increased locally, the light superfluid phase is achieved for a smaller detuning strength.

Conclusion

We show that quench dynamics induce a first-order like phase transition in coupled resonator arrays doped with a two-level system. The nucleation of simulated superfluid states has been demonstrated by numerical simulation and by a mean field theoretical approach. In the quench dynamics the abrupt change of the order parameter, instead of sharper crossover driven by adiabatic dynamics, is explained by the non uniform transition from

Mott-Insulator to superfluid, which locally depends of the connectivity. Since the quench dynamics exhibits the same behavior independent of the choice of the order parameter, the standard deviation of the polariton number or the bipartite fluctutation, our results reveal the universality of the simulated first order phase transition (also see Supplementary Material). As the number of TLS is increased the averaged standard deviation of the superfluid phase depends linearly on the connectivity. At an increased scale, for large networks of doped optical/microwave resonators, our system may enter the field of quantum simulators. In particular, as far as we understand, there is no known microscopic mechanism for predicting nucleation in first-order phase transitions. In this context, our results provide an exact geometrical description for the appearance of domain nucleation due to the number of connections. Thus, our results may be used to predict, and manipulate, the nucleation of a superfluid phase of light in complex-random networks.

References

1. Kapitza, P. Viscosity of liquid helium below the λ-point. *Nature* **141**, 74 (1938).
2. Leggett, A. J. *Quantum Liquids* (Oxford University Press, 2006).
3. Anderson, M. H., Ensher, J. R., Matthews, M., Wieman, C. E. & Cornell, E. A. Observation of bose-einstein condensation in a dilute atomic vapor. *Science* **269**, 198–201 (1995).
4. Onofrio, R. *et al*. Observation of superfluid flow in a bose-einstein condensed gas. *Phys. Rev. Lett.* **85**, 2228–2231 (2000).
5. Zwierlein, M. W. e. a. Observation of bose-einstein condensation of molecules. *Phys. Rev. Lett.* **91**, 250401 (2003).
6. Schiró, M., Bordyuh, M., Öztop, B. & Türeci, H. E. Phase transition of light in cavity qed lattices. *Phys. Rev. Lett.* **109**, 053601 (2012).
7. Greiner, M., Mandel, O., Esslinger, T., Hansch, T. W. & Bloch, I. Quantum phase transition from a superfluid to a mott insulator in a gas of ultracold atoms. *Nature* **415**, 39–44 (2002).
8. Regal, C. A., Greiner, M. & Jin, D. S. Observation of resonance condensation of fermionic atom pairs. *Phys. Rev. Lett.* **92**, 040403 (2004).
9. Lerario, G. *et al*. Room-temperature superfluidity in a polariton condensate. *Nature Physics* **13**, 837–841 (2017).
10. Wertz, E. *et al*. Spontaneous formation and optical manipulation of extended polariton condensates. *Nature Physics* **6**, 860–864 (2010).
11. Byrnes, T., Kim, N. Y. & Yamamoto, Y. Exciton-polariton condensates. *Nature Physics* **10**, 803–813.
12. Houck, A. A., Türeci, H. E. & Koch, J. On-chip quantum simulation with superconducting circuits. *Nature Physics* **8**, 292–299.
13. Raftery, J., Sadri, D., Schmidt, S., Türeci, H. E. & Houck, A. A. Observation of a dissipation-induced classical to quantum transition. *Phys. Rev. X* **4**, 031043 (2014).
14. Fitzpatrick, M., Sundaresan, N. M., Li, A. C. Y., Koch, J. & Houck, A. A. Observation of a dissipative phase transition in a one-dimensional circuit qed lattice. *Phys. Rev. X* **7**, 011016 (2017).
15. Hartmann, M. J., Brandão, F. G. S. L. & Plenio, M. B. Strongly interacting polaritons in coupled arrays of cavities. *Nature Physics* **2**, 849–855 (2006).
16. Angelakis, D. G., Santos, M. F. & Bose, S. Photon-blockade-induced mott transitions and *xy* spin models in coupled cavity arrays. *Phys. Rev. A* **76**, 031805 (2007).
17. Greentree, A. D., Tahan, C., Cole, J. H. & Hollenberg, L. C. L. Quantum phase transitions of light. *Nature Physics* **2**, 856–861 (2006).
18. Birnbaum, K. M. *et al*. Photon blockade in an optical cavity with one trapped atom. *Nature* **436**, 87–90 (2005).
19. Imamoğlu, A., Schmidt, H., Woods, G. & Deutsch, M. Strongly interacting photons in a nonlinear cavity. *Phys. Rev. Lett.* **79**, 1467–1470 (1997).
20. Greentree, A. D., Vaccaro, J. A., R de Echaniz, S., Durrant, A. V. & Marangos, J. P. Prospects for photon blockade in four-level systems in the n configuration with more than one atom. *Journal of Optics B: Quantum and Semiclassical Optics* **2**, 252 (2000).
21. Jaynes, E. T. & Cummings, F. W. Comparison of quantum and semiclassical radiation theories with application to the beam maser. *Proceedings of the IEEE* **51**, 89–109 (1963).
22. Hartmann, M., Brandão, F. & Plenio, M. Quantum many-body phenomena in coupled cavity arrays. *Laser & Photonics Reviews* **2**, 527–556 (2008).
23. Hartmann, M. J. & Plenio, M. B. Strong photon nonlinearities and photonic mott insulators. *Physical Review Letters* **99**, 103601 (2007).
24. Rossini, D., Fazio, R. & Santoro, G. Photon and polariton fluctuations in arrays of qed-cavities. *EPL (Europhysics Letters)* **83**, 47011 (2008).
25. Na, N., Utsunomiya, S., Tian, L. & Yamamoto, Y. Strongly correlated polaritons in a two-dimensional array of photonic crystal microcavities. *Phys. Rev. A* **77**, 031803 (2008).
26. Koch, J. & Le Hur, K. Superfluid mott-insulator transition of light in the jaynes-cummings lattice. *Phys. Rev. A* **80**, 023811 (2009).
27. Halu, A., Garnerone, S., Vezzani, A. & Bianconi, G. Phase transition of light on complex quantum networks. *Phys. Rev. E* **87**, 022104 (2013).
28. Rossini, D. & Fazio, R. Mott-insulating and glassy phases of polaritons in 1d arrays of coupled cavities. *Phys. Rev. Lett.* **99**.
29. Aichhorn, M., Hohenadler, M., Tahan, C. & Littlewood, P. B. Quantum fluctuations, temperature, and detuning effects in solid-light systems. *Phys. Rev. Lett.* **100**, 216401 (2008).
30. Pippan, P., Evertz, H. G. & Hohenadler, M. Excitation spectra of strongly correlated lattice bosons and polaritons. *Phys. Rev. A* **80**, 033612 (2009).
31. Schmidt, S. & Blatter, G. Strong coupling theory for the jaynes-cummings-hubbard model. *Phys. Rev. Lett.* **103**, 086403 (2009).
32. Hartmann, M. J. Quantum simulation with interacting photons. *Journal of Optics* **18**, 104005 (2016).
33. Noh, C. & Angelakis, D. G. Quantum simulations and many-body physics with light. *Rep. Prog. Phys.* **80**, 016401 (2016).
34. Angelakis, D. G. (ed.) *Quantum Simulations with Photons and Polaritons*. Quantum Science and Technology (Springer, 2017).
35. Rachel, S., Laflorencie, N., Song, H. F. & Le Hur, K. Detecting quantum critical points using bipartite fluctuations. *Phys. Rev. Lett.* **108**, 116401 (2012).
36. Koch, J. *et al*. Charge-insensitive qubit design derived from the cooper pair box. *Phys. Rev. A* **76**, 042319 (2007).
37. Rozenberg, M. J. Integer-filling metal-insulator transitions in the degenerate hubbard model. *Phys. Rev. B* **55**, R4855–R4858 (1997).

Acknowledgements

This work was supported by the Fondo Nacional de Investigaciones Científicas y Tecnológicas (FONDECYT, Chile) under grants No. 1150806 (FT), No. 1160639 (MK,JR), 1150718 (JAV), 11596590659 (GR), Grants-FA9550-16-1-0122 (FT,MK) and FA9550-18-1-0438 CEDENNA through the "Financiamiento Basal para Centros Científicos y Tecnológicos de Excelencia-FB0807" (FT, JR, MK and JAV).

Author Contributions

F.T., G.R., M.K., J.R. and J.A.V. supervised and contributed to the theoretical analysis. J.F. carried out all analytical and numerical calculations, F.T. and G.R. wrote the manuscript. All authors contributed to the discussion of the results and revised the manuscript.

Additional Information

Supplementary information accompanies this paper at https://doi.org/10.1038/s41598-018-30789-9.

Competing Interests: The authors declare no competing interests.

Publisher's note: Springer Nature remains neutral with regard to jurisdictional claims in published maps and institutional affiliations.

PROCEEDINGS OF SPIE

SPIEDigitalLibrary.org/conference-proceedings-of-spie

Nucleation of superfluid-light domains

Joaquin Figueroa, Jose Rogan, Juan Alejandro Valdivia, Miguel Kiwi, Guillermo Romero, et al.

Joaquin Figueroa, Jose Rogan, Juan Alejandro Valdivia, Miguel Kiwi, Guillermo Romero, Felipe Torres, "Nucleation of superfluid-light domains," Proc. SPIE 10734, Quantum Nanophotonics 2018, 1073403 (11 September 2018); doi: 10.1117/12.2319764

SPIE.

Event: SPIE Nanoscience + Engineering, 2018, San Diego, California, United States

Nucleation of superfluid-light domains

Joaquin Figueroa[a,b], Jose Rogan[a,b], Juan Alejandro Valdivia[a,b], Miguel Kiwi[a,b], Guillermo Romero[c], and Felipe Torres[a,b]

[a]Departamento de Física, Facultad de Ciencias, Universidad de Chile, Casilla 653, Santiago, Chile 7800024.
[b]Centro para el Desarrollo de la Nanociencia y Nanotecnología, CEDENNA, Avenida Ecuador 3493, 9170124, Santiago, Chile.
[c]Departamento de Física, Universidad de Santiago de Chile (USACH), Avenida Ecuador 3493, 9170124, Santiago, Chile

ABSTRACT

Electromagnetic coupled resonator arrays (CRAs) doped with a quantum two-level system allow for the quantum simulation of a Mott-insulator to superfluid phase transition. We demonstrate that the order of this simulated phase transition depends on the type of dynamics. Thus, a first order like phase transition can be induced by a quench dynamics, while a second order like phase transition is produced by an adiabatic dynamics. In addition, we show that the underlying macroscopic behavior of the phase transition in other many body systems, such as domain nucleation and phase coexistence, can also be observed in CRAs. This universal behavior emerges from the light-matter interaction and the topology of the array. Therefore, the latter can be used to manipulate the photonic transport properties of the simulated superfluid phase.

Keywords: Quantum Simulation, Topology effect, Polariton Dynamics

1. INTRODUCTION

Remarkable progress has been made in controlling light-matter interactions in quantum systems, for instance, in the microwave regime of circuit quantum electrodynamics (QED), ultra-cold atoms in optical lattices,[1] trapped gases of interacting fermionic atom pairs,[2] and exciton-polariton condensates,[3–5] which have provided a suitable scenario for studying strongly correlated effects with light.[6–8] Quantum phase transitions, from Mott insulator to superfluid phase, have been observed in the aforementioned physical platforms. The absence of energy dissipation in the flow dynamics of a quantum fluid is one of the most fascinating effects of strongly correlated condensates.[9–14] Coupled resonator arrays (CRAs) each doped with a two-level system (TLS) allow for the formation of dressed quantum states (polaritonic states) and effective photon-photon interactions. The underlying physics is well described by the Jaynes-Cummings-Hubbard (JCH) model.[15–17] In this case, if the frequencies of the single resonator mode and the TLS are close to resonance, the effective photonic repulsion prevents the presence of more than one polaritonic excitation in the resonator, due to the photon-blockade effect.[18–20] Detuning the atomic and photonic frequencies diminishes this effect and leads the system to a photonic superfluid.[16] The quantum dynamics of this model has been studied for linear lattices,[15,16] and its equilibrium properties at zero temperature have been studied by means of density matrix renormalization group,[21] and by means of mean field (MF) theory, for two-dimensional lattices[17,22,23] and complex networks.[24] The latter studies have provided evidence of a quantum phase transition from Mott-insulating to a superfluid. Beyond the MF approach there have been important contributions from the numerical and analytical viewpoint for extracting the phase boundaries,[25–28] the study of critical behavior,[27,28] and the excitation spectrum.[26–28] For a general overview on the many-body physics with photons relevant literature is available.[29–31]

Unlike the Bose-Einstein condensation in optical lattices, polariton condensation includes two kind of excitations, atomic and photonic, and the transition from Mott-insulator to superfluid is accompanied by a transition

Further author information: (Send correspondence to Joaquin Figueroa)
Joaquin Figueroa: E-mail: joafigue@ing.uchile.cl

Quantum Nanophotonics 2018, edited by Jennifer A. Dionne, Mark Lawrence, Matthew T. Sheldon, Proc. of SPIE Vol. 10734, 1073403 · © 2018 SPIE
CCC code: 0277-786X/18/$18 · doi: 10.1117/12.2319764

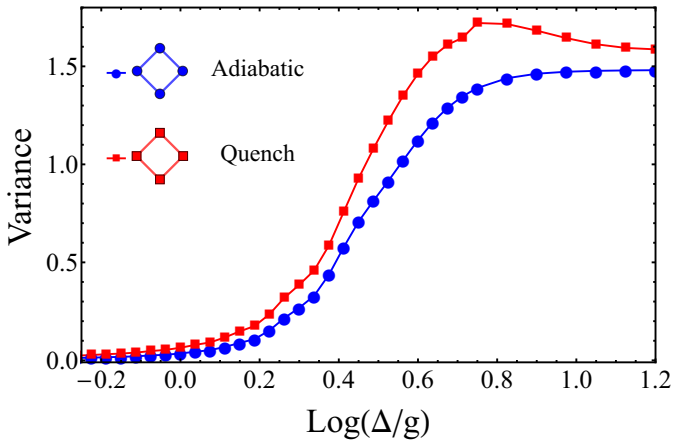

Figure 1. (color online) Simulated phase transition from Mott-insulator to superfluid in light-matter CRAs systems as a function of the detuning parameter. Four CRAs coupled in a square lattice with $g = 10^{-2}\omega$, and $J = 10^{-2}g$. First (Second)-like phase transition can be induced by a quench (adiabatic) dynamics (details concerned with theoretical model will be addressed in the next section).

of the excitations from polaritonic to photonic.[16] Usually the study of the simulated Mott-Superfluid phase transition in CRAs considers the initial state of the system to be in a Mott-insulating state, and an adiabatic change of the detuning between light and matter frequencies applies. This yields a smooth change in the order parameter, namely the variance of the polaritons number per site, thus leading to a second order phase transition. When we prepare the JCH system in the Mott state with a filling factor of one net excitation per site, and a sudden quench of the detuning between the single resonator mode and its corresponding TLS is applied for each site, we find a first-order like phase transition in the collective system, which can be described by two polaritonic excitations of the lower and upper polariton branch. Here we show how a first (second)-order like phase transition of the simulated superfluid phase of polaritons in CRAs can be induced by a quench (adiabatic) dynamics as described by the JCH model. We find that a localized nucleated superfluid photon state emerges, which depends on the topology of the array. As shown in Fig.1, quench (adiabatic) dynamics produces a first (second) order like phase transition. The first-order like Mott Insulator to superfluid phase transition can be observed with a sudden quench of the detuning parameter Δ, where the whole system initially prepared in the Mott-insulating state $|\psi_0\rangle = \bigotimes_{i=1}^{L} |1,-\rangle_i$, at the resonance condition $\Delta = 0$ for each lattice site. From this state a sudden quench of the detuning applied to the JCH cavities generates a discontinuity of the order parameter, see Fig.1. It is noteworthy that the initial state obtained is a linear superposition of the upper and lower polaritonic states ($\Delta \neq 0$), so that the quantum dynamics will be dominated by these two polariton branches.

The model

Let us consider an array of CRAs, as described by the JCH model, which consists of a QED resonator doped with a TLS to be a real or artificial atom. The whole system is described by the Jaynes-Cummings-Hubbard model[15–17]

$$H_{\rm JCH} = \sum_{i=1} H_i^{\rm JC} - J \sum_{\langle i,j \rangle} A_{ij} a_i^\dagger a_j + \text{h.c.}, \tag{1}$$

where i indicates the site at the array, $a_i(a_i^\dagger)$ is the annihilation (creation) bosonic operator, J is the photon-photon hopping amplitude, A_{ij} takes values $A_{ij} = 1$ if two sites of the lattice are connected and $A_{ij} = 0$ otherwise. Also, $H_i^{\rm JC} = \omega a_i^\dagger a_i + \omega_0 \sigma_i^+ \sigma_i^- + g(\sigma_i^+ a_i + \sigma_i^- a_i^\dagger)$ is the Jaynes-Cummings (JC) Hamiltonian describing light-matter interaction.[32] Here, $\sigma_i^+(\sigma_i^-)$ is the raising (lowering) operator acting on the TLS Hilbert space, and ω, ω_0, and g are the resonator frequency, TLS frequency, and light-matter coupling strength, respectively. Notice that the total number of elementary excitations (polaritons) in this system $N_{JCH} = \sum_i^L (a_i^\dagger a_i + \sigma_i^\dagger \sigma_i)$ is the

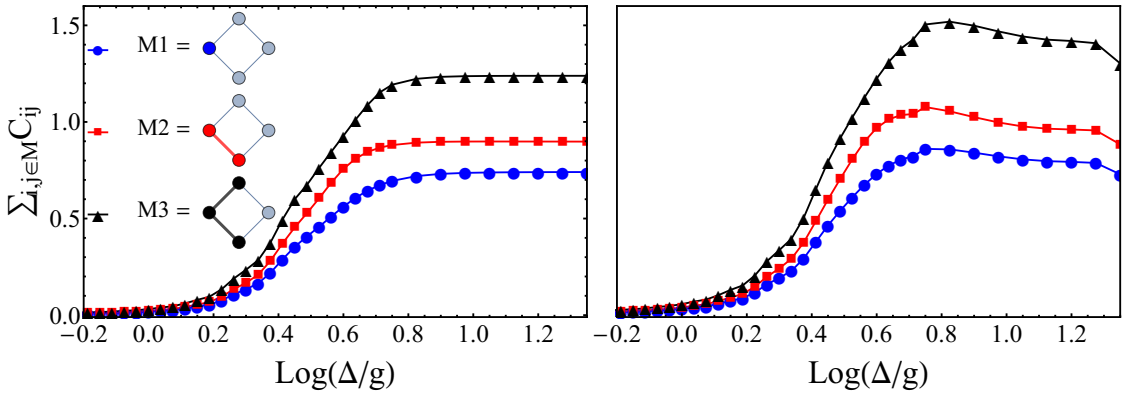

Figure 2. (color online) Mott-insulator to superfluid first (second)-like phase transition induced by an adiabatic (left) and an quench (right) dynamics as a function of the time averaged bipartite fluctuations. The simulated phase transition behavior aid remains independent from the order parameter choice.

conserved quantity[33,34] $[N, H_{JCH}] = 0$. The Mott-Insulator to Superfluid phase transition may be quantified by means of the time averaged bipartite fluctuations[21,35]

$$C_{i,j} = \frac{1}{T}\int_0^T dt\Big(\langle n_i\, n_j\rangle - \langle n_i\rangle\langle n_j\rangle\Big), \tag{2}$$

or by means of the variance $\sum_i C_{ii}$ with $T = J^{-1}$, which can be used as a global descriptor of the phase of the system. In a simulated Mott-insulator transition, where an adiabatic dynamics drives the passage, it has been shown that a suitable order parameter corresponds to the variance of the number of excitations per site. Fig. 2 shows the archetypal behavior of the order parameter as a function of the detuning Δ in the adiabatic dynamic regime, and for an integer filling factor of one net excitation per site.[16] As to compare the difference between the adiabatic and quenched transition, we run the simulations for 4-sites cycle networks in both dynamics, shown in Fig. 2. The simulated Mott-insulator to Superfluid phase transition strongly depends on the type of dynamics, where the adiabatic dynamics exhibits a second order phase transition which leads to a continuous change of the state of the system. On the other hand, the quench dynamics takes place accompanied by a discontinuous change of the state, analogous to the Metal-Insulator transition of oxides.[36]

For the initialization process the scheme proposed by Angelakis et al.[16] is considered. For instance, in circuit QED[7,8] one can cool down the whole system reaching temperatures around $T_0 \sim 15$mK. In this case, the system will be prepared in its global ground state $|G\rangle = \bigotimes_{i=1}^{L} |0,-\rangle_i$. Then, depending if the dynamics of interest is adiabatic or quenched, some variations need to be included. For example, in the adiabatic dynamics one can apply individual magnetic fields on the TLSs, each implemented via a transmon qubit,[37] such that the desired condition $\Delta \neq 0$ is achieved. This way one can address individually each cavity with an external AC microwave current or voltage tuned to the transition $|\downarrow, 0\rangle_i \to |1,-\rangle_i$, with a driving frequency $\omega_D = \frac{\omega+\omega_0}{2} - \frac{1}{2}\sqrt{(\omega-\omega_0)^2 - 4g^2}$, such that the system will be prepared in the desired initial state $|\psi_0\rangle = \bigotimes_{i=1}^{L} |1,-\rangle_i$. A similar procedure is available for quenched dynamics, by changing the initial detuning to a resonant state $\Delta = 0$ and modifying the initial driving frequency to $\omega_D = \omega - g$, in order to perform a sudden quench in the detuning $\Delta \neq 0$ to the desired value. We carry out full numerical calculations for the parameters $g = 10^{-2}\omega$ and $J = 10^{-2}g$, and we consider up to 6 Fock states per bosonic mode for an integration time $T = J^{-1}$ as this time is a characteristic time for the hopping effect to act on the system, and the fact that the behavior of the system stabilizes for times longer than this characteristic time.

As shown Fig.2, as compared to Fig.1, the order of the simulated phase transition is independent of the order parameter choice.

We can generalize these results even further. Considering that the JCH model is in the same universality class as the Bose-Hubbard Model (BH model), we also extended our analysis to the BH model, which is the

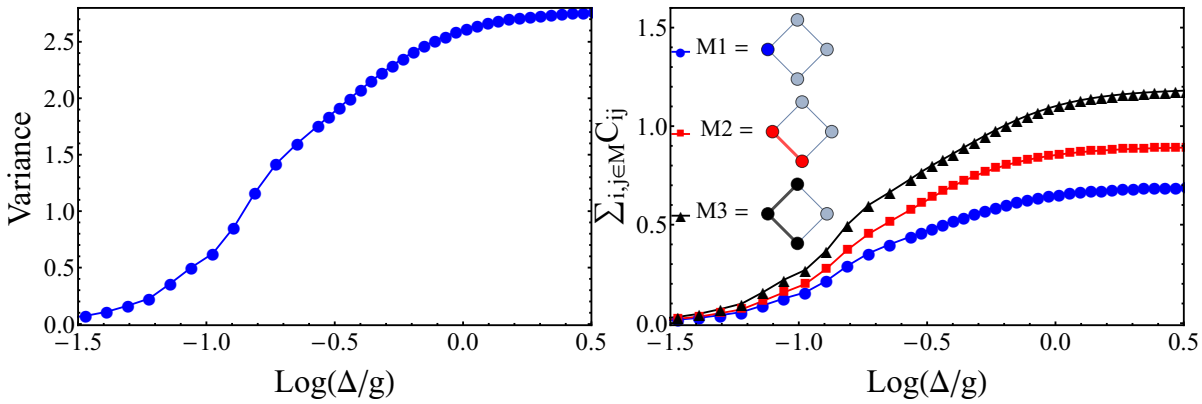

Figure 3. (color online) Simulated phase transition from Mott-insulator to superfluid in Bose-Hubbard model as a function of the detuning parameter. The order parameter of the transition correspond to the variance (left) and the bipartitte fluctuations (right).

paradigmatic model to study bosonic ultra cold atoms, which take the role of the model excitations.[38] For the theoretical description of the system, we rely on the BH model in the canonical ensemble whose Hamiltonian reads

$$H_{\rm BH} = \frac{1}{2}U\sum_{i=1} n_i(n_i-1) - J\sum_{\langle i,j\rangle} A_{ij}a_i^\dagger a_j + \text{h.c.}, \tag{3}$$

where L is the number of lattice sites, U is the strength of the on-site photonic repulsion, $a_i(a_i^\dagger)$ is the annihilation (creation) bosonic operator, J is the hopping amplitude, A_{ij} is the connectivity between sites, which takes values $A_{ij}=1$ if two sites of the array are connected and $A_{ij}=0$ otherwise. Notice that the in the BH model just as the JCH model, the total number of excitations $N_{BH}=\sum_i^L a_i^\dagger a_i$ is a conserved quantity $[N_{BH}, H_{BH}]=0$. As shown in Fig.3, simulated second-like phase transition in the Hubbard model do not depend on the order parameter.

2. NUCLEATION OF SUPERFLUID-LIGHT DOMAIN

Now our aim is to describe how complex arrangements of CRAs affect the simulated phase transition, from Mott insulator to superfluid, inducing localized superfluid nucleation. In order to do so, we first focus our attention on the phase transition in presence of quench dynamics, which already exhibits a fist-order like phase transition. We show that in the presence of complex arrangements nucleation emerges, as shown in Fig. 4 where the on-site variance was used to exhibit connectivity nucleation.

Conclusions

We have demonstrated that quench dynamics induces a first-order like phase transition in coupled resonator arrays doped with a two-level system. The nucleation of simulated superfluid states has been demonstrated by numerical simulation as a function of the local connectivity. In the quench dynamics the abrupt change of the order parameter, instead of sharper crossover driven by adiabatic dynamics, is explained by the non uniform transition from Mott-Insulator to superfluid, which locally depends on the connectivity. Since the quench dynamics exhibits the same behavior, independent of the choice of the order parameter, the variance of the polariton number or the bipartite fluctuations, our results reveal the universality of the simulated first order like phase transition. We show that phase transition for adiabatic dynamics in the JCH model, and the phase transition in the BH model, are capable of exhibiting nucleation, by changing the topology of the network.

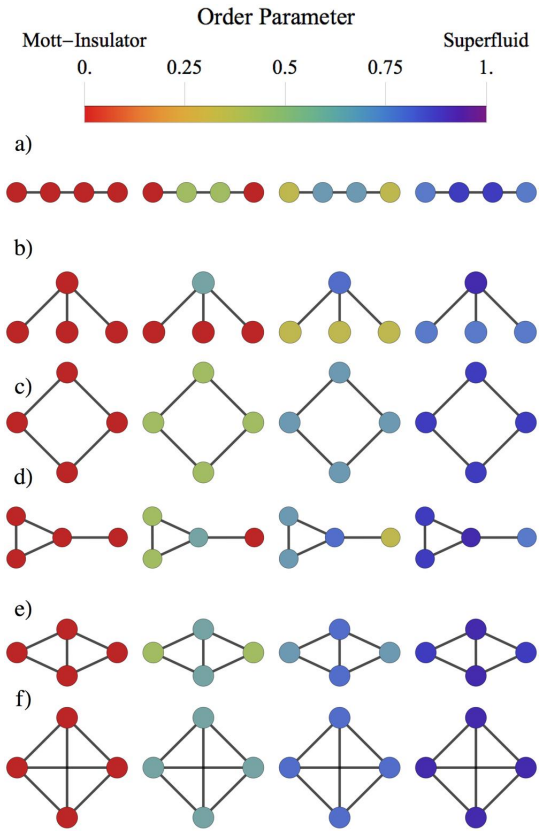

Figure 4. (color-online) Numerical simulation of the quench dynamics. The full set of four node arrays, with (a-b) three; (c-d) four; (e) five; and (f) six connections. Connectivity per site a) (1,2,2,1), b) (1,1,1,3), c) (2,2,2,2), d) (1,3,2,2), e) (2,3,3,2), and f) (3,3,3,3). As the connectivity is increased locally the superfluid phase is achieved with a lower detuning strength. For each array and from left to right we have considered parameters $\log(\Delta/g) = (0.5, 0.7, 0.75, 0.8)$, and $g = 10^{-2}\omega$, $J = 10^{-3}\omega$, where ω is the resonator frequency.

Therefore, we are able to provide a mechanism to change the nature of the phase transition from second-order like to first-order like.

As far as we understand, there is no known microscopic mechanism for predicting nucleation in first-order phase transitions. In this context, our results provide a geometrical description for the appearance of domain nucleation due to the number of connections. Thus, our results may be used to predict, and manipulate, the nucleation of a photonic superfluid phase in complex-random networks.

REFERENCES

[1] Greiner, M., Mandel, O., Esslinger, T., Hänsch, T. W., and Bloch, I., "Quantum phase transition from a superfluid to a mott insulator in a gas of ultracold atoms," *Nature* **415**(6867), 39–44 (2002).

[2] Regal, C. A., Greiner, M., and Jin, D. S., "Observation of resonance condensation of fermionic atom pairs," *Physical Review Letters* **92**(4), 040403 (2004).

[3] Lerario, G., Fieramosca, A., Barachati, F., Ballarini, D., Daskalakis, K. S., Dominici, L., Giorgi, M. D., Maier, S. A., Gigli, G., Kéna-Cohen, S., and Sanvitto, D., "Room-temperature superfluidity in a polariton condensate," *Nature Physics* **13**(9), 837–841 (2017).

[4] Wertz, E., Ferrier, L., Solnyshkov, D. D., Johne, R., Sanvitto, D., Lemaître, A., Sagnes, I., Grousson, R., Kavokin, A. V., Senellart, P., Malpuech, G., and Bloch, J., "Spontaneous formation and optical manipulation of extended polariton condensates," *Nature Physics* **6**(11), 860–864 (2010).

[5] Byrnes, T., Kim, N. Y., and Yamamoto, Y., "Exciton-polariton condensates," *Nature Physics* **10**(11), 803–813 (2014).
[6] Houck, A. A., Türeci, H. E., and Koch, J., "On-chip quantum simulation with superconducting circuits," *Nature Physics* **8**(4), 292–299 (2012).
[7] Raftery, J., Sadri, D., Schmidt, S., Türeci, H. E., and Houck, A. A., "Observation of a dissipation-induced classical to quantum transition," *Physical Review X* **4**(3), 031043 (2014).
[8] Fitzpatrick, M., Sundaresan, N. M., Li, A. C. Y., Koch, J., and Houck, A. A., "Observation of a dissipative phase transition in a one-dimensional circuit qed lattice," *Physical Review X* **7**(1), 011016 (2017).
[9] KAPITZA, P., "Viscosity of liquid helium below the λ-point," *Nature* **141**(3558), 74–74 (1938).
[10] Leggett, A. J., [*Quantum Liquids: Bose Condensation and Cooper Pairing in Condensed-Matter Systems*], Oxford University Press (Sept. 2006).
[11] Anderson, M. H., Ensher, J. R., Matthews, M. R., Wieman, C. E., and Cornell, E. A., "Observation of bose-einstein condensation in a dilute atomic vapor," *Science* **269**(5221), 198–201 (1995).
[12] Onofrio, R., Raman, C., Vogels, J. M., Abo-Shaeer, J. R., Chikkatur, A. P., and Ketterle, W., "Observation of superfluid flow in a bose-einstein condensed gas," *Physical Review Letters* **85**(11), 2228–2231 (2000).
[13] Zwierlein, M. W., Stan, C. A., Schunck, C. H., Raupach, S. M. F., Gupta, S., Hadzibabic, Z., and Ketterle, W., "Observation of bose-einstein condensation of molecules," *Physical Review Letters* **91**(25), 250401 (2003).
[14] Schiró, M., Bordyuh, M., Öztop, B., and Türeci, H. E., "Erratum: Phase transition of light in cavity qed lattices [phys. rev. lett.109, 053601 (2012)]," *Physical Review Letters* **109**(22), 229901 (2012).
[15] Hartmann, M. J., Brandão, F. G. S. L., and Plenio, M. B., "Strongly interacting polaritons in coupled arrays of cavities," *Nature Physics* **2**(12), 849–855 (2006).
[16] Angelakis, D. G., Santos, M. F., and Bose, S., "Photon-blockade-induced mott transitions andxyspin models in coupled cavity arrays," *Physical Review A* **76**(3), 031805 (2007).
[17] Greentree, A. D., Tahan, C., Cole, J. H., and Hollenberg, L. C. L., "Quantum phase transitions of light," *Nature Physics* **2**(12), 856–861 (2006).
[18] Birnbaum, K. M., Boca, A., Miller, R., Boozer, A. D., Northup, T. E., and Kimble, H. J., "Photon blockade in an optical cavity with one trapped atom," *Nature* **436**(7047), 87–90 (2005).
[19] Imamoḡlu, A., Schmidt, H., Woods, G., and Deutsch, M., "Strongly interacting photons in a nonlinear cavity," *Physical Review Letters* **79**(8), 1467–1470 (1997).
[20] Greentree, A. D., Vaccaro, J. A., de Echaniz, S. R., Durrant, A. V., and Marangos, J. P., "Prospects for photon blockade in four-level systems in the n configuration with more than one atom," *Journal of Optics B: Quantum and Semiclassical Optics* **2**(3), 252–259 (2000).
[21] Rossini, D., Fazio, R., and Santoro, G., "Photon and polariton fluctuations in arrays of qed-cavities," *EPL (Europhysics Letters)* **83**(4), 47011 (2008).
[22] Na, N., Utsunomiya, S., Tian, L., and Yamamoto, Y., "Strongly correlated polaritons in a two-dimensional array of photonic crystal microcavities," *Physical Review A* **77**(3), 031803 (2008).
[23] Koch, J. and Hur, K. L., "Superfluid-mott-insulator transition of light in the jaynes-cummings lattice," *Physical Review A* **80**(2), 023811 (2009).
[24] Halu, A., Garnerone, S., Vezzani, A., and Bianconi, G., "Phase transition of light on complex quantum networks," *Physical Review E* **87**(2), 022104 (2013).
[25] Rossini, D. and Fazio, R., "Mott-insulating and glassy phases of polaritons in 1d arrays of coupled cavities," *Physical Review Letters* **99**(18), 186401 (2007).
[26] Aichhorn, M., Hohenadler, M., Tahan, C., and Littlewood, P. B., "Quantum fluctuations, temperature, and detuning effects in solid-light systems," *Physical Review Letters* **100**(21), 216401 (2008).
[27] Pippan, P., Evertz, H. G., and Hohenadler, M., "Excitation spectra of strongly correlated lattice bosons and polaritons," *Physical Review A* **80**(3), 033612 (2009).
[28] Schmidt, S. and Blatter, G., "Strong coupling theory for the jaynes-cummings-hubbard model," *Physical Review Letters* **103**(8), 086403 (2009).
[29] Hartmann, M. J., "Quantum simulation with interacting photons," *Journal of Optics* **18**(10), 104005 (2016).

[30] Noh, C. and Angelakis, D. G., "Quantum simulations and many-body physics with light," *Reports on Progress in Physics* **80**(1), 016401 (2016).
[31] Angelakis, [*Quantum Simulations with Photons and Polaritons*], Quantum Science and Technology, Springer International Publishing (2017).
[32] Jaynes, E. and Cummings, F., "Comparison of quantum and semiclassical radiation theories with application to the beam maser," *Proceedings of the IEEE* **51**(1), 89–109 (1963).
[33] Hartmann, M., Brandão, F., and Plenio, M., "Quantum many-body phenomena in coupled cavity arrays," *Laser & Photonics Review* **2**(6), 527–556 (2008).
[34] Hartmann, M. J. and Plenio, M. B., "Strong photon nonlinearities and photonic mott insulators," *Physical Review Letters* **99**(10), 103601 (2007).
[35] Rachel, S., Laflorencie, N., Song, H. F., and Hur, K. L., "Detecting quantum critical points using bipartite fluctuations," *Physical Review Letters* **108**(11), 116401 (2012).
[36] Rozenberg, M. J., "Integer-filling metal-insulator transitions in the degenerate hubbard model," *Physical Review B* **55**(8), R4855–R4858 (1997).
[37] Koch, J., Yu, T. M., Gambetta, J., Houck, A. A., Schuster, D. I., Majer, J., Blais, A., Devoret, M. H., Girvin, S. M., and Schoelkopf, R. J., "Charge-insensitive qubit design derived from the cooper pair box," *Physical Review A* **76**(4), 042319 (2007).
[38] Jaksch, D., Bruder, C., Cirac, J. I., Gardiner, C. W., and Zoller, P., "Cold bosonic atoms in optical lattices," *Physical Review Letters* **81**(15), 3108–3111 (1998).